32001

National Library of Canada / Bibliothèque nationale du Canada

CANADIAN THESES ON MICROFICHE / THÈSES CANADIENNES SUR MICROFICHE

NAME OF AUTHOR/*NOM DE L'AUTEUR* Daniel John Kenway

TITLE OF THESIS/*TITRE DE LA THÈSE* A study of the Photoluminescence of Cuprous Oxide

UNIVERSITY/*UNIVERSITÉ* University of Alberta, Edmonton

DEGREE FOR WHICH THESIS WAS PRESENTED/ *GRADE POUR LEQUEL CETTE THÈSE FUT PRÉSENTÉE* M. Sc.

YEAR THIS DEGREE CONFERRED/*ANNÉE D'OBTENTION DE CE GRADE* 1977

NAME OF SUPERVISOR/*NOM DU DIRECTEUR DE THÈSE* F. L. Weichman

Permission is hereby granted to the NATIONAL LIBRARY OF CANADA to microfilm this thesis and to lend or sell copies of the film.

The author reserves other publication rights, and neither the thesis nor extensive extracts from it may be printed or otherwise reproduced without the author's written permission.

*L'autorisation est, par la présente, accordée à la BIBLIOTHÈQUE NATIONALE DU CANADA de microfilmer cette thèse et de prêter ou de vendre des exemplaires du film.*

*L'auteur se réserve les autres droits de publication; ni la thèse ni de longs extraits de celle-ci ne doivent être imprimés ou autrement reproduits sans l'autorisation écrite de l'auteur.*

DATED/*DATÉ* April 11, 77 SIGNED/*SIGNÉ* Daniel Kenway

PERMANENT ADDRESS/*RÉSIDENCE FIXÉ* #102 10915 - 83 Ave
Edmonton, Alberta

NL-91 (3-74)

National Library of Canada

Cataloguing Branch
Canadian Theses Division

Ottawa, Canada
K1A 0N4

Bibliothèque nationale du Canada

Direction du catalogage
Division des thèses canadiennes

## NOTICE

The quality of this microfiche is heavily dependent upon the quality of the original thesis submitted for microfilming. Every effort has been made to ensure the highest quality of reproduction possible.

If pages are missing, contact the university which granted the degree.

Some pages may have indistinct print especially if the original pages were typed with a poor typewriter ribbon or if the university sent us a poor photocopy.

Previously copyrighted materials (journal articles, published tests, etc.) are not filmed.

Reproduction in full or in part of this film is governed by the Canadian Copyright Act, R.S.C. 1970, c. C-30. Please read the authorization forms which accompany this thesis.

THIS DISSERTATION
HAS BEEN MICROFILMED
EXACTLY AS RECEIVED

## AVIS

La qualité de cette microfiche dépend grandement de la qualité de la thèse soumise au microfilmage. Nous avons tout fait pour assurer une qualité supérieure de reproduction.

S'il manque des pages, veuillez communiquer avec l'université qui a conféré le grade.

La qualité d'impression de certaines pages peut laisser à désirer, surtout si les pages originales ont été dactylographiées à l'aide d'un ruban usé ou si l'université nous a fait parvenir une photocopie de mauvaise qualité.

Les documents qui font déjà l'objet d'un droit d'auteur (articles de revue, examens publiés, etc.) ne sont pas microfilmés.

La reproduction, même partielle, de ce microfilm est soumise à la Loi canadienne sur le droit d'auteur, SRC 1970, c. C-30. Veuillez prendre connaissance des formules d'autorisation qui accompagnent cette thèse.

LA THÈSE A ÉTÉ
MICROFILMÉE TELLE QUE
NOUS L'AVONS REÇUE

THE UNIVERSITY OF ALBERTA

# A STUDY OF THE PHOTOLUMINESCENCE OF CUPROUS OXIDE

by

© DANIEL JOHN KENWAY

A THESIS

SUBMITTED TO THE FACULTY OF GRADUATE STUDIES AND RESEARCH

IN PARTIAL FULFILLMENT OF THE REQUIREMENTS FOR THE DEGREE

OF MASTER OF SCIENCE

DEPARTMENT OF PHYSICS

EDMONTON, ALBERTA

SPRING, 1977

THE UNIVERSITY OF ALBERTA

FACULTY OF GRADUATE STUDIES AND RESEARCH

The undersigned certify that they have read, and recommend to the Faculty of Graduate Studies and Research, for acceptance, a thesis entitled A STUDY OF THE PHOTOLUMINESCENCE OF CUPROUS OXIDE submitted by Daniel John Kenway in partial fulfillment of the requirements for the degree of Master of Science.

.....
Supervisor

.....

.....

.....

Date: January 27, 1977

TO MY WIFE,

AND MY PARENTS

ABSTRACT

This thesis reports an experimental study of the extrinsic photoluminescence of cuprous oxide. While primarily a detailed description of the development and nature of the specific apparatus used, it also includes a broad historical review of previous work and some preliminary results from our current research.

The system developed uses a tunable pulsed dye laser to excite photoluminescence, and a minicomputer system for data acquisition.

The luminescent output is measured as a function of temperature and excitation wavelength. It is found that the behavior of the 0.93 μ luminescence is considerably different from that of the 0.72 μ and 0.83 μ luminescences, the 0.93 μ temperature function shifting with changes in excitation wavelength. Further there is tentative evidence that the excitation functions of the 0.72 μ and 0.83 μ luminescences differ. Neither of these results has been directly reported in the literature.

ACKNOWLEDGEMENTS

I would like to thank F.L. Weichman without whose guidance and support this work would not have been possible; my father and the rest of my family, whose assistance in the production of this thesis was invaluable; and my friends, especially B. Ramage, whose discussion greatly clarified the text.

I would also like to express my appreciation to T. Keosim, K. Chee, G. Christie, and especially C. Duvvury, with whom it has been my privilege to work,

The financial support of the National Research Council of Canada was of great assistance, and warmly appreciated.

Finally I owe a great deal to my wife who has been a constant source of encouragement and support.

TABLE OF CONTENTS


| | | Page |
|---|---|---|
| CHAPTER 1: | INTRODUCTION AND HISTORICAL BACKGROUND | 1 |
| 1.0 | Introduction | 1 |
| 1.1 | Historical Background | 1 |
| CHAPTER 2: | EQUIPMENT | 36 |
| 2.0 | Introduction | 36 |
| 2.1 | The Light Source | 38 |
| 2.1.1 | The Nd:YAG Laser | 38 |
| 2.1.2 | The Dye Laser | 46 |
| 2.1.3 | The Dye Laser Power Monitoring System | 63 |
| 2.1.4 | The Collimation System and Chopper | 84 |
| 2.1.5 | The Wavelength Monitoring System | 87 |
| 2.2 | The Detection System | 89 |
| 2.3 | The Temperature Control and Monitoring System | 94 |
| 2.4 | The Data Acquisition and Processing System | 102 |
| 2.5 | Summary | 134 |
| CHAPTER 3: | RESULTS | 136 |
| 3.0 | Results | 136 |
| 3.1 | Summary and Conclusions | 174 |
| REFERENCES | | 177 |
| ADDITIONAL BIBLIOGRAPHY | | 188 |
| APPENDIX I: | COMPUTER PROGRAMS | 190 |
| APPENDIX II: | LIST OF DATA | 195 |

LIST OF FIGURES

CHAPTER 1


| Figure | | Page |
|---|---|---|
| 1-1 | Excitons and the band structure of $Cu_2O$. | 3 |
| 1-2 | Band structure for the model of Mott and Gurney. | 3 |
| 1-3 | The optical data of Karkhanin and Lashkarev. | 8 |
| 1-4 | Temperature dependence observed by Karkhanin and Lashkarev. | 8 |
| 1-5 | Mechanism for photoconductivity and luminescence (after Grillot). | 10 |
| 1-6 | Data of Garlick. | 10 |
| 1-7 | Emission as observed by Bloem and Van der Houven van Oordt. | 13 |
| 1-8 | Dependence of luminescence emission on oxygen pressure during preparation (after Bloem). | 15 |
| 1-9 | Theoretical results of Bloem. | 15 |
| 1-10 | The band scheme of Garlick. | 16 |
| 1-11 | The band scheme as modified by Bloem. | 16 |
| 1-12 | The model of Gorban, Rudko and Shishlovskii. | 21 |
| 1-13 | Excitation spectrum observed by Karkhanin and Vorob'ev. | 23 |
| 1-14 | The optical data of Gorban and Rudko. | 25 |
| 1-15 | The impurity band scheme. | 25 |
| 1-16 | Superlinearity observed by Bonch-Bruevich and Tolstoi. | 27 |
| 1-17 | The model of Tolstoi and Bonch-Bruevich. | 27 |

| Figure | | Page |
|---|---|---|
| 1-18 | The saturation data of Tolstoi and Abramov. | 29 |
| 1-19 | The high intensity results of Berkovskii and Schreter. | 29 |
| 1-20 | The excitation spectrum of Taylor and Weichman. | 30 |
| 1-21 | Excitation characteristics observed by Duvvury, Kenway and Weichman. | 33 |
| 1-22 | Excitation shift with temperature. | 33 |
| | CHAPTER 2 | |
| 2-1 | Basic experiment. | 37 |
| 2-2 | Resonant charging network. | 40 |
| 2-3 | D.C. supply schematic. | 40 |
| 2-4 | Q switch timing. | 41 |
| 2-5 | Original Q-switch timing circuit. | 42 |
| 2-6 | Quartz-stabilized Q switch timing circuit. | 42 |
| 2-7 | Laser output-photograph. | 43 |
| 2-8 | Three level scheme. | 47 |
| 2-9 | Four level scheme. | 47 |
| 2-10 | Dye laser energy bands. | 48 |
| 2-11 | Absorption and fluorescence of rhodamine 6G in ethanol. | 50 |
| 2-12 | Dye circulation system. | 52 |
| 2-13 | Optical pumping configuration. | 52 |
| 2-14 | Detail of dye absorption. | 53 |

| Figure | | Page |
|---|---|---|
| 2-15 | Hemispherical cavity. | 54 |
| 2-16 | Improved dye laser configuration. | 56 |
| 2-17 | Prism tuned cavity. | 56 |
| 2-18 | Brewster prism and angles. | 58 |
| 2-19 | Interfaces at dye cell window. | 59 |
| 2-20 | Dye cell resonator. | 60 |
| 2-21 | Actual dye laser optics. | 61 |
| 2-22 | Naive photoluminescence experiment. | 64 |
| 2-23 | Photo-luminescence signal through corning 7-57 filter. | 64 |
| 2-24 | Internal photodiode optics. | 65 |
| 2-25 | Internal photodiode circuit. | 65 |
| 2-26 | Improved acquisition technique. | 66 |
| 2-27 | Typical data photograph pair. | 68 |
| 2-28 | Computer controlled data acquisition system. | 70 |
| 2-29 | Simplified computer program. | 71 |
| 2-30 | Block diagram of fast pulse integrator sample and hold. | 72 |
| 2-31 | Fast pulse integrator sample and hold. | 73 |
| 2-32 | Fast monitoring acquisition system. | 76 |
| 2-33 | ECL anticoincidence gate. | 77 |
| 2-34 | Actual monitoring system. | 77 |
| 2-35 | Actual mounting of beam monitor. | 80 |
| 2-36 | Laser power level distribution. | 81 |
| 2-37 | Power level indication. | 81 |

| Figure | | Page |
|---|---|---|
| 2-38 | Laser feedback circuit. | 83 |
| 2-39 | Chromatic dispersion of dye laser output. | 84 |
| 2-40 | Collimation system and chopper. | 86 |
| 2-41 | Light source. | 88 |
| 2-42 | Photocathode sensitivity vs wavelength. | 90 |
| 2-43 | Detection system. | 93 |
| 2-44 | Cryostat used in experiment. | 95 |
| 2-45 | Nitrogen transfer pump. | 98 |
| 2-46 | A nitrogen transfer system. | 98 |
| 2-47 | Temperature control and monitoring circuit. | 101 |
| 2-48 | Actual experimental system. | 110 |
| 2-49 | Diagram of S/H amplifier. | 111 |
| 2-50 | Sample and hold schematic. | 112 |
| 2-51 | Fairchild μA 749. | 113 |
| 2-52 | Acquisition timing. | 115 |
| 2-53 | Computer I/O. | 119 |
| 2-54 | Program groupings. | 120 |
| 2-55 | Acquisition program. | 123 |
| 2-56 | Fast acquisition subroutine. | 127 |
| 2-57 | Chopper geometry. | 130 |
| 2-58 | Ring sector approximation. | 130 |
| | CHAPTER 3 | |
| 3-1 | 0.72 μ luminescence excited by 5960 Å. | 140 |
| 3-2 | 0.72 μ luminescence excited by 6080 Å. | 141 |

| Figure | | Page |
|---|---|---|
| 3-3 | 0.72 μ luminescence excited by 6080 Å. | 142 |
| 3-4 | 0.72 μ luminescence excited by 6080 Å. | 143 |
| 3-5 | 0.72 μ luminescence excited by 6200 Å. | 144 |
| 3-6 | 0.72 μ luminescence excited by 6320 Å. | 145 |
| 3-7 | 0.83 μ luminescence excited by 5960 Å. | 146 |
| 3-8 | 0.83 μ luminescence excited by 6080 Å. | 147 |
| 3-9 | 0.83 μ luminescence excited by 6080 Å. | 148 |
| 3-10 | 0.83 μ luminescence excited by 6080 Å. | 149 |
| 3-11 | 0.83 μ luminescence excited by 6080 Å. | 150 |
| 3-12 | 0.83 μ luminescence excited by 6200 Å. | 151 |
| 3-13 | 0.83 μ luminescence excited by 6320 Å. | 152 |
| 3-14 | 0.83 μ luminescence excited by 6330 Å. | 153 |
| 3-15 | 0.83 μ luminescence excited by 6320 Å. | 154 |
| 3-16 | 0.93 μ luminescence excited by 5905 Å. | 155 |
| 3-17 | 0.93 μ luminescence excited by 5905 Å. | 156 |
| 3-18 | 0.93 μ luminescence excited by 5905 Å. | 157 |
| 3-19 | 0.93 μ luminescence excited by 5960 Å. | 158 |
| 3-20 | 0.93 μ luminescence excited by 6080 Å. | 159 |
| 3-21 | 0.93 μ luminescence excited by 6200 Å. | 160 |
| 3-22 | 0.93 μ luminescence excited by 6320 Å. | 161 |
| 3-23 | 0.93 μ luminescence excited by 6330 Å. | 162 |
| 3-24 | 0.93 μ luminescence excited by 6320 Å. | 163 |
| 3-25 | Cumulative 0.72 μ data. | 164 |
| 3-26 | Cumulative 0.83 μ data. | 165 |
| 3-27 | Non-normalized 0.72 μ data. | 167 |

| Figure | | Page |
|---|---|---|
| 3-28 | Non-normalized 0.83 μ data. | 168 |
| 3-29 | Non-normalized 0.93 μ data. | 169 |
| 3-30 | Comparison of the 0.72 μ and 0.83 μ luminescence temperature functions. | 170 |
| 3-31 | Excitation spectrum of the 0.72 μ luminescence at 77 K. | 172 |
| 3-32 | Excitation spectrum of the 0.83 μ luminescence at 160 K. | 173 |

# CHAPTER 1

# INTRODUCTION AND HISTORICAL BACKGROUND

## 1.0 Introduction

The work presented here is an incomplete attempt to resolve some difficulties and contradictions in the observations and theory of the photoluminescence of cuprous oxide. It is primarily an experimental effort concerned with the utilization of a pulsed dye laser as a variable wavelength high power source of stimulating radiation.

## 1.1 Historical Background

The study of the optical properties of cuprous oxide has been intimately related to the theory of the exciton. In its simplest conception (following Mott[1], and Gurney and Mott[2]) an exciton can be thought of as a hydrogenic system formed in a semiconductor and consisting of a positively charged hole bound by Coulomb attraction to a negatively charged electron. The energy levels are usually approximately hydrogenic in structure and are specifically determined by the effective masses of the hole and electron and other details of the semiconductor's structure and properties. Further, the energy

required to form an exciton is just slightly less than the energy required to excite an electron into the conduction band. This is very natural if one considers attainment of the conduction band to be equivalent to the $n=\infty$ state of the exciton. As cuprous oxide has a fairly complicated band structure (including several valence bands), it is possible for more than one type of excitonic system to exist (see figure 1-1).

The theory of Gurney and Mott[2] (1939) considered excitons as important to absorption, but defects as the source of luminescence. Their thermodynamic model for luminescence is based on very simple probability and energy level considerations. If we assume that the energy levels at a defect are likely to be spatially dependent, and we specifically assume a dependence like the one shown in figure 1-2 where the bands closely approach each other at a finite distance from their minima, two principal modes of decay are suggested:

1. a direct transition from the minimum of the upper band resulting in the emission of a photon, or

2. an indirect transition involving the absorption of heat at the upper level which allows the electron in the excited state to spatially move out to point C and switch bands. The majority of the electron's energy will then be lost in heat as the electron settles to point A.

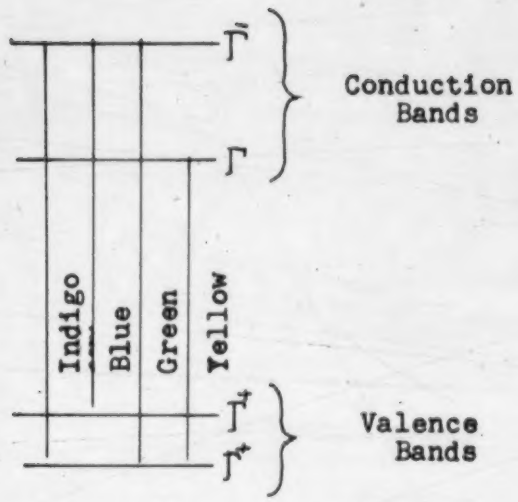


Figure 1-1 Excitons & The Band Structure of $Cu_2O$

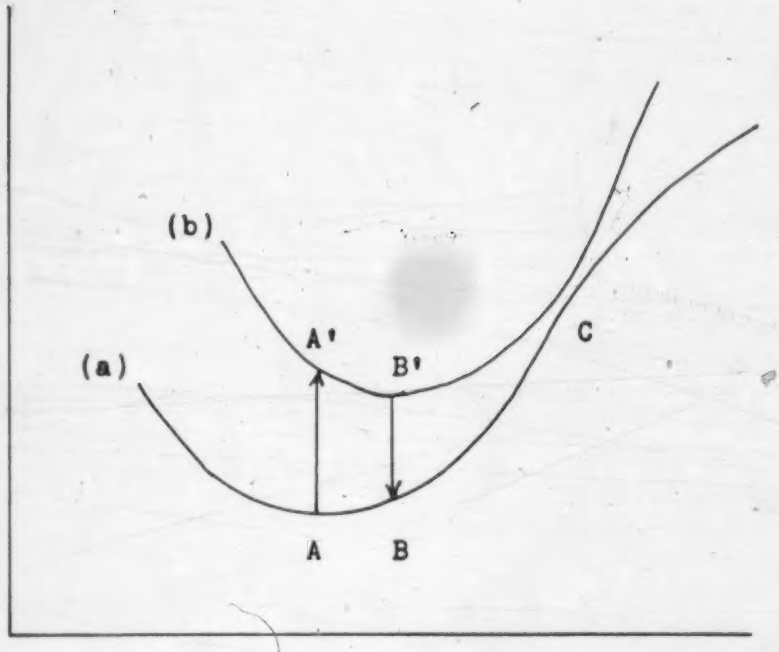


Figure 1-2 Band Structure For The Model of Mott and Gurney

Let us suppose that the probability of the first type of decay is A. The second decay will be dependent upon the available thermal energy and will have (in the simple Boltzman approximation) probability

$$Be^{-\frac{\Delta E}{kT}}$$

where $\Delta E$ is the energy difference between the excited state minimum and the crossover point. The probability of luminescent emission will therefore be given by:

$$L(T) = \frac{A}{A + Be^{-\Delta E/kT}} = \frac{1}{1 + (B/A)e^{-\Delta E/kT}} \quad .$$

It is very interesting to note that a very similar formula for the thermodynamic behavior of luminescence can be arrived at with Fermi-Dirac statistics applied to an electron with an available excited state. If one considers the luminescence to be proportional to the number of electrons available for excitation from the ground state at temperature T, then the temperature dependence of luminescence will be given by:

$$L(T) \propto 1 - \frac{1}{1 + e^{\Delta E/kT}} = \frac{1}{1 + e^{-\Delta E/kT}} \quad .$$

This formula is very similar to the formula of Gurney and Mott except for the absence of the factor preceding the exponential. As a result the temperature dependence of the simple Fermi-Dirac occupation model is limited to a

drop to 1/2 of the low temperature maximum, whereas the Gurney-Mott luminescence may drop to

$$\frac{1}{1 + (B/A)}$$

which can be arbitrarily small (depending on B/A). It is difficult to find conventional arguments for such a factor in a Fermi system.

Luminescence in $Cu_2O$ is well known and has been studied extensively over a long period of time with a great variation in results. Luminescence in the region of 1 micron was first reported by M. Seibt[3] in 1939. After the war the luminescence was independently rediscovered by V.E. Lashkarev and K.M. Kossonogova[4] (1946) who made three important observations:

1. That the luminescence was between 0.9 and 1 microns;

2. That the luminescence yield varied widely from sample to sample depending upon sample preparation and was greatest for samples annealed in a vacuum;

3. That the luminescence was strongly temperature dependent and approximately followed the formula of Gurney and Mott:

$$L \propto \frac{1}{1 + Ae^{-\Delta E/kT}} .$$

Interest blossomed and in the next few years a number of papers reporting on various aspects of the luminescence were published. Karkhanin[5] (1952) published the first curve showing the distribution of the luminescence over its output wavelength. The curve is bell shaped with a maximum in the vicinity 0.96 μ and a half-width of about 0.1 μ. This was confirmed by Garlick and Dumbleton[6] (1954). The peak was observed to shift with temperature by Karkhanin and Lashkarev[7] (1954) who further studied a large number of samples. These findings were later confirmed by many other authors.

Tolstoi and Tkachuk[8] (1954) investigated the time relaxation characteristics finding a very fast exponential decay with a lifetime of approximately $4\times10^{-8}$ seconds. They further found that the relaxation time was independent of excitation intensity but increased anomalously with increasing temperature. A more extensive paper discussing experimental techniques and covering the investigation of a large number of samples prepared in different ways was published by Tolstoi, Tkachuk, and Preobrazhensky[9] (1957).

The excitation characteristics (i.e. the luminescent output as a function of excitation wavelength) were investigated by Karkhanin[5] (1952), Garlick and Dumbleton[6] (1954), Karkhanin and Lashkarev[7] (1954), and by Garlick[10] (1956) with disagreement between the Soviet and English authors.

With the growing number of results it was natural that more specific theoretical conjectures on the nature of the luminescence would be made. It is important to realize that parallel research on the other properties of $Cu_2O$ was yielding some interesting results. Most significant was the observation of a hydrogenic series in the optical absorption edge of $Cu_2O$ by Gross and Karriev[11] (1952). This was the first direct evidence of the existence of excitons (in $Cu_2O$ or any other substance).

It was with this background of supporting data that Karkhanin and Lashkarev[7] (1954) ventured some theories on the mechanism of the IR luminescence. They were aware that the luminescence was greatest in oxygen rich samples, and that the luminescence increased at low temperatures where electrical resistance was high. They were further aware that $Cu_2O$ is generally a p-type semiconductor and suspected that copper vacancies were responsible for the acceptor levels. These results supported the idea that the luminescence had its origin in decays at un-ionized copper vacancy defects.

Karkhanin and Lashkarev further applied a strong electric field to the sample, capable of removing (according to their estimation) more than 90% of the photoelectrons generated by optical excitation. Under

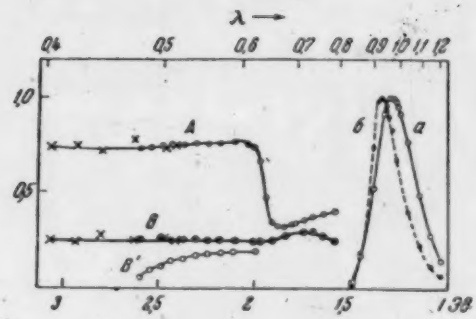


Спектры поглощения, выхода и люминесценции закиси меди. *а* — спектр люминесценции при 20°; *б* — спектр люминесценции при —183°. *A* — спектр поглощения образца закиси меди толщиной 0,3 мм в %; *B* — спектр квантового выхода травленого образца при $T = 20°$ в %; *B'* — спектр квантового выхода нетравленого образца в произвольных единицах. Крестики — результаты измерений, выполненных при помощи интерференционных фильтров

a. Luminescence Output at 20 C

b. Luminescence Output at -183 C

A. Optical Absorption (0.3 mm Sample) in %

B. Quantum Yield (excitation spectrum) at 20 C

B'. Quantum Yield for unpolished sample

**Figure 1-3 The Optical Data of Karkhanin & Lashkarev[7]**

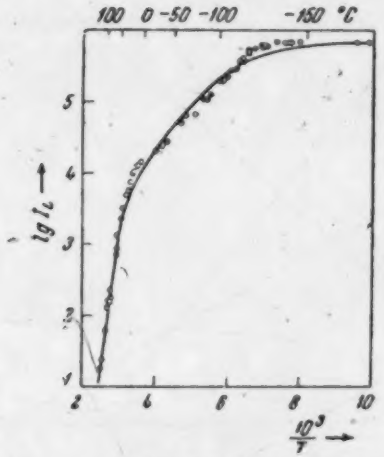


Зависимость интенсивности люминесценции $Cu_2O$ от температуры. Сплошная кривая соответствует формуле (1). Кружки — опытные данные

**Figure 1-4 Temperature Dependence Observed by Karkhanin and Lashkarev[7]**

these conditions they observed virtually no change in the photoluminescence. This, in conjunction with their observation of a change in luminescence, yields for excitation wavelengths greater than 0.65 μ (the optical absorption edge) led them to believe that (at least in the visible) the luminescence was excited through the creation of excitons rather than through the stimulation of photoelectrons.

Their model then was one in which optical excitation created excitons which were then captured by unionized copper vacancies where the excitons decayed giving off luminescence (with the remaining energy and recoil absorbed by the lattice).

Photoconductivity also seemed greatest in oxygen rich samples and increased approximately exponentially with temperature. This encouraged Karkhanin and Lashkarev to make direct comparisons with the excitonic theory of photoconductivity developed by Zhuze and Ryvkin[12] (1952).

These concepts are amplified in a review by Grillot[13] (1955). In his view optically created excitons will decay in one of two ways upon encountering a copper vacancy (see figure 1-5). If the acceptor level created by the vacancy is occupied the decay of the exciton will give rise to a free electron in the conduction band. If the acceptor level is empty the decay will result in the

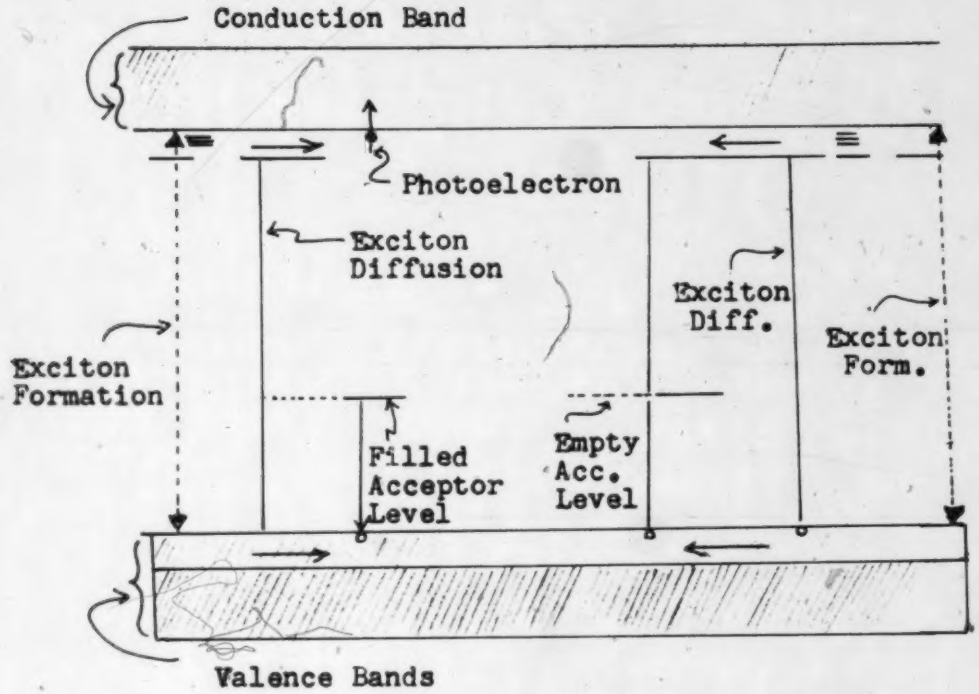


Figure 1-5 (After Grillot[13])
Mechanism for Photoconductivity and Luminescence

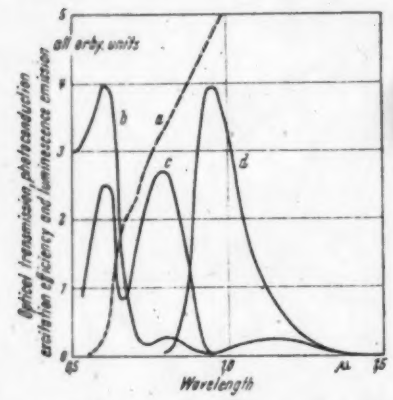


Optical and photoconduction response spectra of a cuprous oxide layer. a Optical transmission. b Photoconduction. c Luminescence excitation spectrum. d Luminescence emission spectrum.

a. Optical Transmission

b. Photoconduction

c. Luminescence Excitation Spectrum

d. Luminescence Emission Spectrum

Figure 1-6 Data of Garlick[10]

luminescent emission of a photon. The complementary thermal behavior of photoconductivity and luminescence then follows as a natural consequence of the thermal filling of the acceptor states at the copper vacancies. (Any difficulties with the Fermi-Dirac statistics are ignored.)

Tolstoi's anomalies in relaxation time may then be detached from the dominant effect and explained by changes in exciton mobility. Tolstoi[14] (1957) reviewed these concepts and extended them with the conjecture that the relaxation time anomaly could be related to temperature changes in the lifetime of the acceptor-exciton complex which would have no effect on the total luminescence yield. This specific conjecture was contested by Khas[15] (1965) who claims to prove theoretically that an exciton-acceptor complex should have a lifetime of greater than $10^{-5}$ seconds (too long to correlate with any of the experimental results).

A somewhat different approach is taken by Garlick[10] (1956) who first notes similarities in the excitation curves of the 0.93 μ luminescence and the photoconductivity (see figure 1-6), both showing peaks at 0.6 μ and 0.8 μ. (It is worth noting that these curves differ substantially from those of Karkhanin and Lashkarev[7], and that strong excitation at 0.8μ is impossible with a purely excitonic mechanism.)

Garlick then, combining this with astute comparison of thermal activation energies (and using the difference between the static and optical dielectric constants), is able to construct a two level model for the excitation of electrons from the valence band (see figure 1-10). Garlick in fact uses the early results of Zhuze and Ryvkin[16] (1949) and Lashkarev and Kossonogova[4] (1946) as a basis for the positioning of the thermal levels: the lower level from photoconductivity activation energies, and the upper from the luminescence activation energy reported by Lashkarev and Kossonogova.

On the basis of this scheme Garlick accounts for the observed luminescence as the result of transitions from the conduction band to level B (see figure 1-10), and predicts at low temperatures (when level A will be empty) a new luminescence at about 0.7 μ.

It was then with some excitement that Bloem and Van der Houven van Oordt[17] (1956) announced in the same year the observation of this new luminescence. In fact they also observed a third luminescence at 0.83 μ which they believed to be due to a splitting of the A level. More detailed analysis appears in a later paper (Bloem[18] (1958)) and it is this work that we will review.

In much of the preceding work a sample to sample variation in properties has been noted (in fact, some author to author disagreement may be due to this variation). The most important parameter affecting the

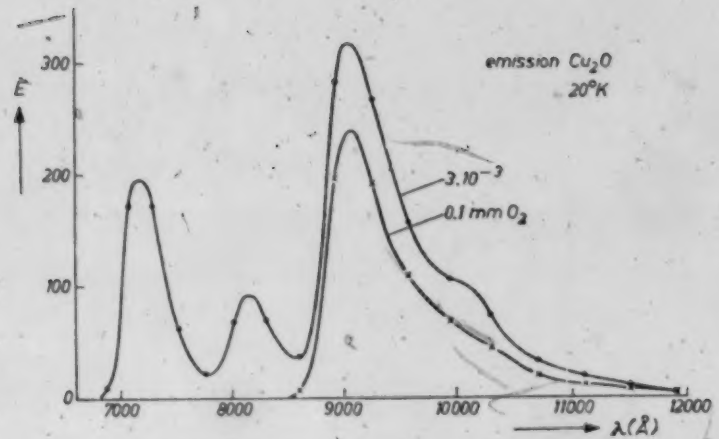


Luminescence emission spectra of some $Cu_2O$ samples at 20 °K (intensities in arbitrary units).

Figure 1-7 Emission as Observed by Bloem and Van Der Houven Van Oordt[17]

luminescence and other properties is the non-stoichiometry of the samples - that is the extent to which the samples are oxygen rich or copper rich. Bloem's principal study was of the precise effects on luminescence (and conductivity) of controlled variation in sample preparation. His polycrystalline samples were annealed at 960 C under carefully controlled partial pressures of oxygen. When equilibrium conditions were reached the samples were quenched in water.

By means of thermodynamic arguments Bloem is able to estimate the concentrations of various vacancies (and complexes of vacancies) present in the samples thus prepared. By comparison between the estimated concentrations of vacancies (and complexes) as a function of oxygen pressure (during preparation), and the observed dependencies of luminescent output on oxygen pressure, he is able to make inferences as to the defects responsible for the various luminescences (see figures 1-8 and 1-9).

Bloem's conclusions then are:

1. That copper vacancies, ionized $V_{Cu}^{+}$ and unionized $V_{Cu}$, are responsible for the 0.9 μ luminescence.

2. That the 0.7 μ (and 0.8 μ) luminescences may be related to the $V_{O}^{-}$ ionized oxygen vacancies, or to the neutral complexes $V_{O}$-$V_{Cu}^{+}$.

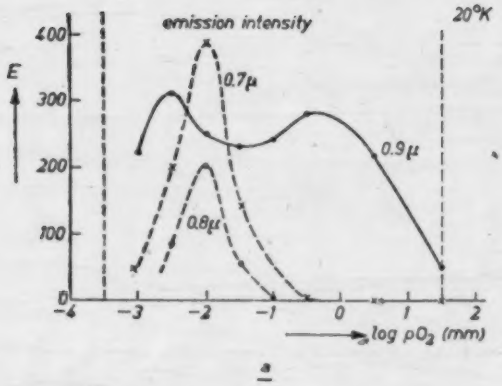


Figure 1-8 Dependence of Luminescence Emission on Oxygen Pressure During Preparation (After Bloem[18])

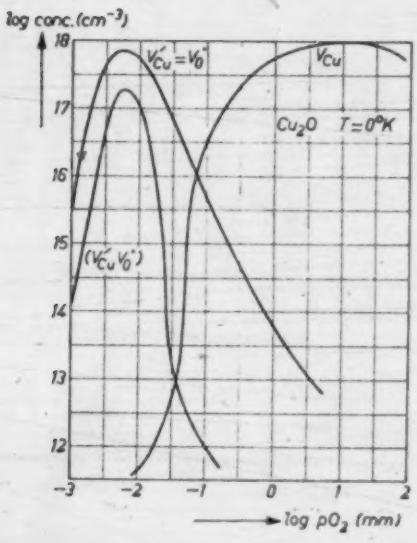


Situation after cooling with internal rearrangements taken into account (see text).

Figure 1-9 Theoretical Results of Bloem[18]

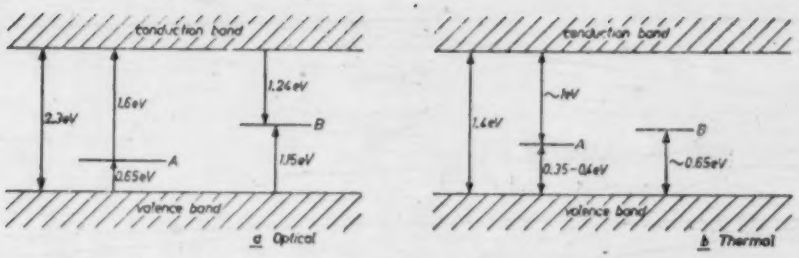


Energy-level diagram for optical and thermal transitions proposed by Garlick

Figure 1-10 The Band Scheme of Garlick[10]

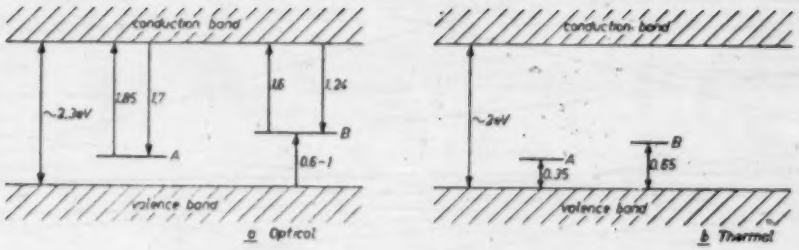


Proposed energy-level diagrams for optical and thermal transitions.

Figure 1-11 The Band Scheme as Modified by Bloem[18]

Bloem further constructs an energy level model (based on luminescence and absorption) very similar to that of Garlick (see figure 1-11). The band gap for the thermal model is adjusted however to agree with more accurate results on the static dielectric constant of $Cu_2O$.

At about this point in time research into the luminescence of $Cu_2O$ split in many directions. Luminescence generated by means other than optical excitation is reported by Frerichs and Weichman[19] (1958) who observed luminescence at 0.9 μ excited by an electron beam. This is followed by papers on ordinary electroluminescence at contact junctions by Frerichs and Handy[20] (1959), and by Frerichs and Liberman[21] (1959).

In an apparent reversal of the early conclusions of Karkhanin and Lashkarev[7] (1954) work by Vorob'ev and Karkhanin[22] (1961) and by Peka and Karkhanin[23] (1961) revealed that the presence of an electric field (generated either directly or by immersion in ionic solutions) seemed to affect the 0.96 μ photoluminescence of $Cu_2O$. This was the beginning of a long series of papers (see references 22, 23, 24, 25, 26, 27, 28, and 29).

The presence of this effect was not held to be contradictory with the exciton capture model for luminescence, the explanation being that the electric field decreases the number of neutral acceptors available as sites for decay.

One useful and interesting by-product of this research was the observation that changes in the atmosphere surrounding the sample (e.g. vacuum, moist air, or dry air) could strongly affect the luminescent output (see references 30, 31, and 32). This correlates with three arguments:

1. that slight changes in the oxygen content (stoichiometry) will affect the luminescence;

2. that additional centres are adsorbed near the surface and non-radiatively capture excitons;

3. the already mentioned field effects.

A more recent development of great interest is the 1968 discovery by Gross and Kreingol'd[33] of direct recombinational exciton luminescence. A sharp peak was observed in the vicinity of 6150 Å which corresponds to the recombination of a "yellow" series exciton in the n = 1 state. Also observed were phonon satellites of this line. This was the first observation of intrinsic luminescence in $Cu_2O$. This luminescence has since been extensively researched (see references 34, 35, 36, 37, 38, 39, 40, 41, 42, 43, 44, 45, 46, and 47). The basic consequences of this research have been:

1. The determination of the energies of the characteristic phonons of the $Cu_2O$ lattice through careful measurements of the energies of the phonon replicas of the recombinational line.

2. Some results on the temperature dependence of these lines.

3. The observation of exciton electroluminescence.

4. A new awareness of the importance of sample preparation and the development of new sample preparation techniques.

5. The possible detection of some further exciton resonances.

Recently Bairamov and Khaskhozhev[48] (1975) claim to have observed further intrinsic luminescence in the ultraviolet.

Cuprous oxide is usually prepared by the high temperature oxidation of copper. By careful adjustment of the temperature and oxygen pressure sample stoichiometry can be approximately controlled (see Bloem[18]). Unfortunately vacancies will be generated at these high temperatures and "frozen in" in cooling. Further, the high temperature transformation from copper to cuprous oxide lattices produces great strain and a large number of dislocations in the crystal. Annealing will somewhat relieve this situation and allow the growth of large crystals. The material produced will however still be rich in defects and under strain.

In their search for exciton luminescence Gross and Kreingol'd[33] employed a new technique developed by Kinoshita and Nakano[49] (1967) for chemically growing $Cu_2O$

crystals from seed at lower temperatures. The Soviet study of exciton luminescence has been made principally with these crystals. References 50, 51, and 52 discuss the effects of crystal growth techniques on luminescence. The basic result of this research is that only the new lower temperature crystals (or very carefully recrystallized high temperature crystals) will show good exciton luminescence. Further, these "good" crystals do not show, or show only weakly, the extrinsic luminescences. The decreasing extrinsic luminescence of the new crystals is of interest in that with more detailed study it could be used to evaluate the types and quantity of defects present in crystalline $Cu_2O$.

Returning however to the main stream of research on the extrinsic photoluminescence we find some new interpretations. The existence of three excitable luminescent emissions at 0.72 μ, 0.83 μ, 0.93 μ was confirmed by Gorban, Rudko, and Shishlovskii[53] (1961) who further confirmed the strong temperature dependence of the 0.7 μ luminescence which appears only at low temperatures. From the energies of the three luminescent outputs they postulated in a straightforward manner an energy level scheme (see figure 1-12). Following Karkhanin and Lashkarev[7] they maintained that exciton capture excited the luminescence at the defects, and that capture was only possible when the acceptor levels at the defect were

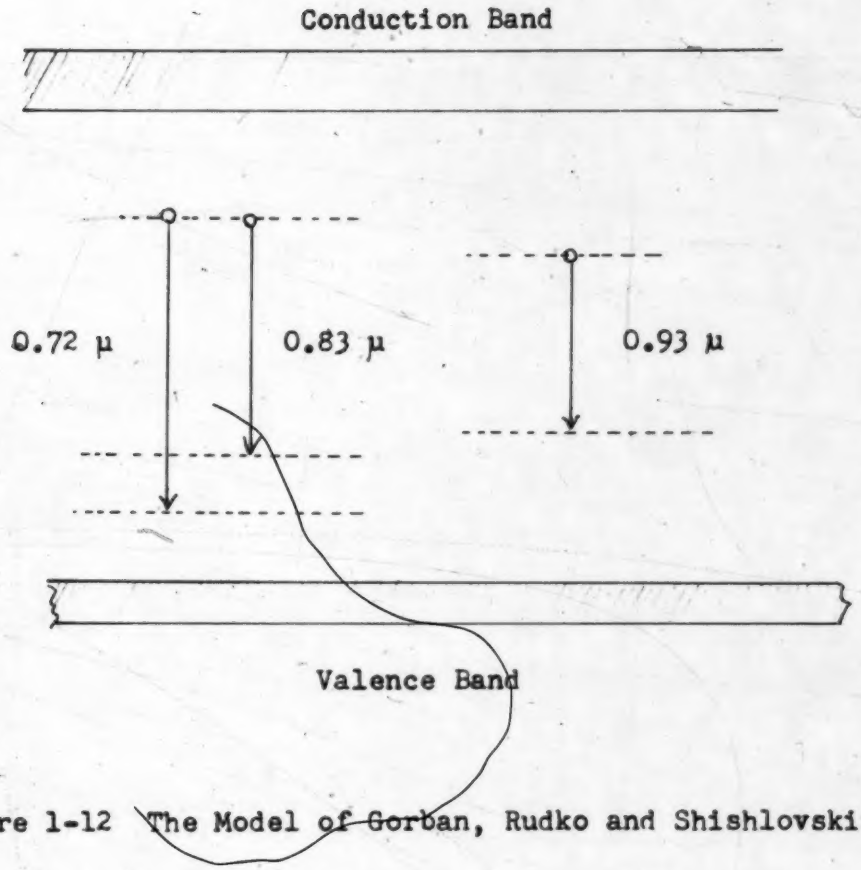


Figure 1-12 The Model of Gorban, Rudko and Shishlovskii[53]

unoccupied. This allowed a simple thermodynamic model following slightly modified Boltzman statistics and basically reproducing the formula of Gurney and Mott.

In a slightly later paper Gorban, Gritsenko, and Rudko[54] (1961) observed extra components in the time decay curve of photoconductivity in samples which display 0.7 μ and 0.8 μ luminescence. They then extend their analysis based upon their previously postulated energy scheme.

This model of excitation and luminescence is strongly challenged by Vorob'ev and Karkhanin[57] (1962) who studied the excitation spectrum of the 0.7 μ - 0.8 μ luminescences (see figure 1-13) and found in it a reflection of the luminescence output spectrum. They further report (in a slightly earlier paper Karkhanin and Vorob'ev[56] (1962)) a relaxation time for the 0.7 - 0.8 μ luminescence of about $4 \times 10^{-8}$ seconds.

Their model of intracentre excitation at defect levels is extended in a later paper (Vorob'ev and Karkhanin[58] (1963)) containing results from several new experiments. They report:

1. Some polarization (about 10%) of output for 0.60- 0.68 μ excitation of the 0.7- 0.8 μ luminescence.

2. The excitation of 0.93 μ luminescence by light in the 0.65 - 0.78 μ region (previously reported

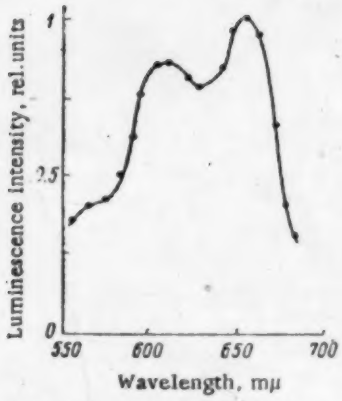


Excitation spectrum of the short-wavelength luminescence of cuprous oxide. Sample No. 1. The ordinate axis gives (in relative units) the luminescence intensity per unit energy of the incident light.

**Figure 1-13 Excitation Spectrum Observed by Karkhanin and Vorob'ev[57]**

by Garlick[10]).

3. A sharp increase in the lifetime of the 0.93 μ luminescence with excitation at wavelengths greater than 0.65 μ.

From this they conclude:

1. That the 0.7- 0.8 μ luminescence is largely the result of intracentre excitation.

2. That there are two mechanisms for the 0.93 μ luminescence, direct intracentre excitation in the long wavelength excitation region with possible exciton capture at shorter wavelength excitation.

Their model is approximately based upon the band scheme of Bloem, and accounts for the thermal quenching of the 0.72 μ luminescence by assigning to the lower acceptor level the characteristics of a hole trap. Thus with a large number of holes in the valence band at high temperatures the acceptor levels are kept empty by repeated trapping of holes and the luminescence is quenched.

The next attempt at a model is made by Gorban and Rudko[55] (1967) who combine measurements of excitation, absorption, and luminescence (see figure 1-14) to produce an elaborated energy level scheme (see figure 1-15). Excitation is assumed to be intracentre for most cases with a possible contribution to the 0.93 μ luminescence from excitonic capture in the visible region. Their

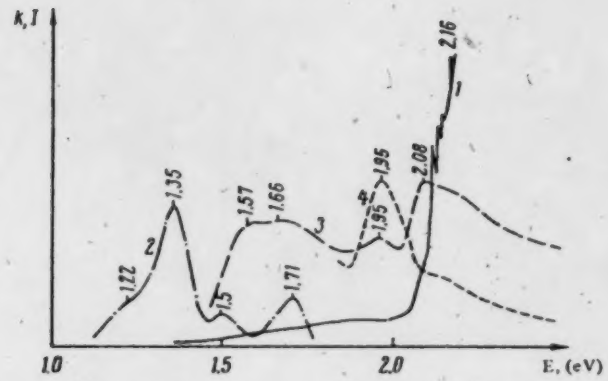


Absorption spectrum (curve 1), photoluminescence spectrum (curve 2), and excitation spectra for long-wave (curve 3) and short-wave (curve 4) photoluminescence of $Cu_2O$ crystal at 77° K.

**Figure 1-14 The Optical Data of Gorban & Rudko[55]**

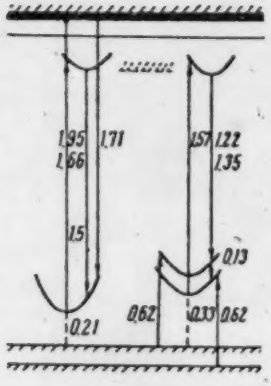


The energy levels of copper-oxide crystals.

**Figure 1-15 The Impurity Band Scheme[55]**

data are also notable in that they report evidence of an additional band at 1.01 μ. Unfortunately, their model correlates only weakly with the other properties of $Cu_2O$.

The most recent Soviet model is that of Bonch, Bruevich and Tolstoi[62,63] (1971). It is based upon some interesting new observations:

1. That the relaxation time of the 0.72 μ and the 0.83 μ luminescences are different.

2. That the output of 0.83 μ luminescence increases in the temperature range where the output of the 0.72 μ luminescence sharply drops.

3. That at high excitation intensities the output of the 0.72 μ luminescence seems to increase at the expense of the 0.83 μ luminescence (see figure 1-16).

The first observation gravely damages the model of Vorob'ev and Karkhanin[57] which makes little distinction between these luminescences. The second observation is in direct contradiction with the 1967 model of Gorban and Rudko[55] which predicts approximately the same thermodynamic behavior for the 0.72 μ and 0.83 μ luminescences.

On the basis of these new results a model is proposed for the 0.72 μ and 0.83 μ luminescences. It assumes that oxygen vacancies introduce a pair of low lying acceptor states (see figure 1-17), and that excitation of the singly ionized defect produces 0.72 μ luminescence, and excitation of the neutral defect produces 0.83 μ luminescence. Further it is assumed that

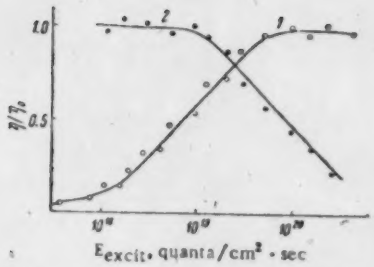


Fig. 2. Dependence of the normalized yield of (1) SL, and (2) ML on the excitation intensity. $\eta_0$ is the value of the yield corresponding to the region of linear change of intensity of the steady state luminescence with variation of E. T = 77°K, interband excitation.

**Figure 1-16 Superlinearity Observed by Bonch-Bruevich and Tolstoi[62]**

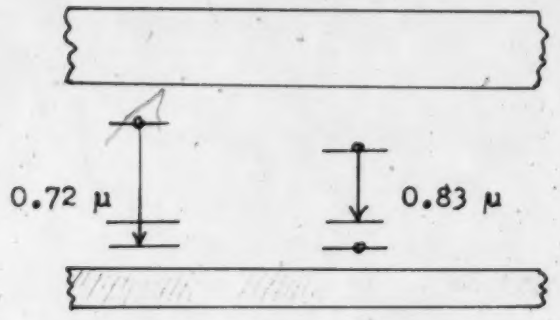


**Figure 1-17 The Model of Tolstoi and Bonch-Bruevich[62]**

decay in a neutral defect is to the upper acceptor level. Local and lattice excitation mechanisms are both allowed.

In this way at high excitation intensities in the visible, holes will be generated in the valence band and the trapping of these holes will convert the 0.83 μ centres to 0.72 μ centres. The efficiency of the 0.83 μ emission will therefore decrease, while the newly created singly ionized states will increase the efficiency of the 0.72 μ emission. Further, with increasing temperature the occupation of the upper level of the doublet will increase converting 0.72 μ centres into 0.83 μ centres thus increasing the efficiency of the 0.83 μ emission at the expense of the 0.72 μ emission.

It is interesting to note however that Tolstoi and Abramov[60] (1967) and Tolstoi, Bonch-Bruevich and Gerlovin[61] (1969) report saturation of the 0.93 μ luminescence at high excitation intensities (see figure 1-18) which appears to be similar to that of the 0.83 μ luminescence. Berkovskii and Shreter[59] (1968) further report (from studies with electron beam excitation) increases in the output of 0.72 μ luminescence at the expense of 0.93 μ luminescence at high excitation intensities (see figure 1-19).

These results, of course, weaken the Tolstoi-Bonch-Bruevich theory.

One last major contribution remains and that is the work of Taylor and Weichman[64] (1969), and Taylor, Lomnes,

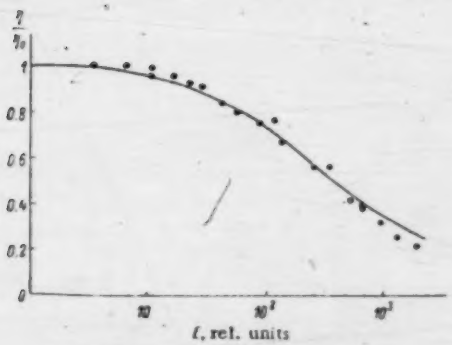


Dependence of the luminescence yield of $Cu_2O$ on the excitation intensity. $\lambda = 0.93\ \mu$, T = 300°K.

**Figure 1-18 The Saturation Data of Tolstoi and Abramov[60]**

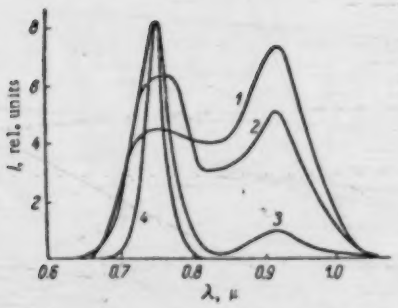


Luminescence spectra of $Cu_2O$ for various electron current densities j ($A/cm^2$): 1) 0.01; 2) 0.025; 3) 0.05; 4) 3.0. T = 80°K.

**Figure 1-19 The High Intensity Results of Berkovskii and Schreter[59]**

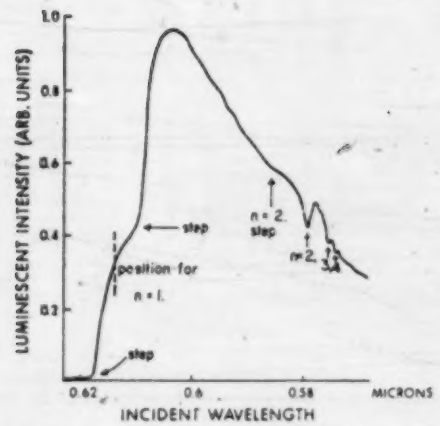


FIG. 3. Luminescence-excitation curve for a weakly luminescing sample; exciton structure is clearly visible. Temperature is 77°K.

Figure 1-20 The Excitation Spectrum of Taylor and Weichman[64]

and Weichman[65] (1971). They very carefully studied the excitation spectrum of the 0.93 μ luminescence. Although in general varying widely from sample to sample (see Taylor, Weichman, and McClung[67] (1971)) consistent excitation spectra were obtainable for "weakly luminescent samples" (i.e. samples with room temperature quantum efficiencies of less than 0.1%). Within these spectra they were able to resolve clearly the hydrogenic series of exciton lines. (An earlier attempt by Pastrnak[66] (1961) to observe these lines had negative results.) The presence of these lines indicates almost incontestably that for visible excitation exciton capture does contribute to the luminescent process. Taylor, Lomnes, and Weichman[65] were further able to show that excitons with low kinetic energies were most easily captured.

Briefly summarizing the reliable results we then have:

1. That copper vacancies (or their complexes) are responsible for the 0.93 μ luminescence.

2. That oxygen vacancies (or their complexes) are responsible for the 0.72 μ and 0.83 μ luminescences.

3. That 0.93 μ luminescence can be excited through excitonic capture.

4. That 0.93 μ luminescence can be excited through nonexcitonic means.

5. That the excitation spectra of the 0.72 μ and 0.83 μ luminescences differ from that of the 0.93 μ luminescence.

6. That under high intensity excitation the 0.72 μ luminescence is superlinear.

7. That the 0.72 μ luminescence is a low temperature phenomenon.

8. That the 0.83 μ luminescence has a peak emission at about 160 K.

9. That the 0.93 μ luminescence remains at higher temperatures than either the 0.72 μ or 0.83 μ luminescences.

Also worth noting are the inconsistencies, incompleteness, and contradictions in the results thus far. The approach to the problem has been of necessity phenomenological, and as a consequence these inconsistencies have seriously impaired the development of a satisfactory model.

Our own research (with C. Duvvury and F. Weichman) into the extrinsic luminescence was the offshoot of some studies on samples in support of a far infrared (10 μ) luminescence experiment. Unaware of the bulk of the Soviet literature we independently observed:

1. the dominance of the 0.72 μ luminescence at high excitation intensities;

2. the low temperature nature of the 0.72 μ luminescence;

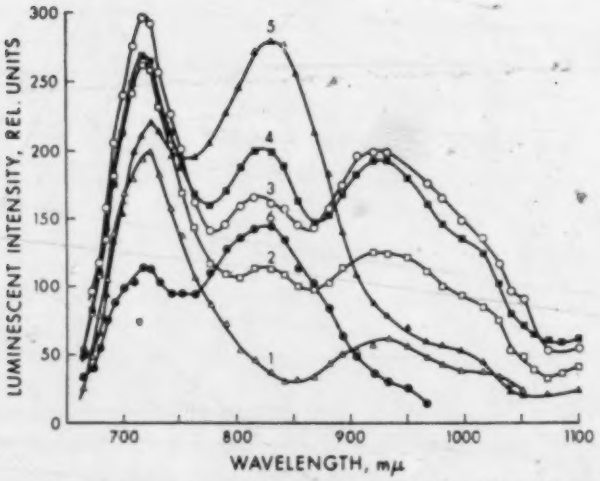


Luminescence emission spectrum of $Cu_2O$ at 193 K for various excitation wavelengths: 5320 A (curve 1), 5800 A (curve 2), 6000 A (curve 3), 6200 A (curve 4), 6350 A (curve 5), and 6420 A (curve 6).

**Figure 1-21 Excitation Characteristics Observed by Duvvury, Kenway, and Weichman[68]**

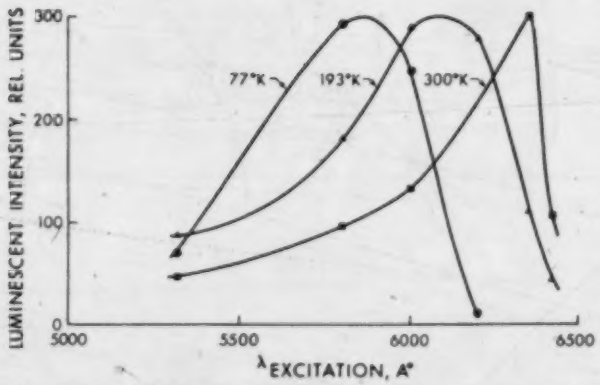


Excitation spectrum for the long-wave luminescence (0.93 μm) at 77, 193 and 300 K.

**Figure 1-22 Excitation Shift with Temperature[68]**

3. the plateau in the 0.83 μ output at 160 K;

and other details of the luminescent behavior.

In 1975 we published some preliminary results[68] on the excitation characteristics of the three luminescences. The most interesting result notable from our reported data (see figure 1-21) is the apparent difference in the dependence of the 0.83 and 0.72 μ luminescences on wavelength of excitation. This data was taken at about 193 K with a power density of about 1000 watts/$cm^2$. Also observed was an apparent change with temperature in the excitation spectrum of the 0.93 μ luminescence. (This effect is also reported by Gorban and Rudko[55].)

Further in unpublished research we have observed that the 0.83 μ luminescence seems to require about 110 μsec to reach its maximum. This is at least two orders of magnitude greater than the time required by either the 0.72 μ or the 0.93 μ luminescences. This is further two orders of magnitude greater than the time constants reported by the Soviets (who seem to have made all their measurements by indirect techniques) and cast some doubt on the accuracy of their lifetime measurements.

These early observations suggested the research of this thesis. In the hope of better resolving the relationships between the various luminescences a program of research was initiated to investigate the

excitation of the luminescence as a function of temperature and wavelength, with additional studies of lifetime and intensity relationships. As a first step an experimental apparatus incorporating the dye laser was developed for this study. It is the development of this apparatus and the preliminary results of this investigation that are reported here.

# CHAPTER 2

# EQUIPMENT

## 2.0 Introduction

Photoluminescence experiments essentially consist of three elements: a light source, the sample to be studied, and a detector.

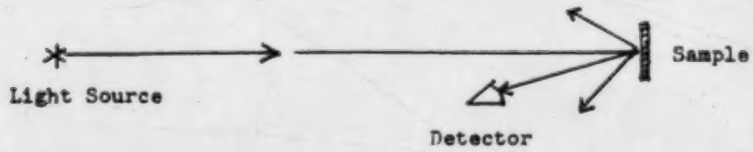


**Figure 2-1 Basic Experiment**

In our case the light source was chosen to be a tunable dye laser driven by a frequency doubled Nd:YAG laser. This source has three outstanding advantages:

1. It produces light of good spectral purity (FWHM ≈ 25Å) and variable wavelength.

2. It produces pulses of short duration (FWHM ≈ 100 ns).

3. It produces pulses of high power (≈ 300 watts).

Thus measurements of: a) luminescent output versus input wavelength, b) relaxation time of luminescence, c) luminescent output versus incident intensity, and d) luminescent output at high excitation intensities, are facilitated.

It also poses a terrific liability in that the consistency of power levels of output pulses is very poor, and in that it seems prone to breakdowns.

Most of my effort was in fact expended in attempting to remedy these problems.

The detection system used consisted of a Leiss double prism monochromator with an RCA 7102 photomultiplier monitoring the output slit. The advantages of this particular combination are:

1. The S1 response of the 7102 extends more deeply into the infrared than does that of almost any other tube available; thereby giving a broad range of sensitivity.

2. The Leiss monochromator (resolution ≈ 20Å) makes possible detailed examination of the emission spectrum.

Finally, the sample holder was constructed so that the sample temperature could easily be varied from 77K to 340K, and we could monitor with some accuracy the parameter $S(\lambda_i, I_i, T, \lambda_o)$ where

$$S(\lambda_i, I_i, T, \lambda_o) = \int_{\lambda_i - \frac{\Delta}{2}}^{\lambda_i + \frac{\Delta}{2}} \int_{I_i - \frac{\kappa}{2}}^{I_i + \frac{\kappa}{2}} \int_{T - \frac{\varepsilon}{2}}^{T + \frac{\varepsilon}{2}} \int_{\lambda_o - \frac{\delta}{2}}^{\lambda_o + \frac{\delta}{2}} L(\lambda_i, I_i, T, \lambda_o) \times d\lambda_i dI_i dT d\lambda_o$$

and hence making the usual smoothness assumptions infer $L(\lambda_i, I_i, T, \lambda_o)$.

The experiment was usually conducted at fixed $I_i$, $\lambda_i$, and $\lambda_o$, varying T; although other combinations were sometimes tried. The actual apparatus for this experiment occupied about 100 square feet of floor space and was composed of several natural subsystems and components:

1. The light source
2. The detection system
3. The temperature control and monitoring systems
4. The data acquisition and processing system.

## 2.1 The light source

The light source is the most complex of the subsystems, and is itself composed of several elements and subsystems:

1. The Nd:YAG laser
2. The dye laser
3. The dye laser power monitoring system
4. The collimation system and chopper
5. The wavelength measuring system.

### 2.1.1 The Nd:YAG laser

The Nd:YAG laser employed is a commercial product; the Chromatix model 1000. As such it is complete including power supplies, control electronics, crystal refrigeration, and laser optics. The device consists of a

flashlamp pumped Nd:YAG crystal which is mounted in a prism tuned cavity. The krypton flashlamp and the Nd:YAG rod are mounted at the two foci of a gold plated elliptical reflector, for efficient pumping. Normally the laser mirrors are angled so that the cavity is resonant at 1.064 μ (a strong line of the Nd ions in the YAG matrix). The cavity in normal operation also contains a frequency doubling $LiIO_3$ crystal which at high intensities converts a fraction of the 1.064 μ energy to energy at 0.532 μ, a front mirror which is highly reflective to 1.064 μ and highly transparent at 0.532 μ , and a rear mirror very highly reflective to 1.064 μ. The net effect is that of a coherent amplifier with positive feedback at 1.064 μ, and with output being accomplished through the doubler and the front mirror transmission at the doubled frequency.

Also present in the cavity is a quartz Q-switch which can be used to "spoil" the feedback loop. This allows a larger population inversion to be achieved in the Nd:YAG crystal. When the feedback loop is restored, the optical amplifier has higher gain, and shorter pulses of high power are produced. It is these Q-switched pulses of up to 3 kilowatts which are used to pump the dye laser.

The control of basic output power is achieved by electronic control of the energy transferred to the

flashlamp at each firing. Flashlamp discharge is initiated by a high voltage spike. The current flowing through the flashlamp builds in an arc with the discharge of the main capacitor bank through the lamp and the intervening inductors. When the bank is substantially drained ignition ceases, and the current still flowing through inductor $L_1$ charges the capacitor bank to a voltage about twice that of the DC supply. In this way energies of up to 4 joules can be transferred to the flashlamp, and the flashlamp power controlled by adjustment of the DC supply voltage.

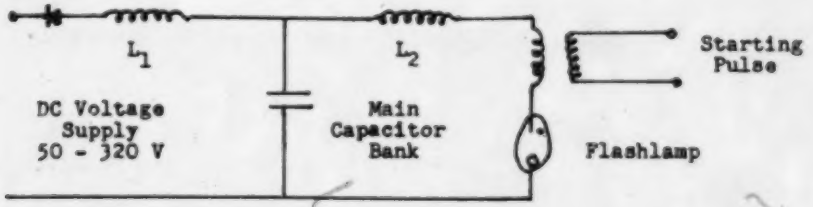


**Figure 2-2 Resonant Charging Network**

The DC supply is simply derived from the 230 volt mains, and the output level adjusted by phase control of the SCR's Q1 and Q2.

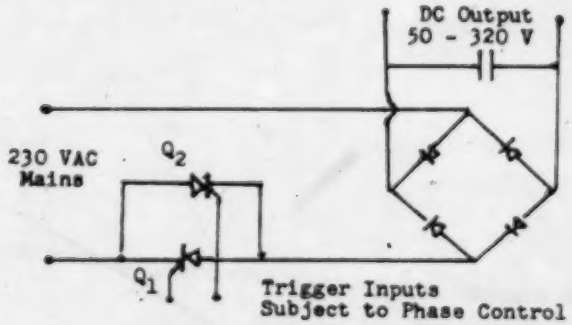


**Figure 2-3**

**DC Supply Schematic**

The Q-switch operates by scattering light off of ultrasonic compression waves travelling perpendicularly across the beam through a quartz crystal mounted in the cavity. When the scattering is present, the Q of the cavity is "spoiled"; as the ultrasonic disturbance is allowed to die out, the Q is restored. The ultrasonic vibration was generated by the application of a 25 MHz RF electric field to a $LiNbO_3$ transducer attached to the quartz crystal. By opening the Q-switch at the peak of the flashlamp discharge, maximum output power is obtained.

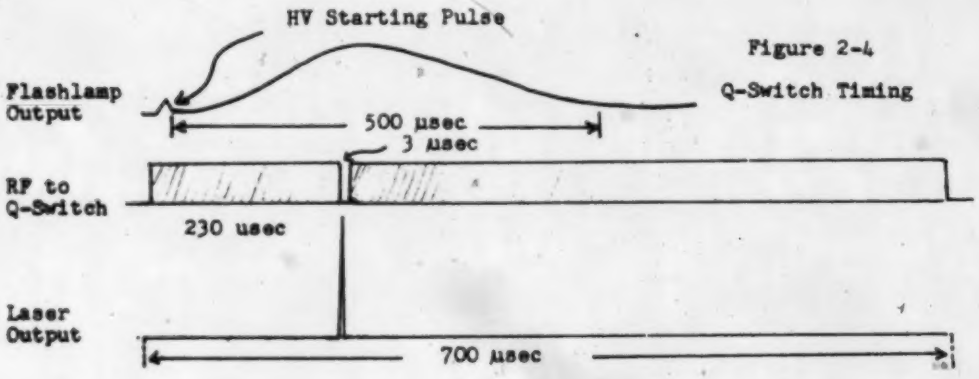


Figure 2-4
Q-Switch Timing

The Q-switch is opened by turning off the RF field for a brief interval (about 3 µs) and allowing the ultrasonics to damp out. In the Chromatix supplied circuitry, Q-switch timing was controlled by RC adjustment of a relaxation oscillator.

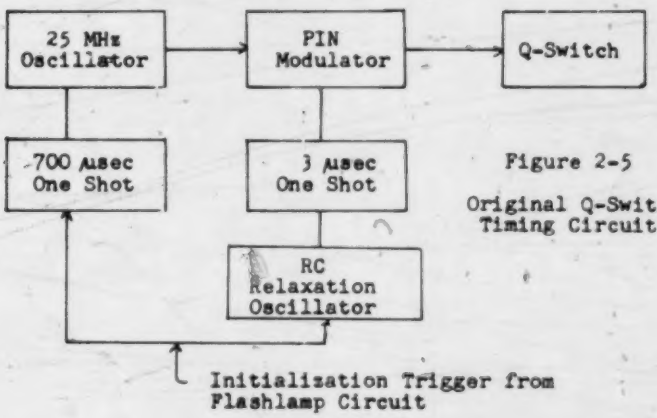


Figure 2-5

Original Q-Switch Timing Circuit

The output pulses produced by this system were highly erratic in amplitude (dynamic range ≈ 10 at fixed power settings), and in timing relative to the flashlamp trigger ($\Delta t/t \approx 0.05$). The amplitude variations were initially attributed to the timing instability of the Q-switch release. As a consequence timing circuitry employing a crystal quartz oscillator was developed and installed.

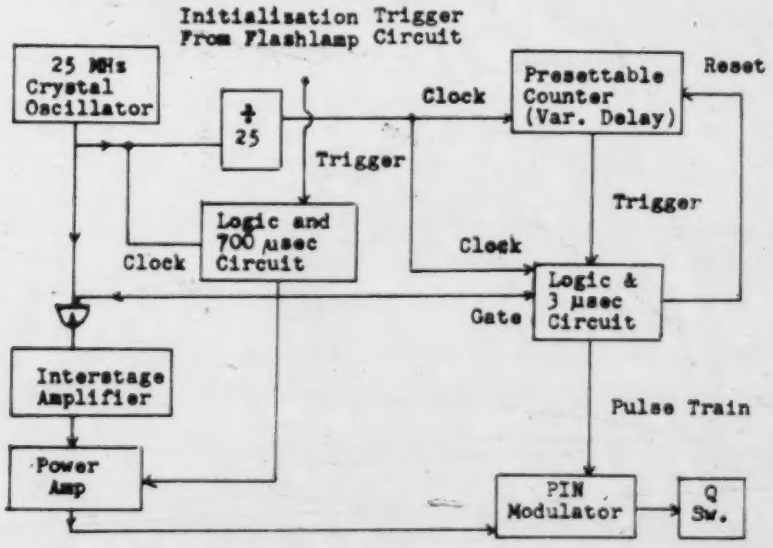


Figure 2-6 Quartz Stabilized Q-Switch Timing Circuit

This modification reduced the timing jitter in the electronic gating of the Q-switch to the order of 5 ns. Unfortunately amplitude jitter in the output pulses remained large with intensity variation of greater than a factor of 2 at fixed power settings. Surprisingly, jitter sometimes seemed to remain in the optical output. In fact by varying power settings a shift of more than 1 μsec was obtainable (obviously far greater than any remaining electronic effect) in the time between the flashlamp trigger and the output pulse. Looking at the oscilloscope trace shown in figure 2-7

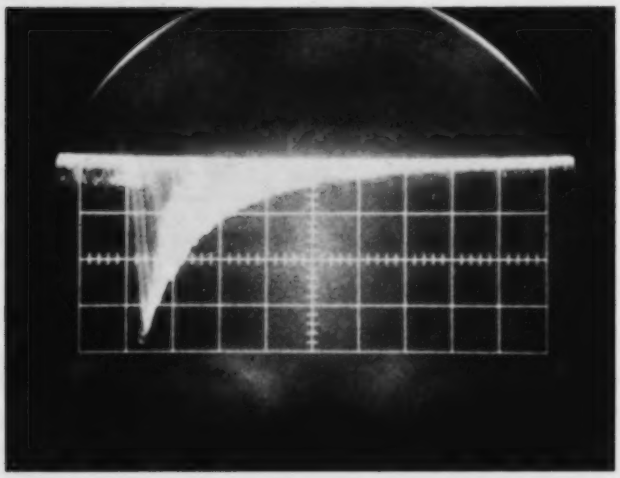

Oscilloscope triggered by Q switch electronics
Horizontal:
0.2 μsec/div.
Vertical:
0.5 V/div.

Figure 2-7. Laser Output

a strong correlation between output amplitude and timing is evident. This is quite understandable considering the effect of the varying flashlamp power levels. At high levels greater population inversion and hence

optical gain are achieved in the Nd:YAG crystal; because of the higher gain, the laser will oscillate with a lower cavity Q. When the RF is turned off and the ultrasonics in the quartz crystal damp out (presumably in a quasi-exponential manner), the Q of the cavity increases monotonically with time. Since lower Q is required at higher population inversions, the high power pulses will appear at an earlier stage of the ultrasonic damping.

What is most alarming however, is that considerable time and amplitude jitter remain at fixed power settings - implying irregularity in the flashlamp output.

This indeed seems to be the crux of the problem. The flashlamp discharge is an arc process and therefore highly unstable and irregular, the path and resistance of the arc being largely determined by the random distribution of ions at the time of the initial spike. Here two things are immediately evident:

1. that the total amount of light from the flashlamp may vary significantly from pulse to pulse;

2. that the spatial distribution of flashlamp output may vary from pulse to pulse, and thus alter the effective gain of the crystal.

This problem of irregularity in flashlamp output is further compounded when one considers fluctuations in the flashlamp power supply. Firstly, the amount of charge transferred to the main capacitor bank through

resonant charging is highly dependent upon both the arc resistance and extinction time. Since these quantities are prone to fluctuation, there will always remain pulse to pulse fluctuations in the energy stored in the main capacitor bank. The second power supply difficulty is more subtle; it arises from the fact that the laser pulses are asynchronous with the 60 Hz mains. As was shown in figure 2-3, the DC supply for the lamps is almost directly tied to the AC mains. The DC power level is maintained by phase control of an SCR pair. This phase control is regulated by a moderately complex feedback loop. Since the design is virtually that of a very low frequency switching regulator, it is clear that recovery ability will depend greatly on loading timing: e.g. the DC supply cannot replenish itself during a zero crossing of the AC line voltage. This problem is aggravated by the fact that the flashlamp power depends upon the square of twice the DC supply voltage; so that small changes in $V_{DC}$ are amplified in effect.

To date, the only successful solution to the amplitude variation problem has been to monitor and discriminate output pulses individually. Many other steps might be tried including:

1. Monitoring the optical output level of the flashlamp, and controlling the Q-switch release by flashlamp thresholds.

2. Running the laser in a Q-switched CW mode.

3. Substantial reworking of the flashlamp firing electronics, so that the lamp idles with a continuous trickle of discharge.

4. Synchronizing the flashlamp discharge with the 60 Hz mains for more stable power supply operation.

### 2.1.2 The dye laser

The output of the frequency doubled Nd:YAG laser is highly limited with respect to variability of wavelength; despite the fact that Neodymium has several laser active levels, retuning is awkward, and at best yields a half-dozen or so discrete output wavelengths. By coupling the output of the Nd:YAG into a tunable dye laser, a continuous choice of output wavelengths covering a large portion of the visible spectrum is available with relatively little difficulty. It was for this reason that we used the dye Rhodamine B (or the dye Rhodamine 6G), lasing in a prism tuned hemispherical resonator, for our output stage.

A laser of course consists of a coherent amplifier operating through the mechanism of stimulated emission, and a positive feedback loop. The term dye laser is usually used to designate a laser which uses an organic dye as its active medium. For various technical reasons, it was not until 1966 that coherent amplification was

actually achieved with an organic dye.

The energy schemes of organic dyes differ considerably from those of the elemental ions which were responsible for the early successes in coherent amplification. The energy spectrum of an elemental ion suitable for laser use usually consisted of a series of discrete lines arranged in an appropriate three or four level scheme. Stimulated emission requires a large

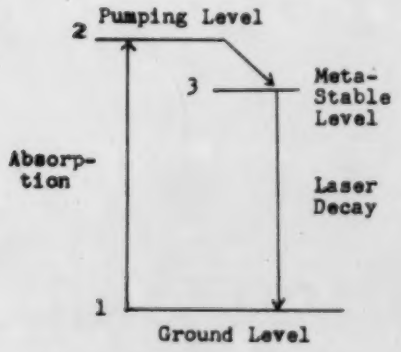


Figure 2-8
Three Level Scheme

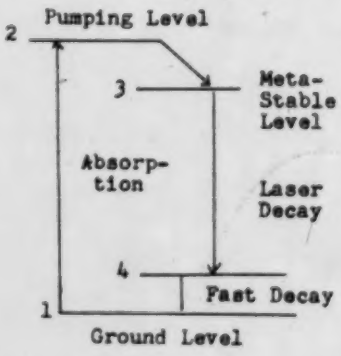


Figure 2-9
Four Level Scheme

population inversion for any significant effect, and hence the first requisite of any energy scheme is a metastable level above the ground state in which electrons may accumulate. With elemental ions this is often a triplet state. Pumping directly to this level would be highly inefficient, since any pumping would be essentially restricted to the blackbody equilibrium with the incident radiation by the combined

effects of absorption and stimulated emission; hence a third and higher pumping level which rapidly empties into the metastable level is required. A four level scheme has the additional advantage of a very sparsely filled lower level in the laser decay.

The principal difference with organic dyes is the large molecular system. Electrons are shared over large parts of the molecule, and their energy spectra display a great number of vibrational and rotational levels. Due to thermal smearing at room temperature, the net effect is that of broad energy bands.

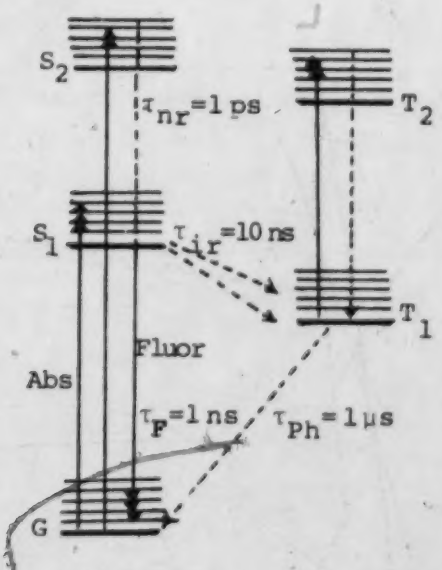


Figure 2-10 Dye Laser Energy Bands

A typical energy scheme is shown in figure 2-10. Triplet levels are usually found just beneath the excited singlet states. Initially the position of the triplet

would suggest a conventional three level scheme, except that non-radiative competing processes usually completely dominate the triplet to ground state decay. In fact, the presence of the triplet states creates difficulties. Over long time periods ($\geq$ 100 ns) singlet to triplet decay will:

1. reduce the number of available electrons in the singlet ground state system;

2. drastically increase triplet - triplet absorption ($T_1 - T_2$) which frequently is in the same band as the lasing singlet - ground decay.

As a consequence, excitation is usually to the top of the $S_1$ band (or to the $S_2$ band), and the fluorescent decay from the bottom of the $S_1$ band to any of the levels in the ground state band provides the coherent amplification. Since this fluorescent decay usually has a relatively short time constant ($\approx$ 1 ns), two things are evident:

1. Fast excitation is favored for efficient extraction of energy. Otherwise, spontaneous emission will dissipate significant amounts of energy before a lasing threshold is reached.

2. The system will have high gain, since the Einstein coefficient for spontaneous emission A is given by $A = T/_{fl}$, and the stimulated emission coefficient B is directly proportion to A ($B = \frac{c^3}{8\pi} \frac{A}{h\nu^3}$).

Since speed is favored to avoid both spontaneous and triplet losses, and significant energies are required to achieve population inversion, the obvious pumping source is a fast pulsed laser operating at an appropriate wavelength. Both Rhodamine 6G and Rhodamine B show absorption maxima in the vicinity of 0.532 μ, so that they are very efficiently pumped by the frequency doubled Nd:YAG.

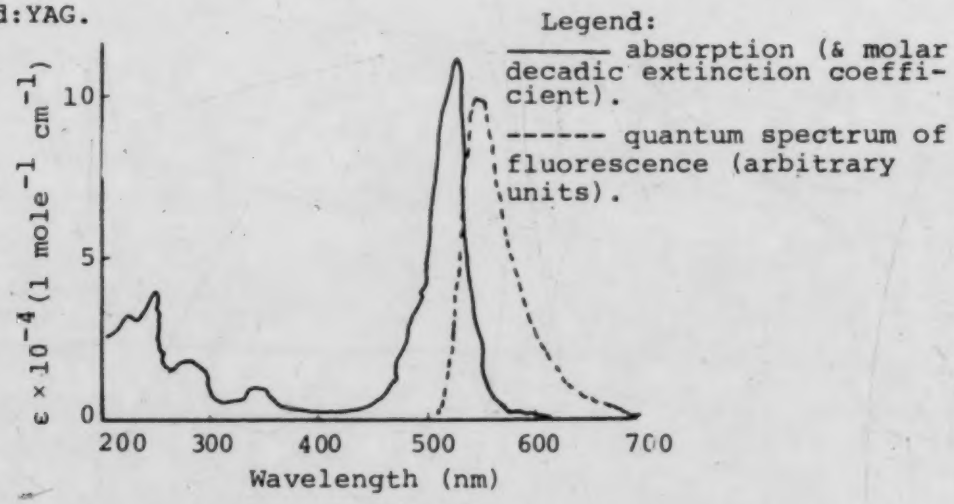


Figure 2-11 Absorption and Fluorescence of Rhodamine 6G in Ethanol.

As the high absorption coefficients of crystalline dye would not allow a cavity length greater than a few microns, it is very practical to dilute the dyes in a transparent solvent. To this end the actual dyes used frequently consist of the organic dye group with an alkali metal or halogen ion attached. This gives good solubility in polar compounds such as water or ethanol. An auxiliary problem is that the dyes often show a tendency to polymerize, or at least to dimerize

in such a solvent. In particular Rhodamine 6G and Rhodamine B dimerize in water. Since the additional levels of the dimer system poison the lasing action, this is to be avoided. The dimerization may be eliminated by the addition of a detergent to the dye solution. The detergent will disperse and form micelles in the solvent to which dye molecules will attach themselves, one dye molecule to the micelle. It is only through this technique that we may use aqueous solvents for the Rhodamine dyes.

There are many benefits consequent to the use of a liquid as the active medium:

1. Flow may be introduced to provide cooling.

2. Molecular damage at high intensities is of little consequence in a flowing medium.

3. High quality optical surfaces may be easily provided through an interface with relatively inexpensive windows of quartz or sapphire.

4. Dyes may be easily replaced, or changed, through a simple flushing procedure.

The dye circulation system used in our configuration is shown in figure 2-12.

The optical pumping of the dye by the laser may be achieved in many configurations, but direct longitudinal pumping is one of the simplest, and the one we employ.

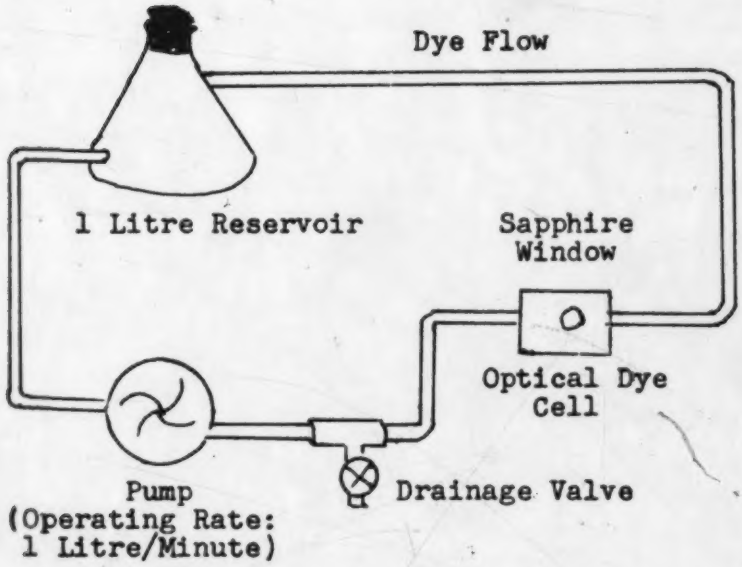


Figure 2-12 Dye Circulation System

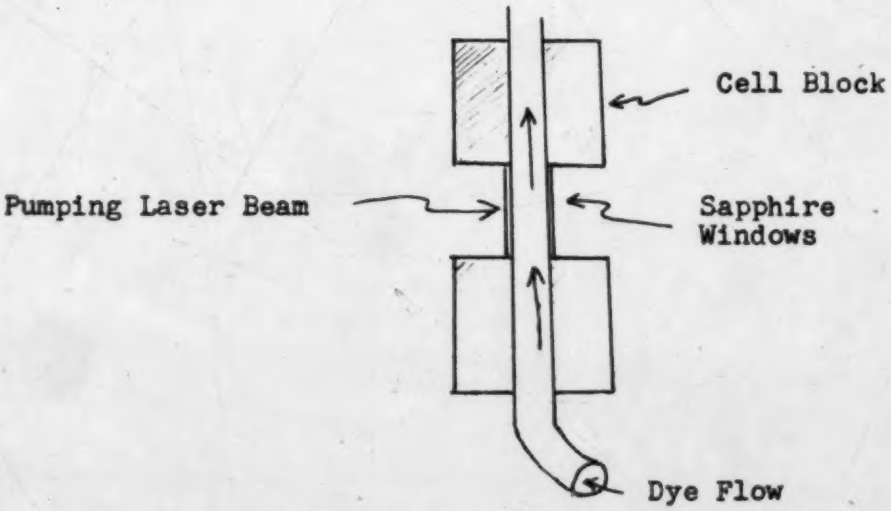


Figure 2-13 Optical Pumping Configuration

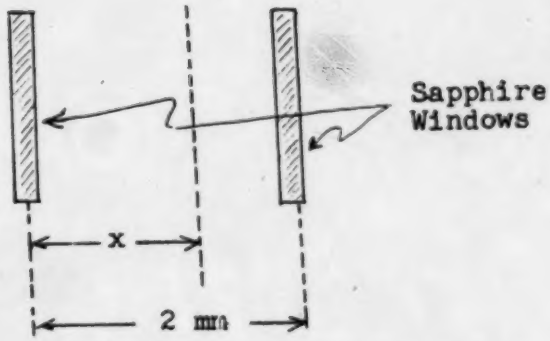


**Figure 2-14 Detail of Dye Absorption**

Considering the incident beam, we have that the intensity remaining after passing distance x into the dye is given by:

$$I(x) = I_o e^{-\alpha x}$$

where $\alpha$ the absorption coefficient in $cm^{-1}$ is given by

$$\alpha = \varepsilon M$$

where $\varepsilon$ is the molar absorption coefficient of the dye in solution in units of $cm^{-1} \cdot litre \cdot mol^{-1}$, and M is the molar concentration of the solution in moles/litre. It is usually most efficient to choose the molar concentration and cell length so that 95 - 99% of the intensity of the pumping beam is absorbed. This choice effectively distributes the incident energy throughout the available volume of dye, and at the same time does not waste the incident beam.

Experiment has verified that solutions of about $4 \times 10^{-4}$ moles/litre of Rhodamine 6G (molecular weight

479), or of $5 \times 10^{-4}$ moles/litre of Rhodamine B (molecular weight 479) were about optimum for our dye cell. The solvent was by volume 95 % deionized water, and 5 % Triton X100, a deaggregating agent (detergent). This is a conservative solvent mix, since experiment seemed to indicate that a 2 % by volume solution of Triton X100 is sufficient to prevent dimerization at such low dye concentrations.

Merely adding reflectivity to the surfaces of the dye cell will produce a laser, and at high excitation intensities the gain of the dye is so high that the reflection at the dielectric boundaries of the cell windows is sufficient to produce laser action. This emission is a nuisance since its wavelength is tuned only by the natural efficiency of the dye. Further it empties electrons from the $S_1$ band, and thus reduces the gain and power available to any mechanically tunable feedback loop. Natural limits to the gain, and hence the power density of the pumping beam, are therefore established; and the Nd:YAG laser is focused only up to the limiting power density.

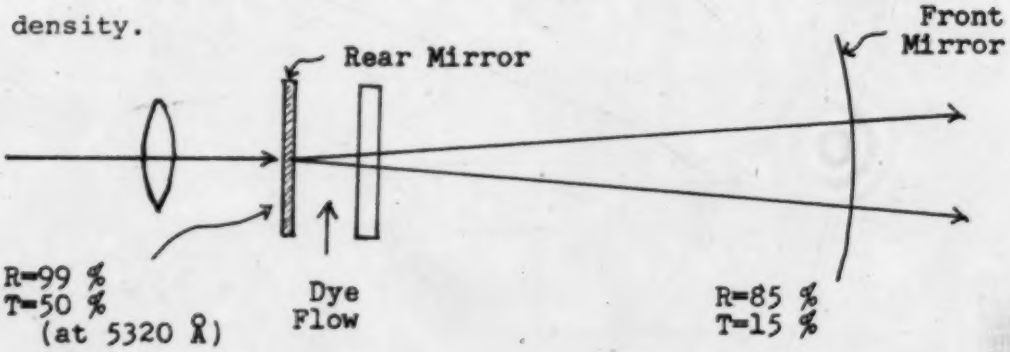


Figure 2-15 Hemispherical Cavity

The main feedback cavity, without the prism tuning elements, would form a simple hemispherical resonator. The advantages of this system are many:

1. A focusing element in the cavity reduces losses due to diffraction and scattering.

2. The hemispherical cavity has a sharp focus at the surface of the flat mirror, which then becomes a convenient entry point for the focused pumping beam. A small volume of optically pumped dye is desirable, since the pumped region must be excited by a high power density of radiation to achieve inversion, and hence to some extent it follows that the smaller the pumped volume, the smaller the power required to achieve high gain, and laser action. The sharp focus at the flat mirror of the hemispherical cavity thus provides a very convenient point for the pumping radiation to enter the dye.

There is also a specific disadvantage to the configuration as drawn: the pumping radiation must pass through the rear mirror. This adds to the cost of the rear mirror, detracts from the quality, and dissipates the energy of the pumping beam, and tends to cause burn holes in the rear mirror. As a consequence we use a slightly less precisely focused system which brings the pumping beam into the dye cell at a low angle from the cavity side.

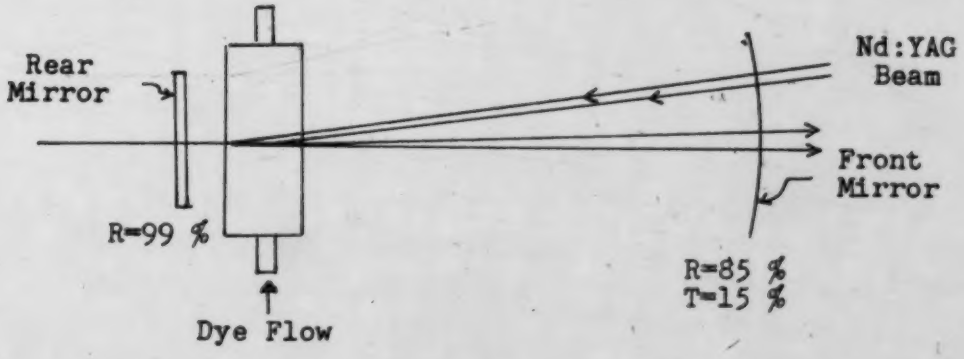


Figure 2-16 Improved Dye Laser Configuration

The reflectivity of the simple cavity is about 0.84 between 5600 Å and 6300 Å with our current mirrors. Additional mirrors covering the ranges 5200 - 5600 Å, and 5900 - 6600 Å have been purchased, but not yet tried.

The most important feature of the dye laser is not apparent until tuning elements are added to the feedback loop. This, of course, is the continuous variability of output wavelength; a direct consequence of the broad band structure of the energy levels.

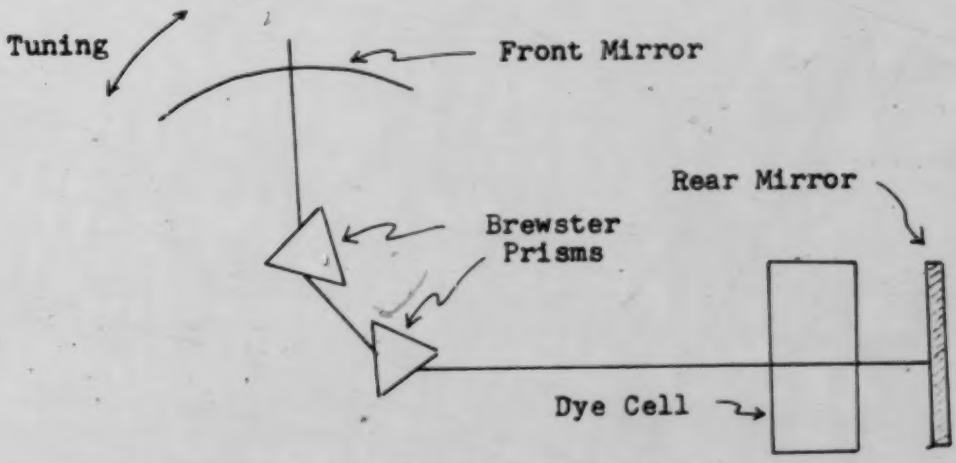


Figure 2-17 Prism Tuned Cavity

In our case wavelength tuning is achieved through the angular dispersion of two prisms placed in the feedback loop. (Actual selection is mechanically achieved by varying the angular orientation of the front mirror.) The prisms are chosen so that the incident radiation enters and exits at approximately Brewster's angle. Virtually 100 % transmission of horizontally electrically polarized light is achieved in this configuration, while significant reflection occurs for vertically polarized light, so that the insertion of the prisms also polarizes the laser. In fact using the formulae:

$$R_v = R_\perp = \left[\frac{(n_1/n_2)\cos\theta_i - \cos\theta_t}{(n_1/n_2)\cos\theta_i + \cos\theta_t}\right]^2$$

$$T_v = T_\perp = \frac{4(n_1/n_2)\cos\theta_i \cos\theta_t}{((n_1/n_2)\cos\theta_i + \cos\theta_t)^2}$$

$$R_h = R_{||} = \left[\frac{-\cos\theta_i + (n_1/n_2)\cos\theta_t}{\cos\theta_i + (n_1/n_2)\cos\theta_t}\right]^2$$

$$T_h = T_{||} = \frac{4(n_1/n_2)\cos\theta_i \cos\theta_t}{(\cos\theta_i + (n_1/n_2)\cos\theta_t)^2}$$

$\theta_i + \theta_t = \pi/2$ Brewster's condition

and $\dfrac{\sin\theta_t}{\sin\theta_i} = \dfrac{n_1}{n_2}$ Snell's law;

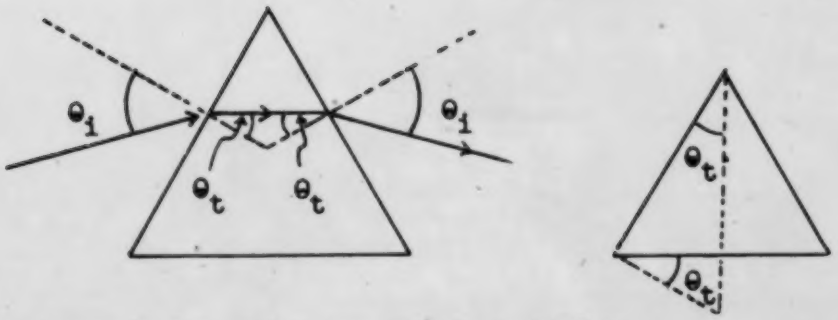


**Figure 2-18 Brewster Prism & Angles**

and the information that the prisms are made of fused quartz, and are approximately cut and mounted so that all radiation enters and exits at Brewster's angle, one finds:

1. The index of refraction of fused quartz at $\lambda$ = 5800 Å, is approximately 1.4588;

2. The dispersion of fused quartz in the region of $\lambda$ = 5800 Å is approximately $3.7 \times 10^{-2}\ \mu^{-1}$;

3. The index of refraction of air at 5800 Å is about 1.00028;

4. $\theta_{\text{incidence from air}} = \theta_{\text{Brewster}} = 55°34'$;

5. The angle of the apex of the Brewster prisms (which is twice $\theta_{\text{transmitted}}$) is 68°53';

6. The transmission coefficient for vertically polarized light is approximately 0.8701 per interface (reflection coefficient 0.1299).

Since there is an equal reflection loss at each of the four interfaces, the total prism transmission is

$(0.8701)^4 = 0.5732$. This gives a cavity reflectivity of 0.4823 for vertically polarized light, compared with 0.8415 for horizontally polarized light. Further calculations show that a 5° misalignment of the angle of incidence produces a reduction of less than 0.01 (i.e. less than 1 %) in the transmission of horizontally polarized light; so that, the angular orientation and apex angles of the prisms are not very critical.

Considering the dielectric interfaces in the dye cell, reflectivities may be calculated. Since the beam

| Dye | Sapphire | Air |
|---|---|---|
| $n \approx 1.33$ | $n = 1.769$ | $n = 1.000$ |

Figure 2-19. Interfaces at Dye Cell Window

at these interfaces passes through approximately perpendicularly, the formulae simplify to:

$$R = \left[\frac{1 - (n_1/n_2)}{1 + (n_1/n_2)}\right]^2$$

$$T = \frac{4(n_1/n_2)}{(1 + (n_1/n_2))^2} \quad .$$

In the region of 5800 Å we have:

1. The index of refraction of sapphire ($Al_2O_3$) is approximately 1.7687;

2. The index of refraction of air is approximately 1.00028;

3. The index of refraction of the dye solution is unknown, but assuming it is close to that of water, it would be approximately 1.33;

so that the reflectivity is 0.077 at the sapphire air interface, and 0.020 at the dye sapphire interface. The significance of this is that some estimates of the single pass gain of the dye cell may now be made. If the rear mirror is aligned parallel to the sapphire window the resulting resonator has a reflectivity of

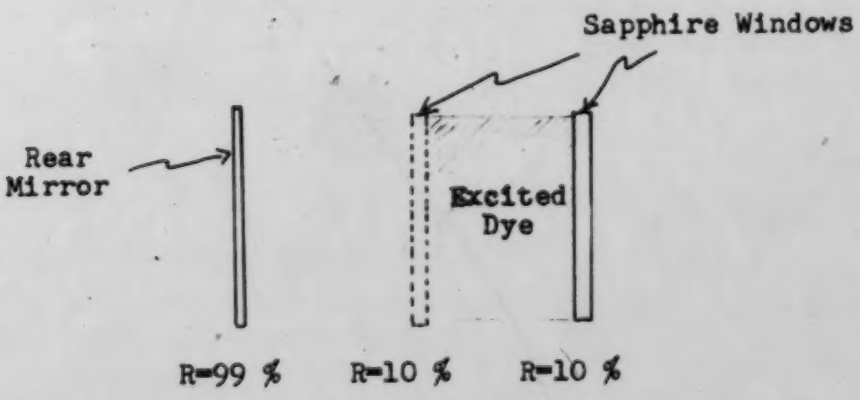


Figure 2-20 Dye Cell Resonator

nearly 0.1. (In normal operation the rear mirror and the dye cell are deliberately misaligned by a small amount to avoid this.) Since, as mentioned earlier, the emission from the dye cell resonator can become a nuisance at high excitation intensities, we may

conclude that under these conditions the single pass gain of the dye must exceed 10 (the reciprocal of the reflectivity). From the simplest considerations we know the gain must be greater than $1.19 = 1/R_{cavity}$, for the laser to function at all at any operating wavelength.

The spectral purity of the output will depend strongly on two things: the dispersion of the prisms; and the solid angle presented by the excited volume of of dye accessible to the resonator. In our case the size and shape of this volume are adjusted by the positioning of a lens which varies the focusing of the

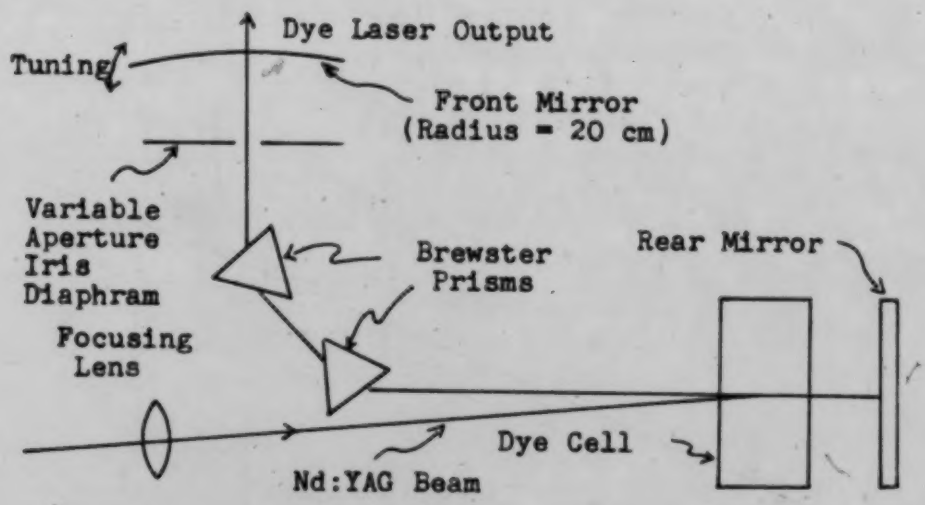


Figure 2-21 Actual Dye Laser Optics

Nd:YAG beam as it enters the dye. Normally the lens is set so that the spectral half width of the output is 20 - 30 Å. This usually occurs when the point of

best focus is just a few centimeters outside of the cell. Any further defocusing reduces the wavelength resolution, and sharper focusing drives the gain of the cell too high. To stabilize the spectral half width, and eliminate unwanted resonances, a variable aperture iris diaphram was also included in the cavity. Output can be easily achieved over the entire range of 5600 Å to 6330 Å with the current mirrors and either dye solution. Rhodamine 6G is favored however in the range to 6200 Å, and Rhodamine B beyond.

The power level of the output depends primarily upon three factors:

1. the power level of the pumping laser;

2. the efficiency of the laser dye at the chosen output wavelength;

3. the efficiency of the resonator at the chosen output wavelength. This last factor can cause unexpected problems, as interferometric losses will occur if the resonator is improperly tuned. With our apparatus efficiencies of about 10 % have been achieved under favorable conditions.

Considering the timing of the output pulse, the dye laser output follows the excitation pulse closely once threshold is attained. This is due to the short lifetime of the metastable level (about 1 ns), and the resonator transit time of less than 1 ns. As a result

the dye laser output pulse is only slightly shorter than the Nd:YAG output pulse, and averages 100 - 125 ns.

The divergence and size of the beam are dependent upon a large number of complex factors, of which the main concerns are the details of focusing within the cavity, and the extent to which the cavity will support true $TEM_{00}$ standing waves. Since the divergence was of little importance to us it was never accurately measured; however, it seems to be of the order of 10 milliradians.

In summary, the dye laser produces pulses of about 100 ns duration, 25 Å spectral halfwidth, and up to 300 watts of power; and is continuously tunable between 5600 Å and 6330 Å. Most important, it is relatively simple to operate and tune.

### 2.1.3 The dye laser power monitoring system

One of the greatest difficulties preventing simple and rapid accumulation of data has been the pulse to pulse variation in output power of both the Nd:YAG and dye lasers. In our earliest photoluminescence experiments with the Nd:YAG laser (before the implementation of the dye laser), no attempts were made to monitor the pulse to pulse laser power output. It was naively hoped that reproducible and relatively constant power levels could be maintained and repeated merely by monitoring the

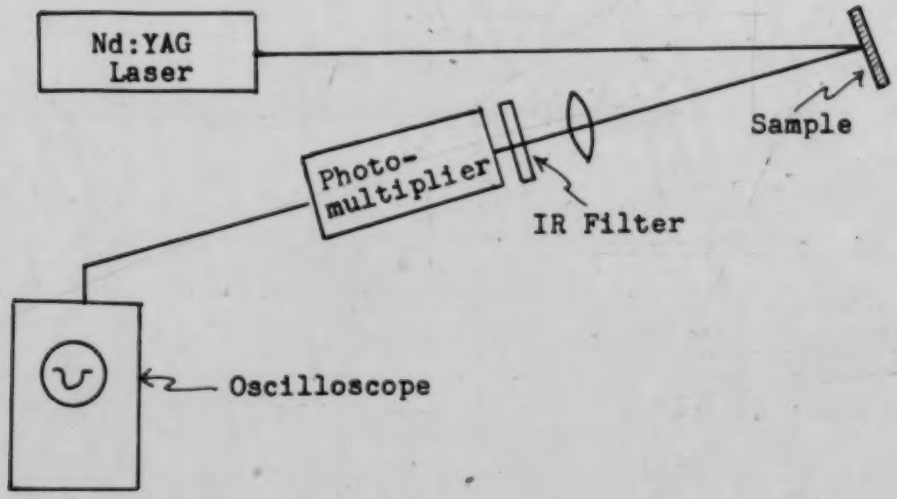


Figure 2-22 Naive Photoluminescence Experiment

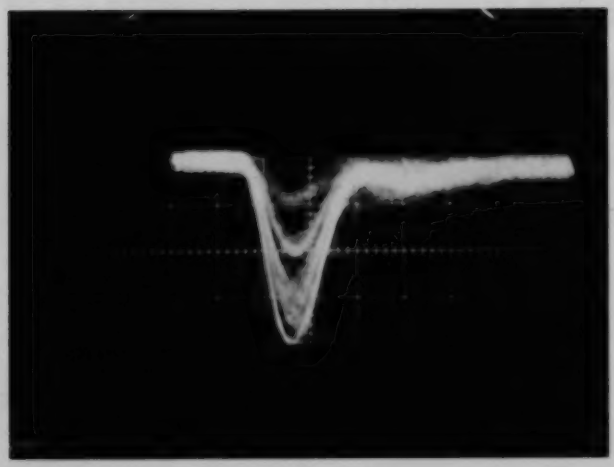

Figure 2-23
Vertical 5 mV/div
Horizontal 0.1
μsec/div.

Luminescence Signal through Corning 7-57 Filter

voltage indicated on the flashlamp power meter. A typical result from this period is shown in figure 2.23. It was not long before the futility of this approach became evident.

The Nd:YAG laser is equipped with a fast internal power level monitor. It consists of a PIN diode which detects radiation scattered by the $LiIO_3$ doubler crystal. This optical coupling suffers from the defect of long term drift, as the coupling efficiency will vary from

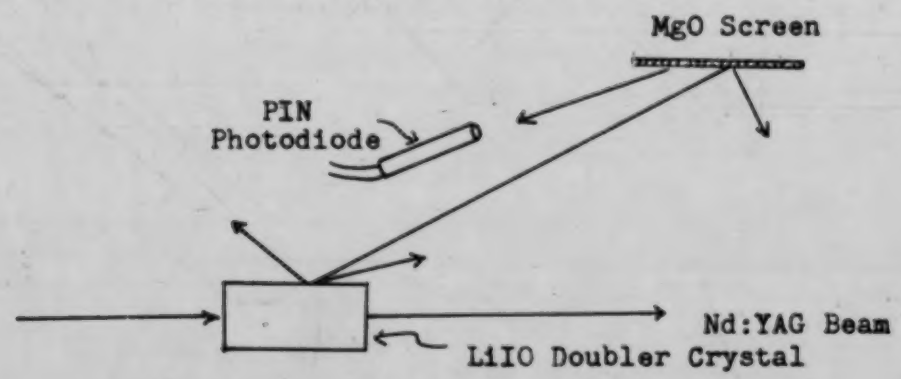


**Figure 2-24 Internal Photodiode Optics**

month to month with slight changes in the alignment of the doubler crystal. Electrically the diode is connected in a simple voltage divider, so that to a first approximation, the output voltage is proportional to the

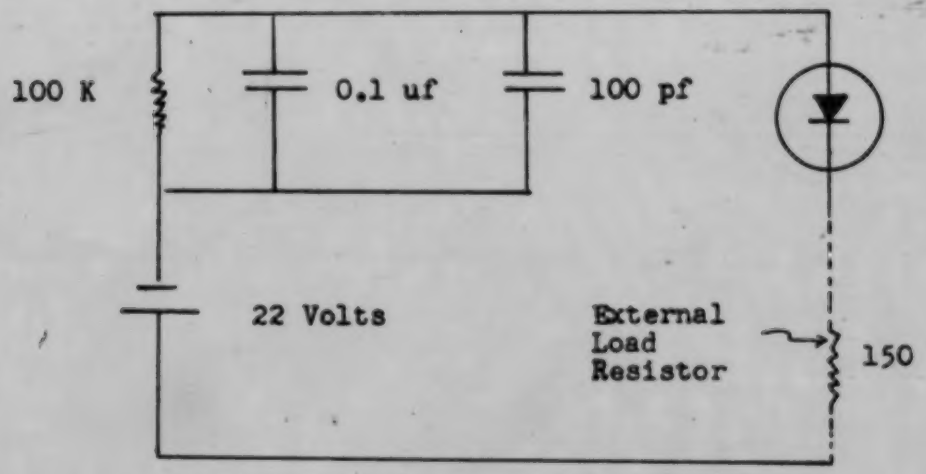


**Figure 2-25 Internal Photodiode Circuit**

incident intensity. Since the PIN photodiode is a very fast detector (rise time < 1 ns) and the circuitry is relatively simple, the fast rise time is preserved, and this detector can easily resolve the amplitude and width of the laser output pulses. Monitoring the output of the internal photodiode on a suitably terminated fast oscilloscope, the wide variation of laser output was verified.

For a short while measurements were made with one oscilloscope by first monitoring the power level with the internal photodiode, and recording the maximum value attained; then quickly measuring the luminescent output and recording the maximum it attained. Unfortunately laser instability makes the process accurate only to about 15 %. Further the maximum of many peak values must be quickly determined and measured from an unstable

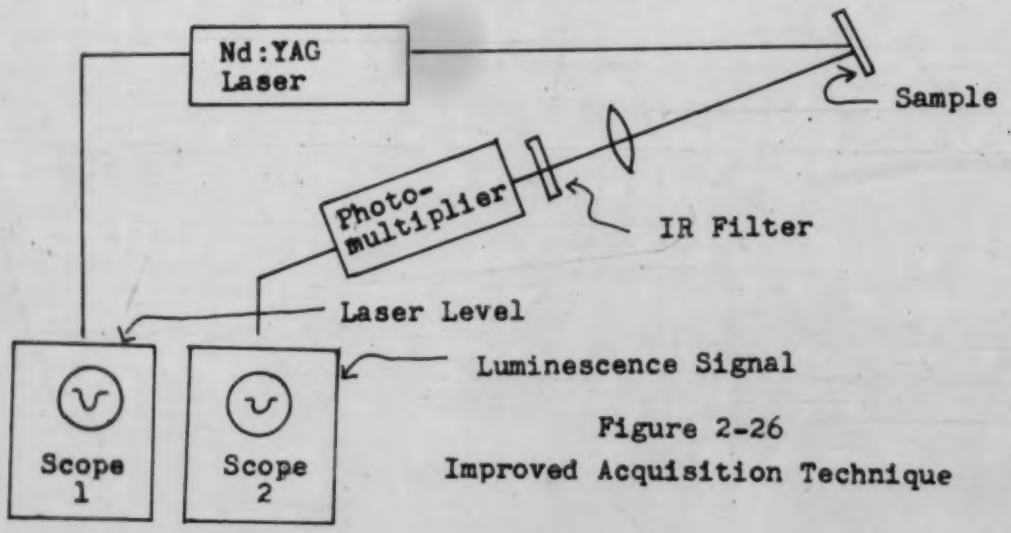


Figure 2-26
Improved Acquisition Technique

oscilloscope trace in real time. This is a difficult and fatiguing task prone to subjective error, and at best yields data of relatively low precision at a low rate.

With the hope of improvement, the complexity of the apparatus was increased. By using two high speed oscilloscopes (Tektronix 541's with type L vertical amplifiers) equipped with Polaroid cameras individual events could be monitored, and the laser and luminescent outputs simultaneously recorded for accurate measurement. To conserve film, two events were recorded on each plate. Typical data acquired are shown in figure 2-26.

Although superior with a reliable basic measurement accuracy of about 4 %, this technique still suffers from many shortcomings. It is a slow data gathering technique, yielding only two data points per pair of photographs. Since the luminescence signal may have a small signal to noise ratio (as small as 0.5), statistical treatment of data is highly favoured. Acquiring any amount of statistical data would be both very slow, and quite expensive in terms of film. Further, since the laser output pulses are of fairly random height at any fixed power setting, obtaining data closely correlated to any specified laser power level would produce a large number of wasted photographs.

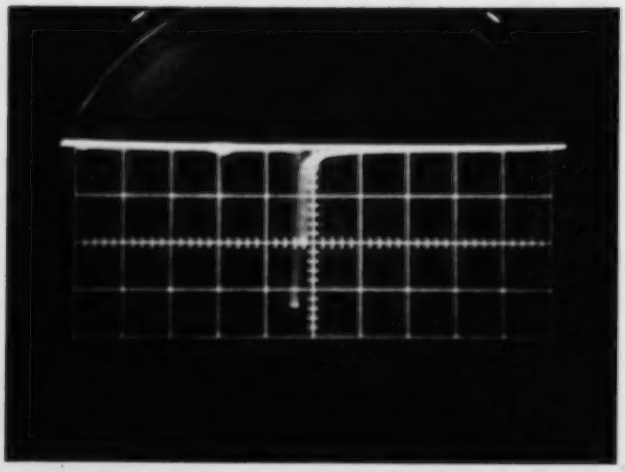

Vertical
0.1 v/div

Horizontal
1 sec/div

Internal Photodiode Output

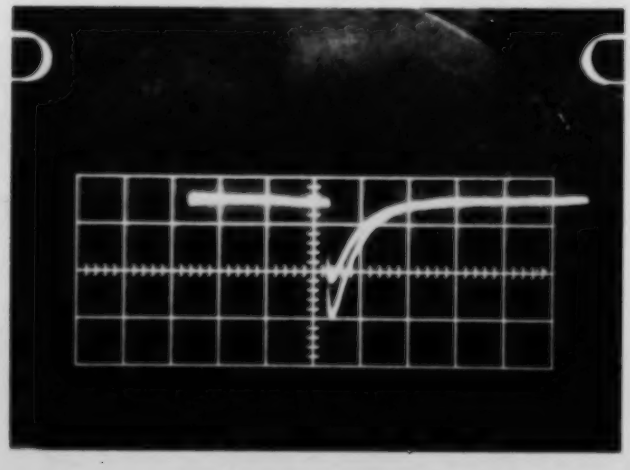

Vertical
0.5 v/div

Horizontal
0.1 msec/div

Luminescence Signal

Figure 2-27 Typical Data Photograph Pair

Bearing in mind the requirement of a large number of experimental events for good data processing, and the capability of the laser to produce pulses at rates of up to 75 pulses per second, the experimental design was reconsidered. The availability of a DEC PDP-8e computer interfaced to an Analogic AN5800 analog to digital converter suggested semi-automated data acquisition. Three circuits were then designed and constructed: a fast integrator and sample and hold amplifier to monitor the output of the internal photodiode, a high gain sample and hold amplifier for the signal channel, and a digital output interface for the computer. With these additional elements a complete system capable of simultaneously monitoring the laser power level and the luminescence signal, on a pulse to pulse basis, was constructed.

The computer was connected and programmed to initiate, control, and synchronize the laser and the various sample and holds. With this system, the laser's fluctuations were monitored with far greater success. Events could be discriminated and sorted according to laser amplitude. Further, data could be accumulated at a much higher rate to allow for statistical averaging. Four major defects remained however:

1. Due to the restrictions of a simple electronic design, the slew rate of the sample and hold amplifiers was slightly too small, restricting the dynamic range of

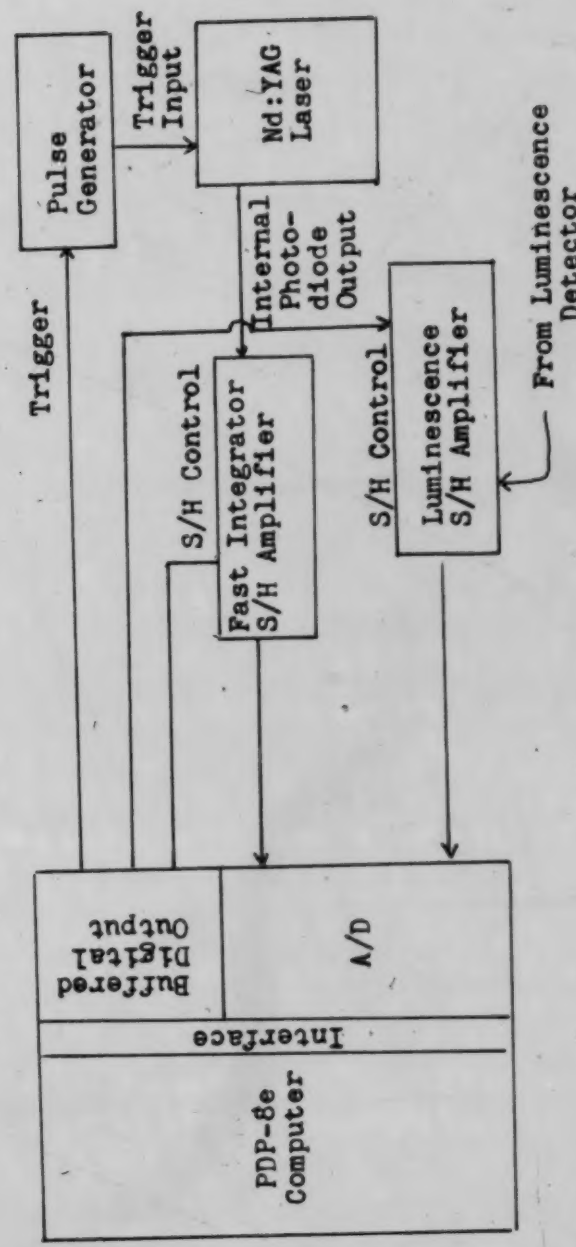


Figure 2-28 Computer Controlled Data Acquisition System

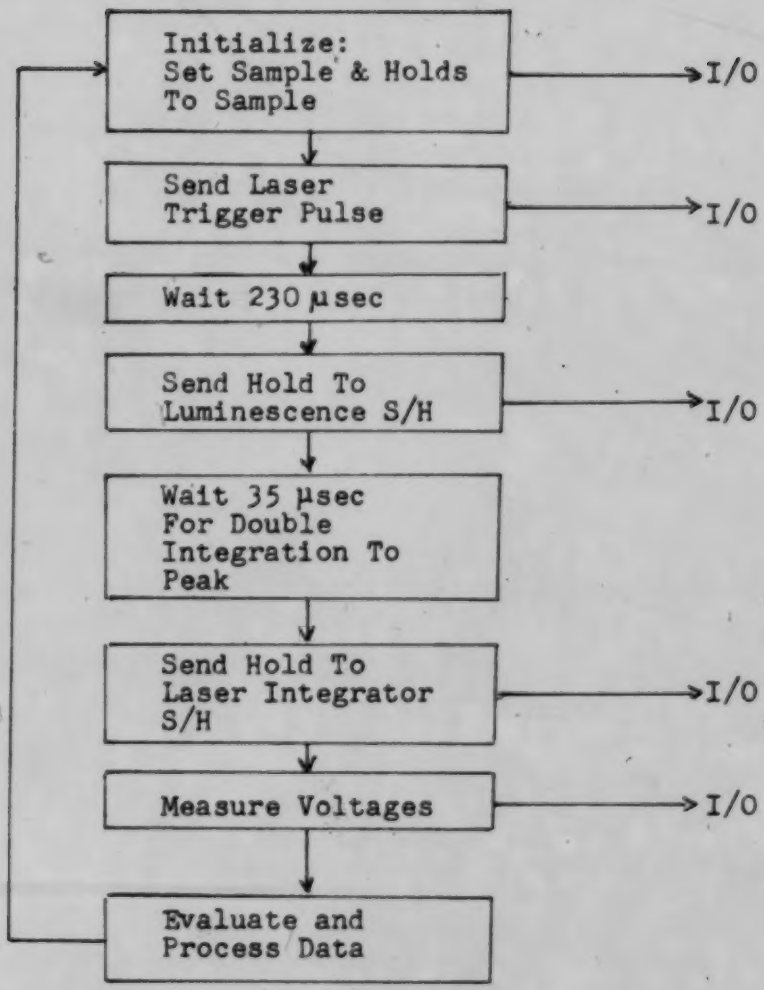


Figure 2 - 29 Simplified Computer Program

Figure 2-30 Block Diagram Of Fast Pulse Integrator Sample And Hold

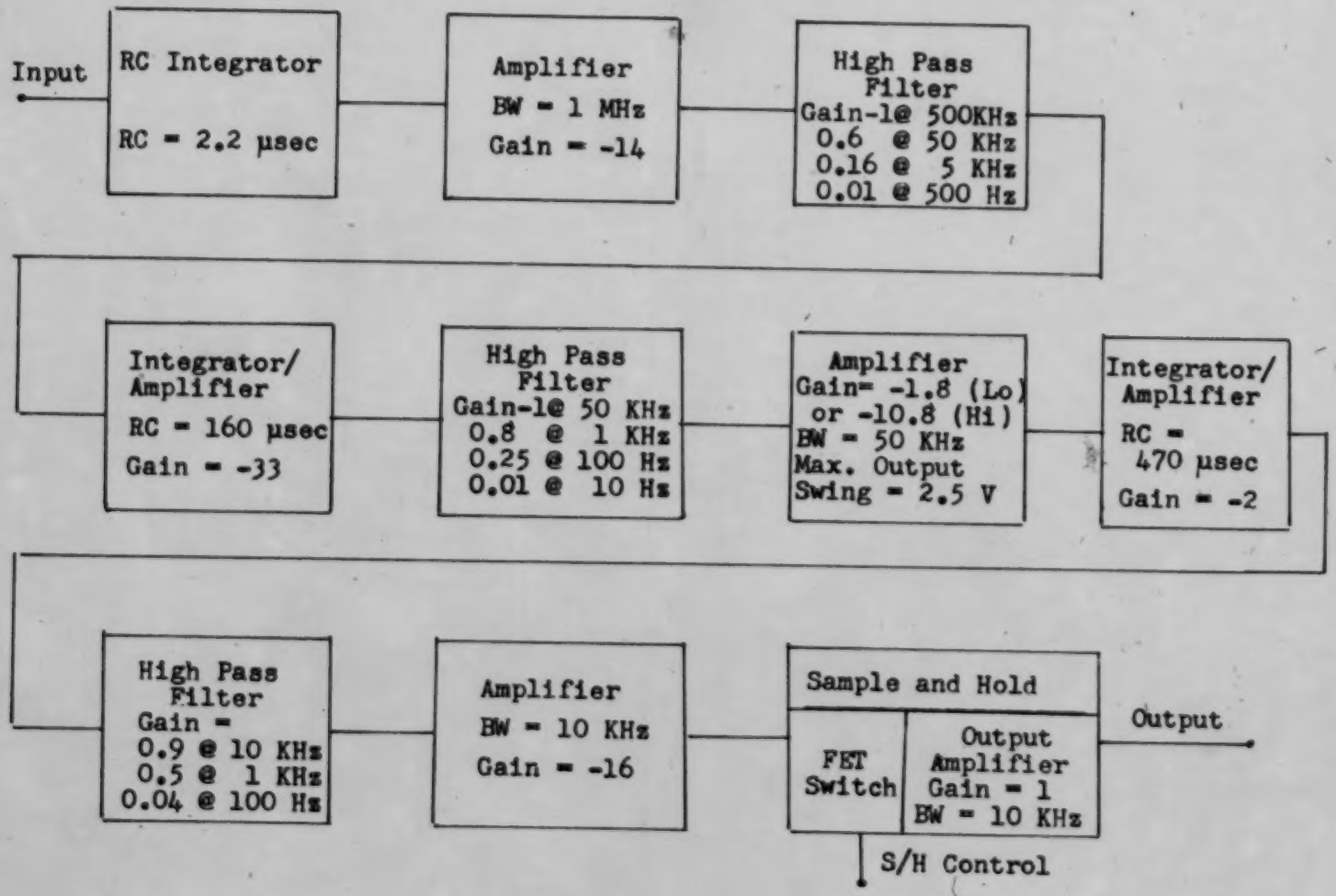

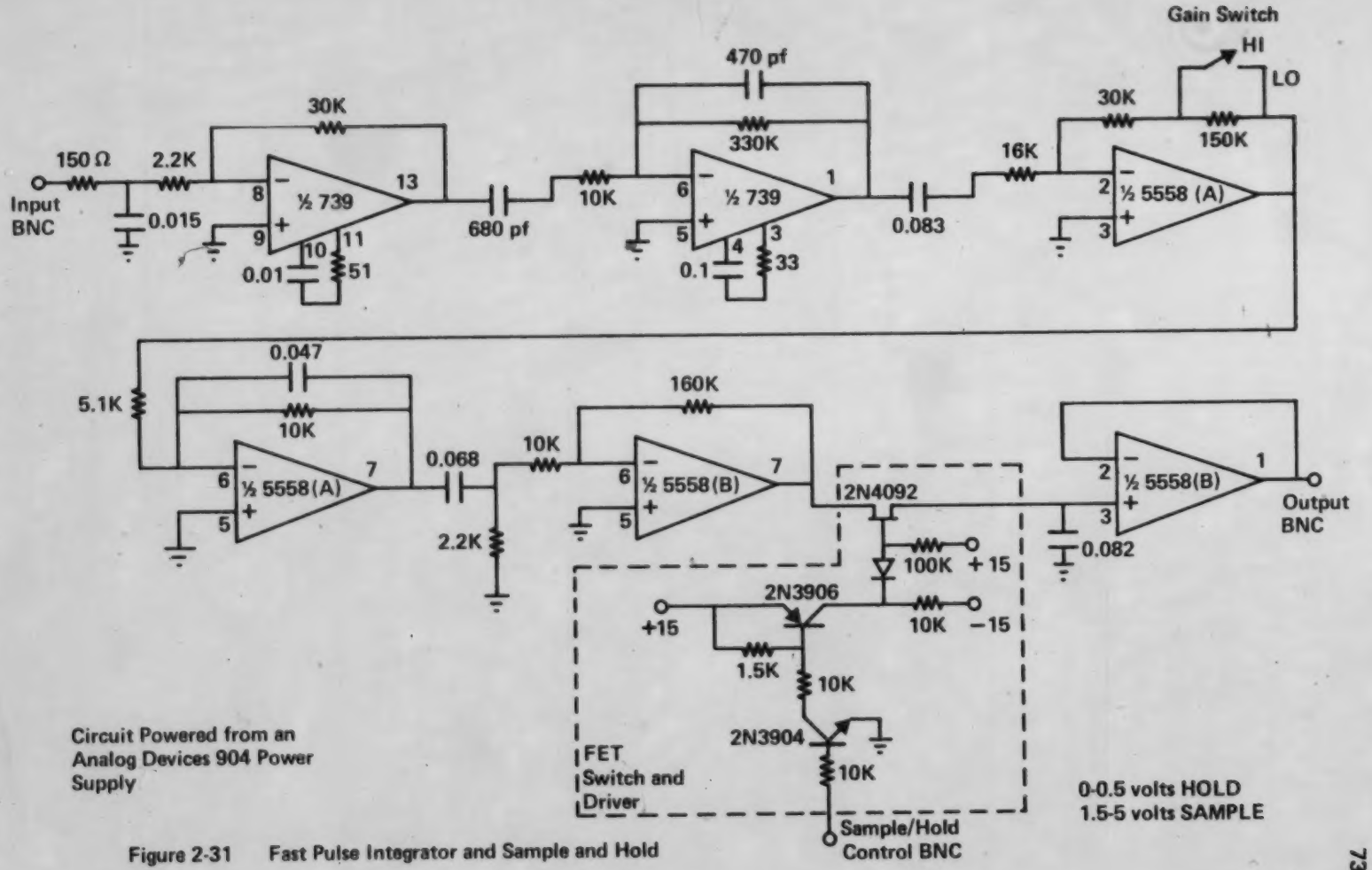


Figure 2-31 Fast Pulse Integrator and Sample and Hold

the circuits.

2. Since the amplifiers in the sample and hold circuit were not fast enough to handle the 100 ns pulse, it was pre-integrated first to 2.2 μsec, amplified, then further integrated to 470 μsec for easy and reliable acquisition. This decreased the resolution of the circuit in two ways. First, there is some jitter in the pulse width of the laser output, therefore integrated discrimination does not correlate directly with peak amplitude discrimination. Second, and more important, the laser output is preceded by large amounts of electrical noise generated by the flashlamp discharge, and the RF bursts to the Q-switch. In an integrated signal the total impulse of this preceding noise remains, and can add considerable fluctuations to the signal.

3. With the implementation of the dye laser, new problems arose. Due to the variation of dye gain with output wavelength, slight variations in dye flow, and other factors, the output power of the dye laser does not correlate directly, or consistently, with the output power of the Nd:YAG laser. As a consequence, the internal photodiode is not an adequate monitor of the dye laser power output. An external PIN photodiode was mounted with a fast preamp constructed by us according to the diode manufacturer's specifications. Unfortunately this circuit has a 1 KΩ output impedance, and the input stage of the

integrator circuit was designed to have an impedance of approximately 150 Ω at 10 MHz in accordance with the requirements of the internal photodiode circuit. Temporary intermediate circuits were constructed, but their performance was not very satisfactory.

4. The Nd:YAG laser is constructed so that its flashlamp firing rate may be varied from 1 - 75 pulses per second by front panel adjustment. It may also be triggered externally, but protection circuitry limits the maximum rate to about 35 pulses per second. Unfortunately the Nd:YAG laser displays far greater stability when the flashlamp is triggered at the highest or near highest rates (55 - 75 pulses per second). This is probably because discharge paths are more stable when the time between firings is shorter. Consequently, it is preferable to trigger the laser internally.

As a result of these problems, system design was again reconsidered. Preference was given to proven commercial components because of the high speeds required at many stages. The resulting design incorporates many improved features. The Nd:YAG laser is allowed to run free at its optimum rate. A fixed fraction of the intensity is taken from the output beam by a beam splitter and directed into a monitoring photomultiplier. The signal from this photomultiplier is fed through a T into two Ortec 436 100 MHz discriminators.

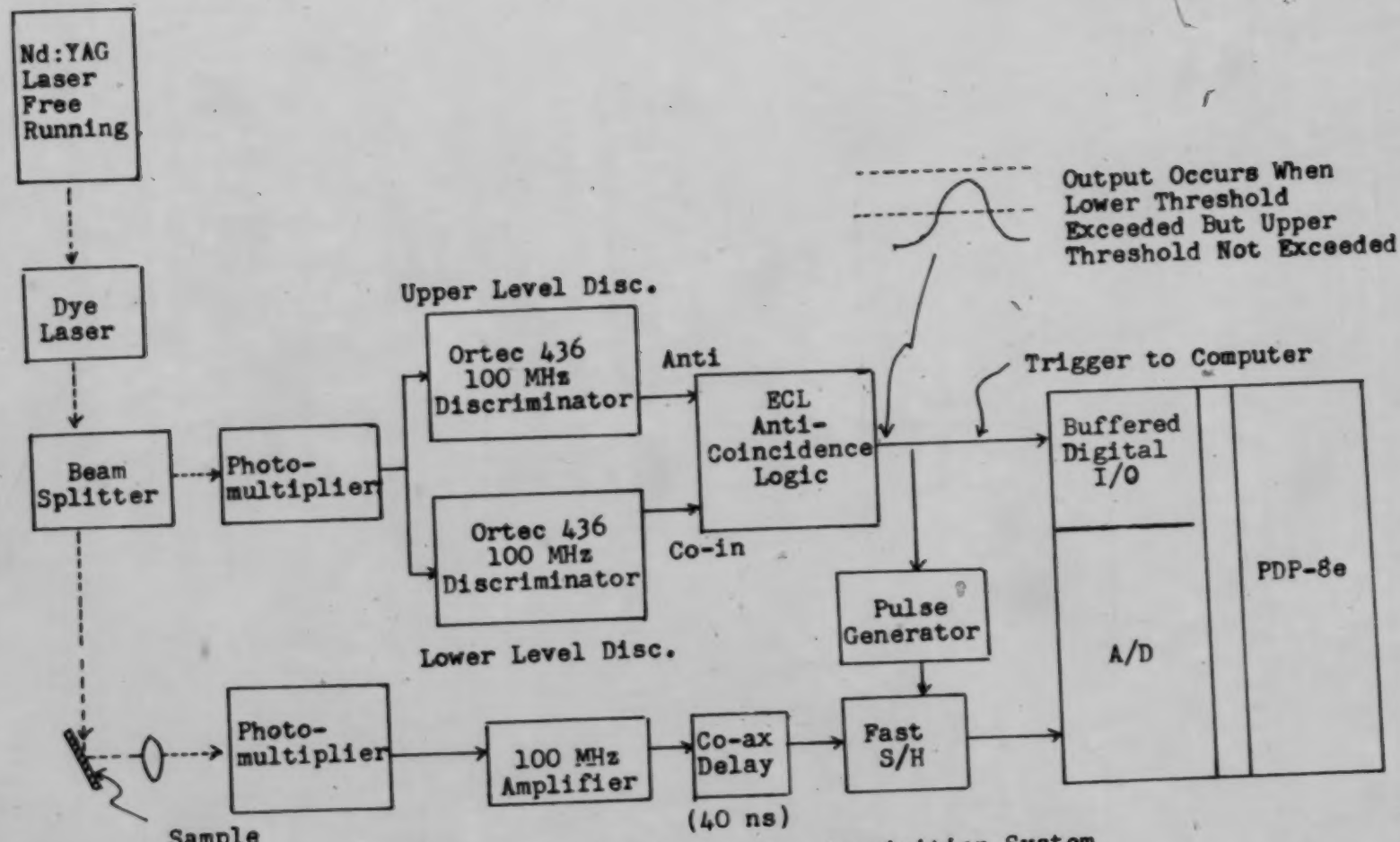


Figure 2-32 Fast Monitoring Acquisition System

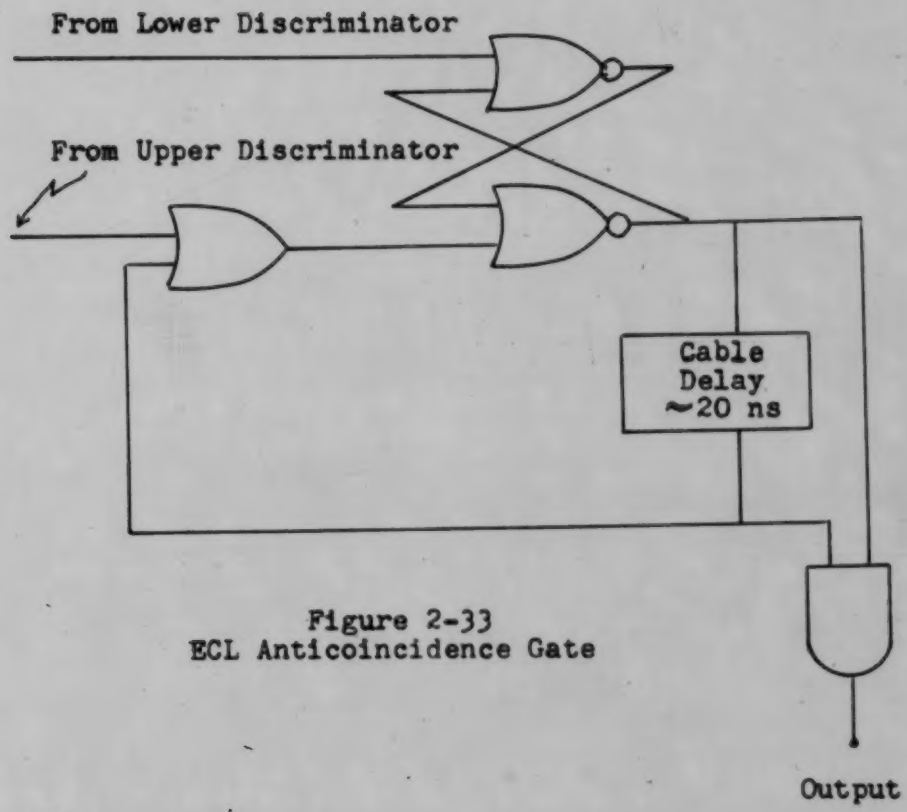


Figure 2-33
ECL Anticoincidence Gate

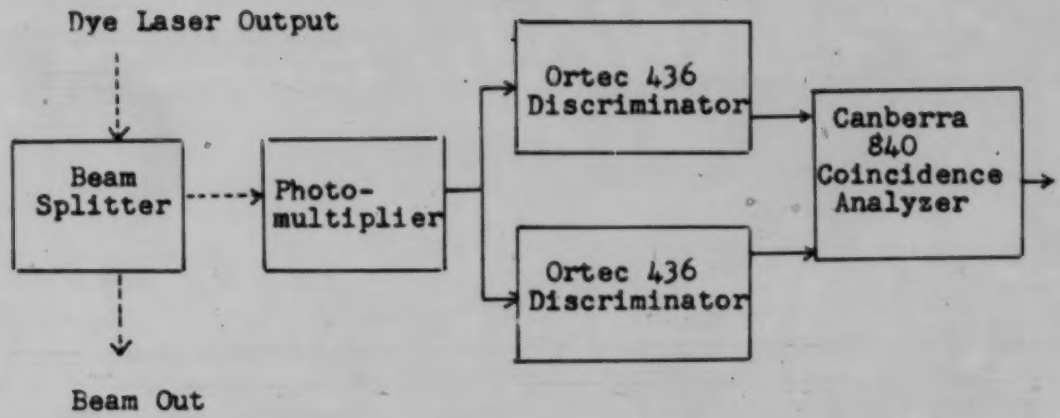


Figure 2-34 Actual Monitoring System

The acceptable "window" of pulse amplitude is determined by the gap between the lower level discriminator setting and the upper level discriminator setting. An anti-coincidence gate is connected to the output of the discriminators to impose this window. The output pulses from this gate serve as trigger and timing mark for the rest of the system.

Most of the data reported here was taken with a partial implementation of this latest generation of design. With the complete design as shown in figure 2-32, discrimination would occur with sufficient speed that the actual unintegrated peak of the luminescence signal could be captured by the sample and hold. However, the ECL anti-coincidence gate was not yet ready, so a standard nuclear instrumentation coincidence gate, the Canberra 840, has been used. This gate has a decision making time of about 1 microsecond (compared with about 30 ns for the ECL circuit) which changes the synchronization somewhat. Integration is used in the signal channel to extend the length of the signal pulse; so that, when the sample and hold amplifier is triggered 1 μsec after the real event, the integrated signal will still be present with very little decay.

The actual optical coupling is achieved using a glass slide as a beam splitter. This works quite satisfactorily as the slide is mounted very rigidly in a fixed

position relative to the output beam. Calculating the reflectivity at each interface for low angles of incidence, one finds about 4 % at each surface, or a total reflectivity of about 8 % for the slide. A beam splitter which would reflect an even smaller amount (such as a pellicle) would be desirable, since the fractional beam from the glass slide must be attenuated by $10^4$ to prevent saturation of the photomultiplier (which further is operated at low voltage). This attenuation is accomplished with a pair of neutral density filters which are mounted immediately in front of the photocathode. A diffuser of ground glass is mounted a few centimeters in front of these filters to reduce any possible effects due to small changes in beam diameter or position.

A photomultiplier was chosen as the monitoring transducer for a number of reasons:

1. It is a relatively fast detector, with a rise time of less than 2.5 ns, and therefore easily capable of resolving the laser pulse.

2. Its output characteristics are exactly those anticipated by the Ortec 436; i.e. it is a fast current source, capable of driving a 50 Ω load to 500 mV without either extreme incident intensities, or intermediate amplification.

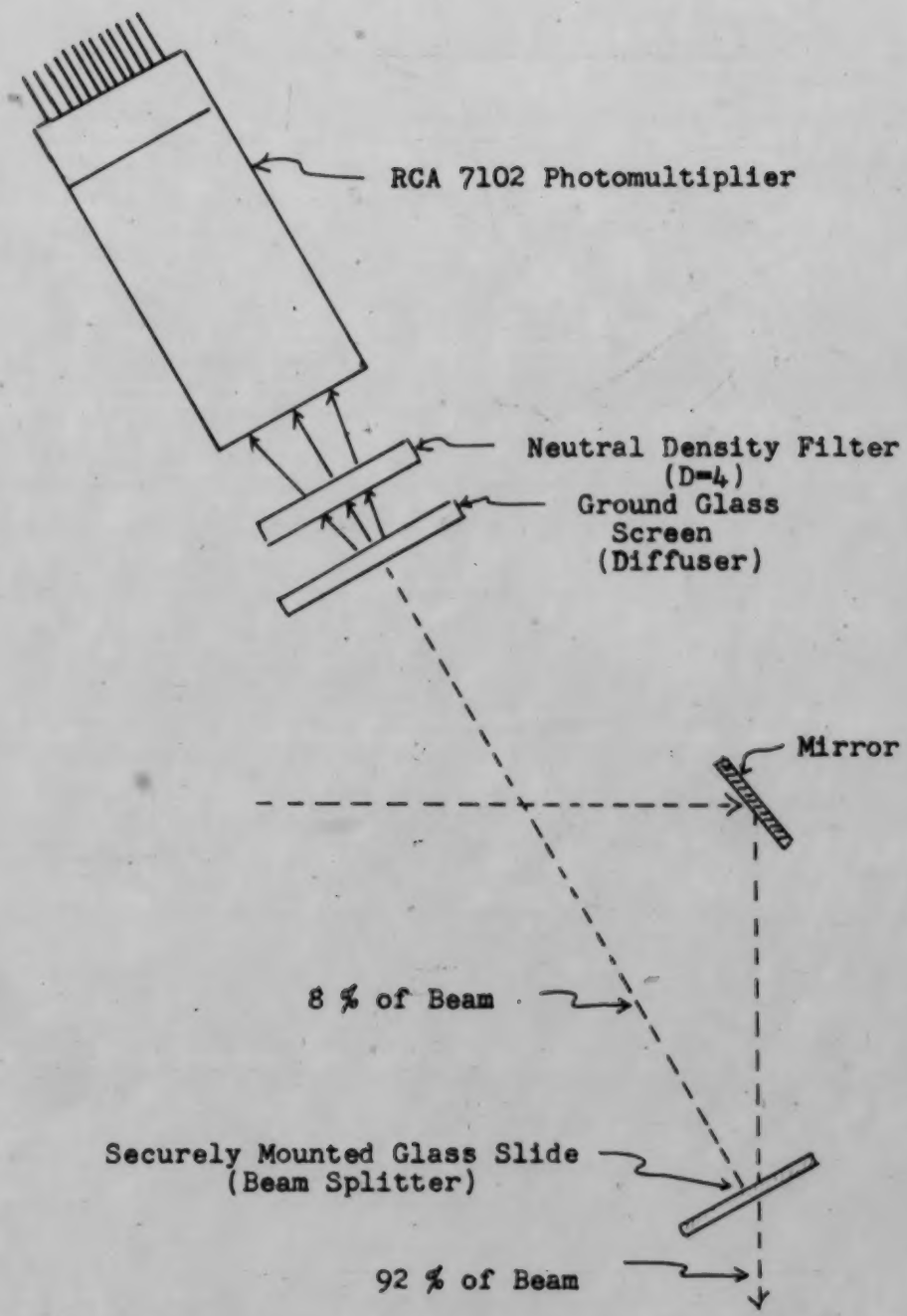


Figure 2-35
Actual Mounting of Beam Monitor

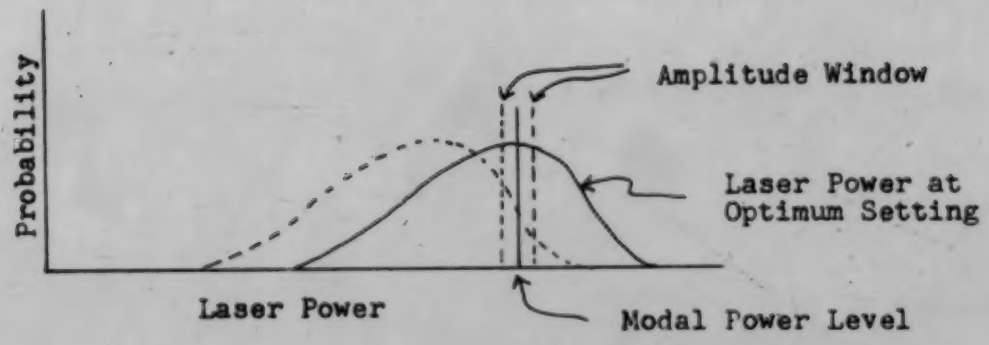


Figure 2-36 Laser Power Level Distribution

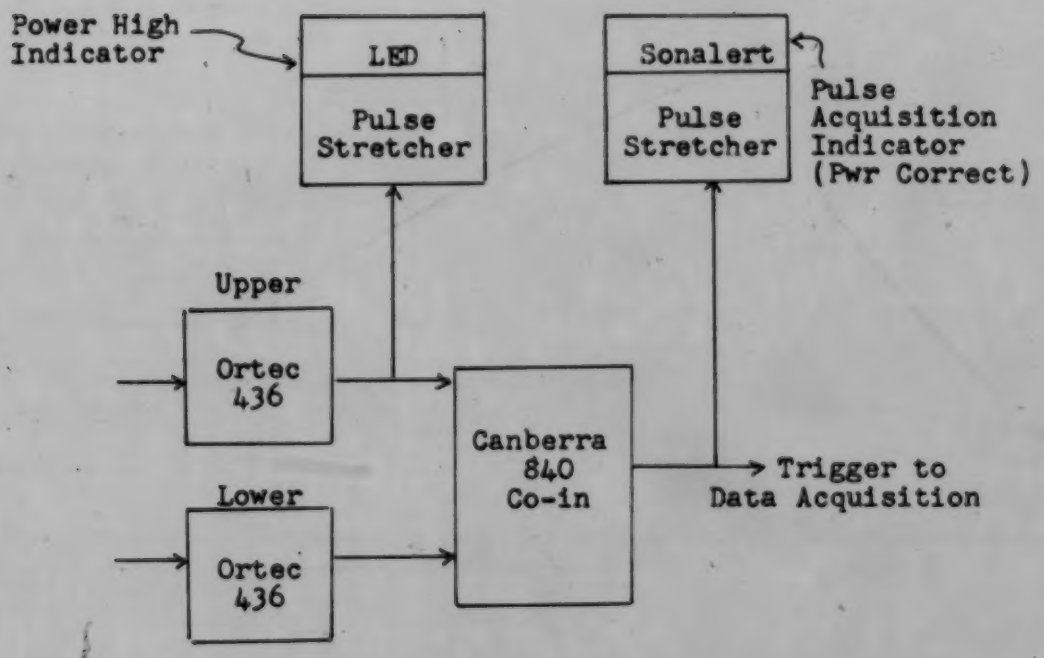


Figure 2-37
Power Level Indication

The RCA 7102 was specifically chosen because:

1. Its S1 spectral response is relatively flat with a sensitivity variation of only 1.8 over the range 5600 Å to 6500 Å. This is bettered only by the multi-alkali and III/V types.

2. It is inexpensive.

3. It was available.

Typical operating voltages in our configuration are in the vicinity of 950 volts.

One last topic relating to the power monitoring system remains. Although the laser pulses fluctuate in power level, at any given setting there will be a statistical distribution of the output power levels, and a statistically modal power level. In well tuned operation this distribution will be approximately gaussian. The discriminator will determine which pulses are of suitable amplitude, but data will be most efficiently collected if the laser power level is adjusted so that the mode corresponds to the center of the acceptable window.

Due to the cumulative instabilities in the Nd;YAG-dye laser system, it displays a tendency to long period ($t \geq$ two minutes) drift. As a result, continual readjustment of the laser power control is necessary. Output transducers have been added to the system to enable the operator to monitor the acquisition rate.

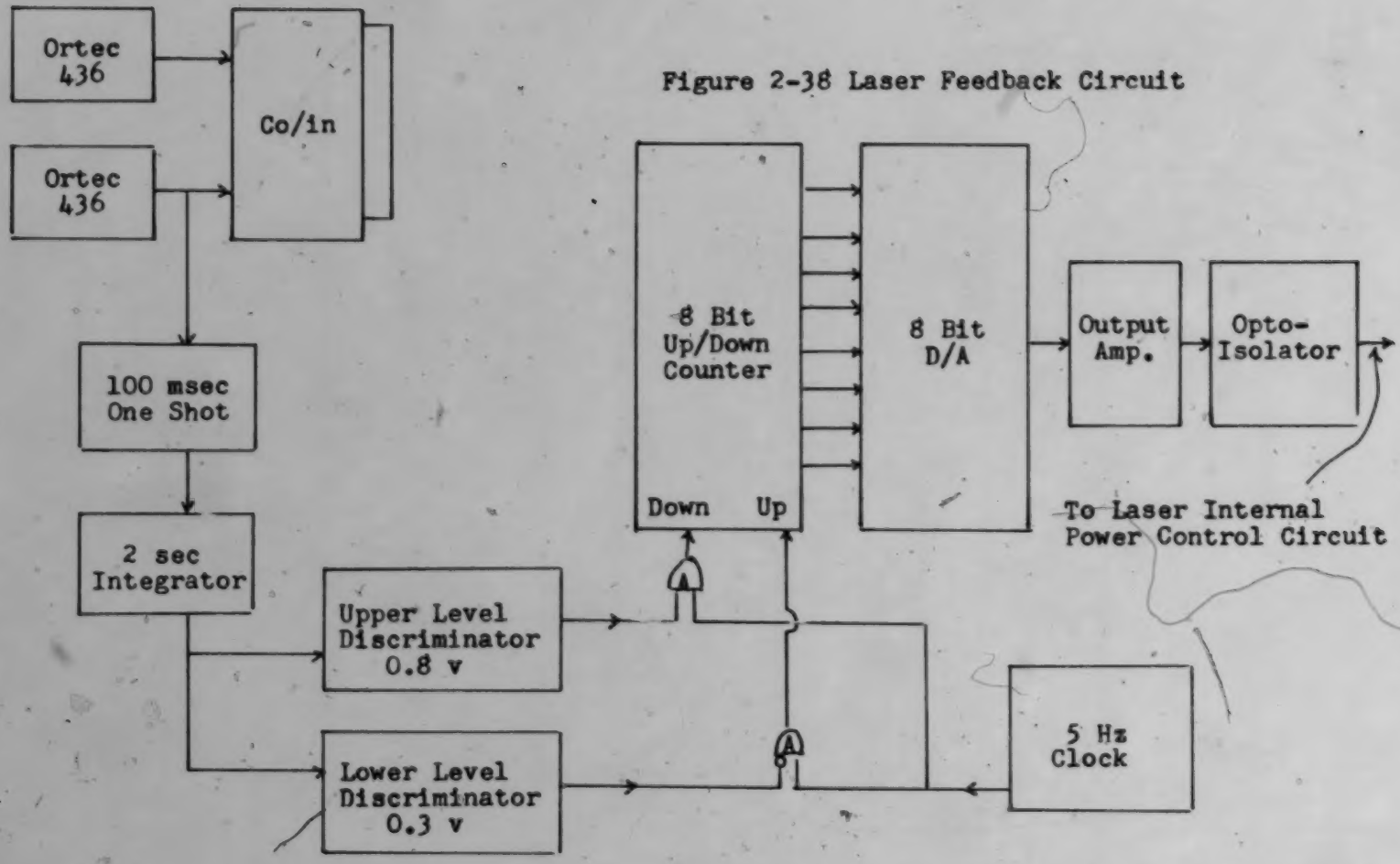


Figure 2-38 Laser Feedback Circuit

With the hope of stabilizing the laser output, the power monitor circuit was linked through a long period feedback loop to the laser power control. The feedback circuit is constructed to monitor the output rate of the lower level discriminator. If the fraction of the pulses whose power exceeds the lower threshold falls below a two second average of 30 %, the flashlamp power is increased; if the fraction exceeds 80 %, the flashlamp power is reduced. The circuit was bread-boarded and tested, with moderately successful results. An improved permanent version may be implemented in the near future.

### 2.1.4 The collimation system and chopper

The dye laser output beam physically shifts with

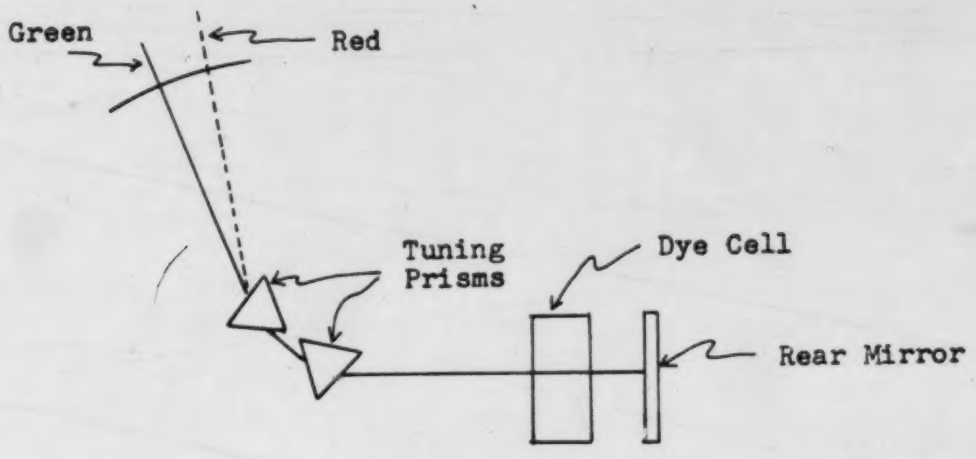


Figure 2-39 Chromatic Dispersion of Dye Laser Output

wavelength changes. This is a natural consequence of the prism tuning, and problematic as it is highly desirable to maintain the focused beam spot in a fixed position on the sample. The simplest and most stable solution is to add a collimator fed by an adjustable reflector. The fixed position collimator insures that the beam path is constant, and the movable reflector allows adjustment to accurately direct the beam energy in this path.

In our case the collimator consists of two apertures, with diameters 1 cm and 0.8 cm, spaced approximately 1.5 meters apart. Since the beam fills the apertures and can be accurately aligned with an error of less than a millimeter, the angular resolution is better than 1 milliradian; thus, with 20 cm remaining between the second aperture and the sample, spot stability of about 0.13 mm is insured.

Because of the stability of the collimation system, it was possible to increase the angular dispersion of the output beam. This was achieved by the addition of two external prisms. The resulting combination of a high dispersion system and a collimator forms a crude prism monochromator, and filters out any unwanted spurious beams that might be generated at high excitation intensities, as well as any remnants of 0.532 μ or 1.064 μ that might be present.

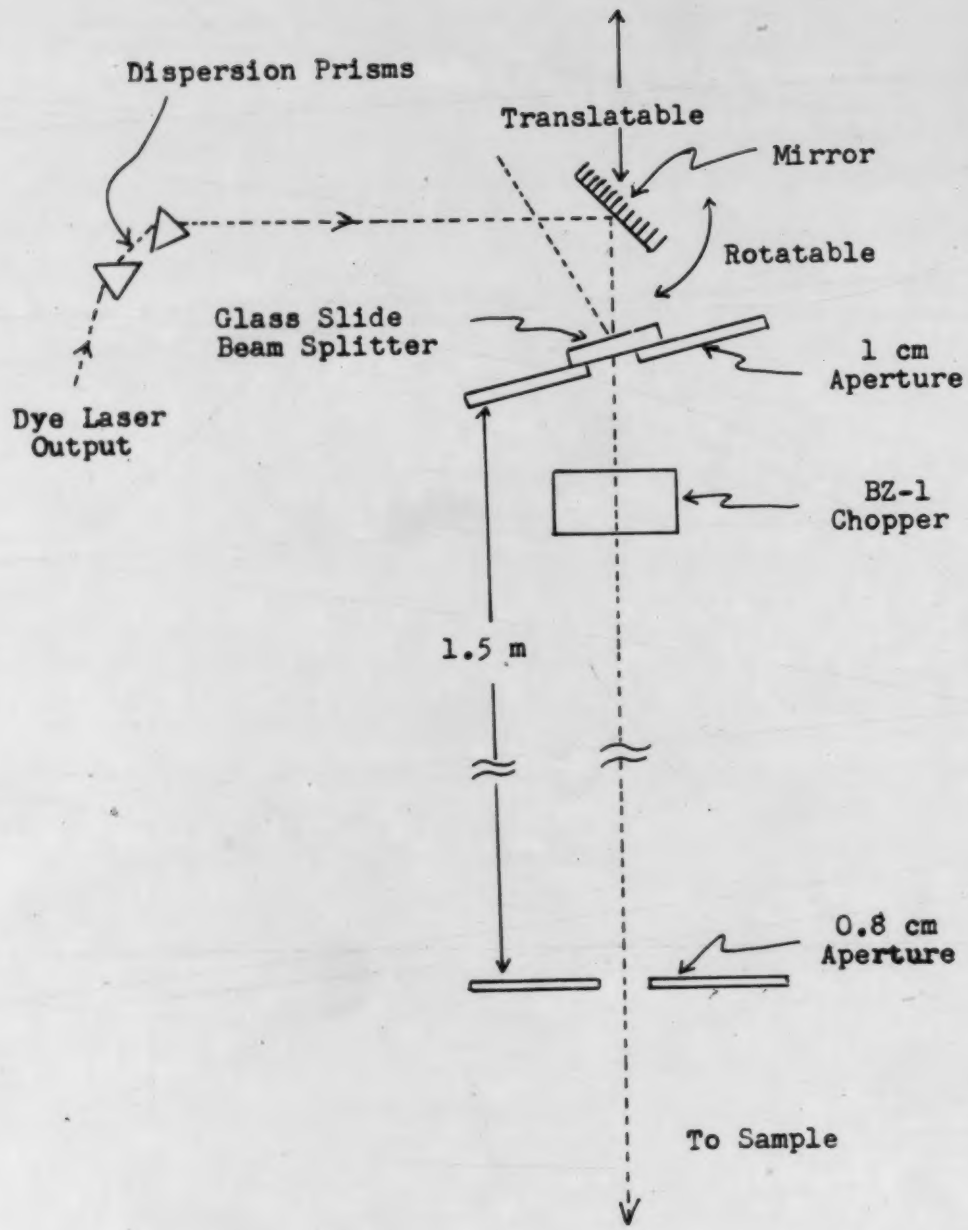


Figure 2-40 Collimation System & Chopper

Further, the secure position and fixed orientation with respect to the beam of the first aperture are very convenient for the mounting of the glass slide beam splitter, which is attached to the front surface of the aperture plate.

Also proximate to the collimator, and in line with the collimated beam, is a PAR BZ-1 mechanical light chopper. This is operated at its lowest frequency, 13 Hz, and is used in conjunction with the data acquisition system to reduce noise and offsets in the signal channel.

### 2.1.5 The wavelength monitoring system

The dye laser output wavelength is measured with a Bausch and Lomb 33-86-45 grating monochromator. This is a 0.5 metre instrument equipped with a 1200 groove per mm grating. Dispersion is about 16.5 Å per mm of slit width, so that operating at a slit width of 0.2 mm, the resolution should be about 3.3 Å, which is more than adequate. The beam is shunted into the monochromator input slit by a removable mirror (normally not present) in the collimator beam path. The output slit of the monochromator is simply monitored by eye.

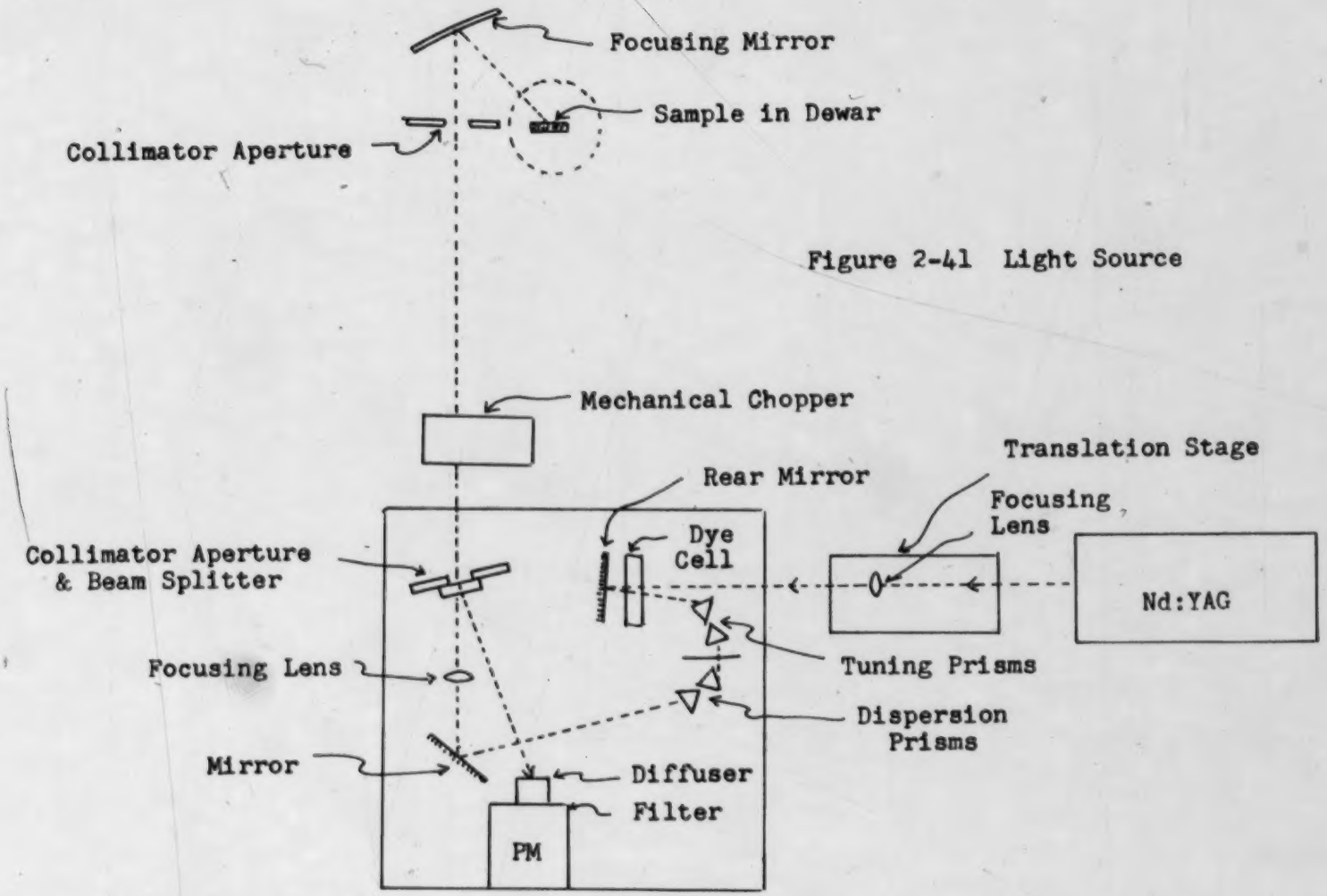


Figure 2-41 Light Source

## 2.2 The detection system

The technical requirements for the detector are quite simple: adequate sensitivity and signal to noise ratio in the spectral region of the luminescent output. To include the impurity bands of $Cu_2O$ this region must encompass at least 0.68 - 1 μ, and for a better study of luminescence 0.5 - 1.1 μ. While there are now many semiconductor photodetectors with high quantum efficiencies and low noise currents that operate in this spectral region (including silicon PIN photodiodes), problems are encountered in amplifying threshold signals up to usable levels. As it is difficult to find a broadband amplifier with better noise characteristics than the electron multiplier, photomultipliers tubes are still superior detectors in spectral regions where photocathode sensitivity is available. There are currently only 3 photocathode types commercially available with usable spectral responses extending to 1 μ. Only two of these extend to 1.1 μ: the Ag-O-Cs S-1 (RCA 101 response, one of the earliest types), and the Ga-In-As type III (RCA 142 response, one of the most recent types). This essentially reduces the choice of an optimum detector to either the RCA 7102, or the RCA C31034D. Comparing the specifications of these photomultipliers at their recommended operating voltages: the 7102 has a sensitivity of 354 A/W at 0.96 μ and a dark current of 1900 nA;

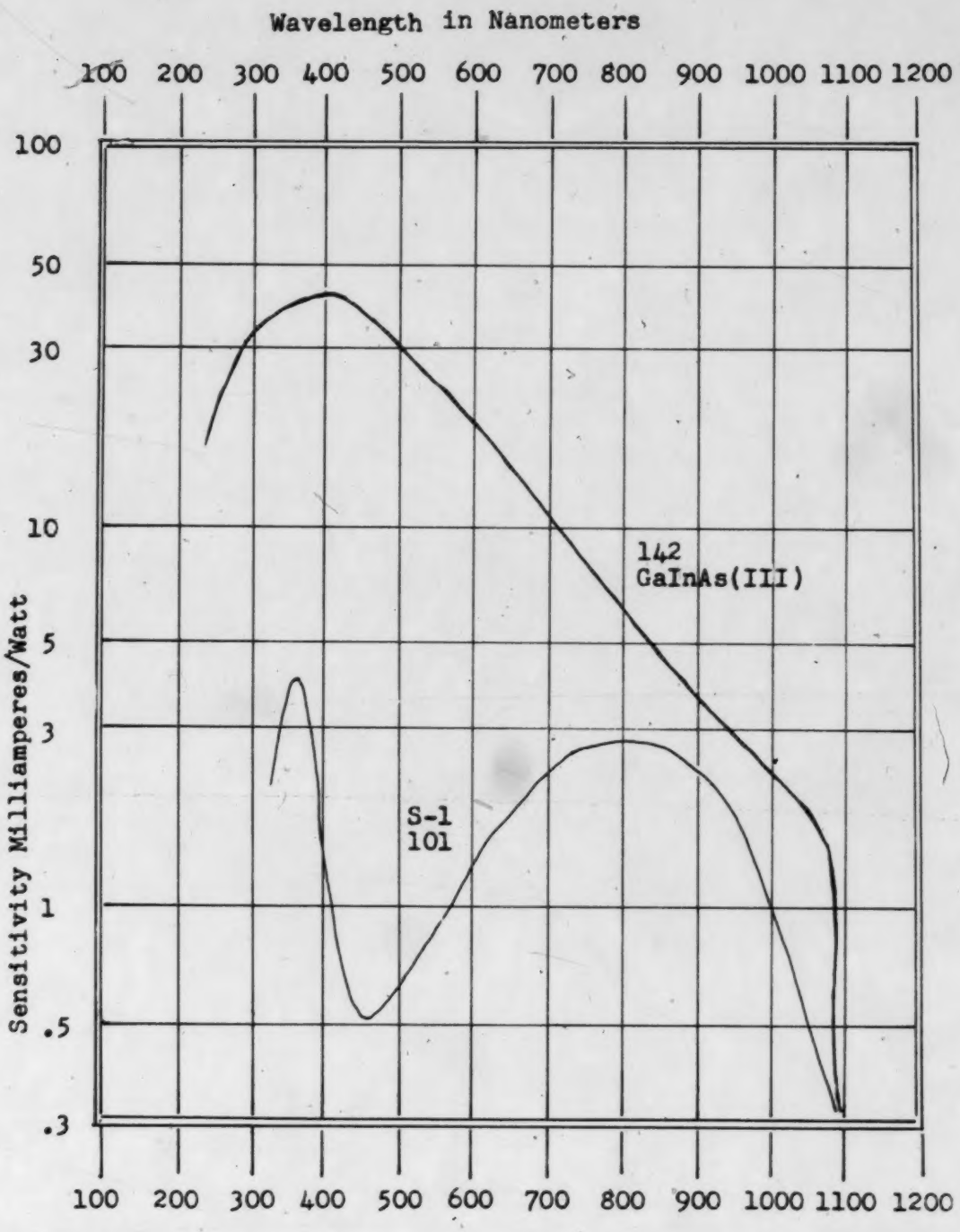


Figure 2-42 Photocathode Sensitivity Vs Wavelength

whereas, the C31034D has a sensitivity of 1093 A/W at 0.96 μ and a dark current of 10 nA. Therefore, considering the simple noise equivalent power, we have $5.4 \times 10^{-9}$ watts for the 7102, and $9.1 \times 10^{-12}$ watts for the C31034D. While the C31034D is therefore at first glance technically preferable, the 7102 was chosen for two reasons: its immediate availability, and its low cost (the price ratio is about 15). Some unsuccessful attempts were made to cool the 7102, and thus reduce noise. The 7102 is operated at the recommended voltage of 1250 volts.

In almost any photoluminescence experiment, the spectral response of the detector must exclude the incident excitation wavelengths. This is usually achieved by filtering the light incident on the detector. In our earliest experiments, the IR transmitting visible absorbing Corning glass filters 7-57, 7-56, and 7-69 were used. While fairly successful in eliminating the excitation radiation, use of these filters did not give much information on the wavelengths of the components of the IR luminescence.

To achieve this resolution, a Leiss double prism mirror monochromator with fused quartz prisms is used. The wavelength resolution of a refracting monochromator depends upon two things: the dispersion of the prisms in spectral region of the output wavelength, and the

total width of the entrance and exit slits. Due to imperfections in the optics of the Leiss, resolution increases with the reciprocal of slit width only to the limit of a total slit width of 0.05 mm. Since the linear dispersion with fused quartz prisms is 0.5 mm/ 10 nm at 500 nm, and the linear dispersion is directly proportional to the dispersion of the fused quartz, we can use the information that the dispersion of fused quartz is about $5.55 \times 10^{-2}$ $\mu^{-1}$ at 0.5 μ, $2.28 \times 10^{-2}$ $\mu^{-1}$ at 0.7 μ, and $1.26 \times 10^{-2}$ $\mu^{-1}$ at 1.0 μ, to compute the linear dispersions at 0.7 μ and 1 μ. We therefore have linear dispersions of 0.205 mm/10 nm at 0.7 μ (700 nm) and 0.114 nm/10 nm at 1.0 μ (1000 nm). Combining this with the limiting slit resolution of 0.05 mm, we have ultimate instrument resolutions of 2.4 at 0.7 μ, and 4.4 nm at 1.0 μ.

Intensities were found to be too low at limiting resolution, so the operational slit widths were chosen to be:

1. 0.18 mm for the entrance slit (18 on the slit micrometer)
2. 0.19 mm for the intermediate slit
3. 0.20 mm for the exit slit.

Summing the entrance and exit slit widths we have a total mechanical slit width of 0.38 mm, and dividing by the linear dispersions we have resolutions of 0.0185 μ

(18.5 nm) at 0.7 μ, and 0.0333 μ (33.3 nm) at 1.0 μ.

Since the luminescent emission will be distributed approximately uniformly over the entire available solid angle of $2\pi$ steraradians, some light gathering mechanism is necessary for efficient detection. The Leiss monochromator fortunately is equipped with light gathering mirror optics specifically designed to image a point source on the entrance slit. The focusing element is a spherical concave mirror with a focal length of 150 mm, and a relative aperture of f/2.5. Focusing with image and object both at approximately 2f, the mirror presents a solid angle of about $4\pi \times 2.5 \times 10^{-3}$ steraradians, and therefore captures about 0.5 % of the available backward luminescent emission. The off axis aberration in the system conveniently renders the images of point

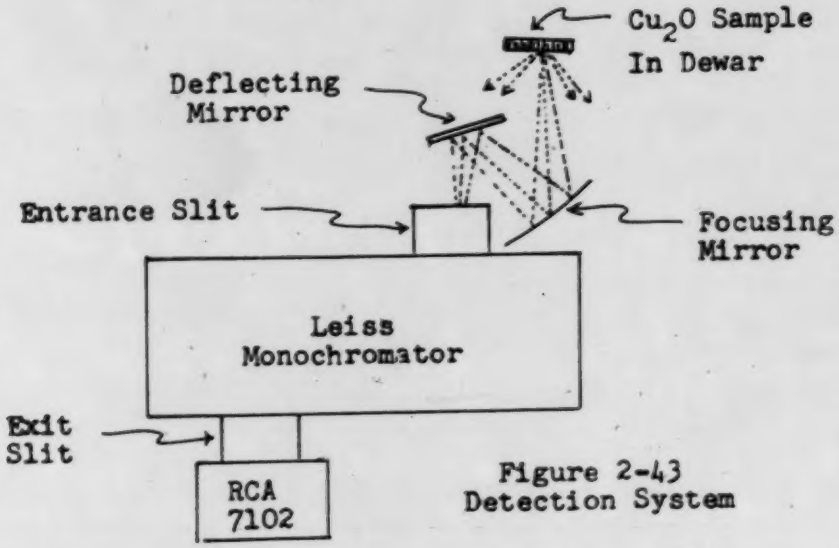


Figure 2-43
Detection System

sources into vertical lines with appropriate mirror adjustment. Since this image has a horizontal breadth of about 1 mm, or about five times that of the entrance slit at its normal setting, only about 0.1 % of the luminescent emission enters the monochromator.

## 2.3 The temperature control and monitoring system

The cooling system used is almost the simplest possible. It consists of a hollow copper cylinder which can be filled with any liquid coolant or cryogen. The sample is attached with vacuum grease to a flattened region on the cylinder's outside surface. Because of availability, ease of handling, low cost, and relatively low temperature, liquid nitrogen is used as the coolant. This system would be adequate in itself except for two problems: temperature gradients within samples exposed to warm air on their outside surface, and frost build-up which optically obscures the sample. As a result, the cylinder is enclosed within a partially silvered dewar which is only slightly larger than the cylinder itself. The small volume of air enclosed quickly reaches equilibrium with the cylinder surfaces. To alleviate any frost problems due to moisture that may be present within the dewar, indicating $CaSO_4$ dessicant fills the remaining volume at the bottom of the dewar, and a greased rubber stopper seals the top.

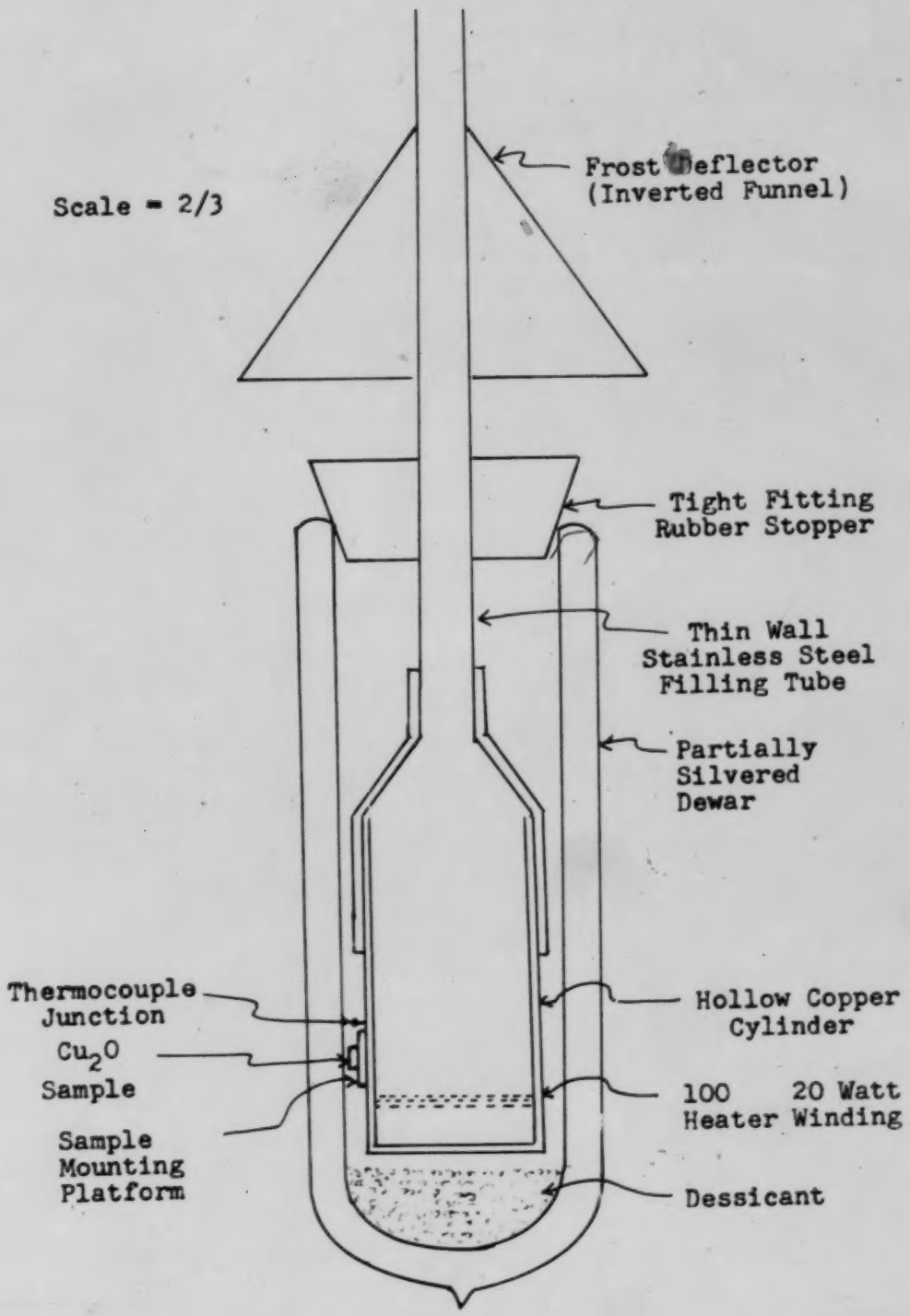


Figure 2-44 Cryostat Used In Experiment

Because of the high insulation value of the dewar, a 100 Ω heater coil is wrapped around the base of the cylinder to provide for rapid warm up, and allow some temperature control after the nitrogen boil off.

The cylinder contains a volume of about 80 ml and has a mass of about 0.27 kg. The heater is operated at about 45 volts and therefore dissipates about 20 watts. For copper, the change in constant pressure enthalpy from 77 K to 300 K is about 74 joules per gram, so that about 20000 joules are required to warm the system to room temperature. From this, and the heater wattage, the time required to heat the cryostat may be calculated, and is about 17 minutes, in good agreement with experimental observation.

With the heater off, the nitrogen boil off will take a maximum of about 50 minutes. Since the latent heat of vaporization of liquid nitrogen is about 199 joules/gm, or 161 joules/ml, the total energy required to boil off the nitrogen is about 13000 joules. Hence, from the time required, we may conclude that at 77 K heat leaks in at a rate of about 4 watts. The heat leakage rate is presumably approximately proportional to the temperature difference. Considering the worst case of heat leakage, we get a temperature stability of about 11 seconds per degree K (after nitrogen boil off). The total warm up time to about 250 K is, however,

about 4 hours with the heater off.

The reservoir can, of course, be boiled dry with the application of heat in about 10 minutes or less, depending upon its fullness.

Quickly calculating the amount of nitrogen required to cool and fill the reservoir, we have 80 ml plus the quotient of the 20000 joule heat capacity of the reservoir, and the 161 joules/ml latent heat of vaporization of the $LN_2$; or a total of about 200 ml. This is a very small amount and transferring directly from a 50 litre storage dewar is wasteful and awkward. As a result, a smaller scale storage and transfer system was constructed. A 5 litre dewar is used as a storage reservoir. To achieve rapid and efficient transfer a simple pressurization system is used. A 50 Ω resistor operated at about 25 volts, and therefore dissipating about 12.5 watts, is immersed in the liquid nitrogen. This vaporizes the liquid producing about 0.9 ml of gas per joule at atmospheric pressure, or about 0.6 ml of gas per joule at 1.5 atmospheres. Since the dewar is sealed (with the vent closed) pressure quickly builds up and forces the liquid nitrogen through the transfer tube. Since a pressure head of about 0.5 atmospheres is required to overcome viscosity, an ultimate flow rate of about 450 ml/minute is achieved.

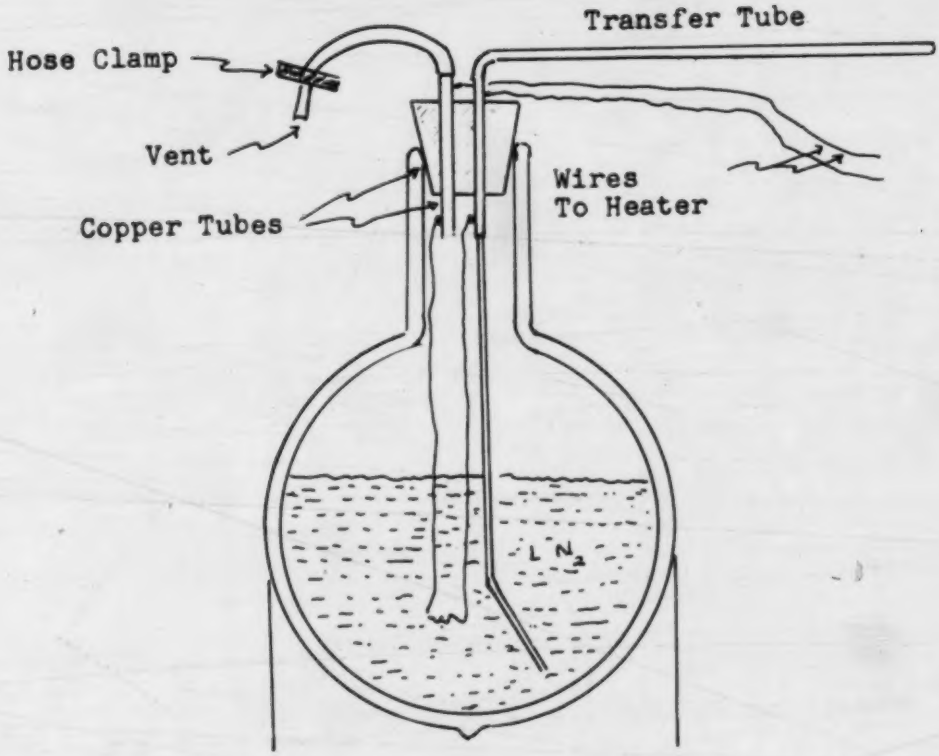


Figure 2-45 Nitrogen Transfer Pump

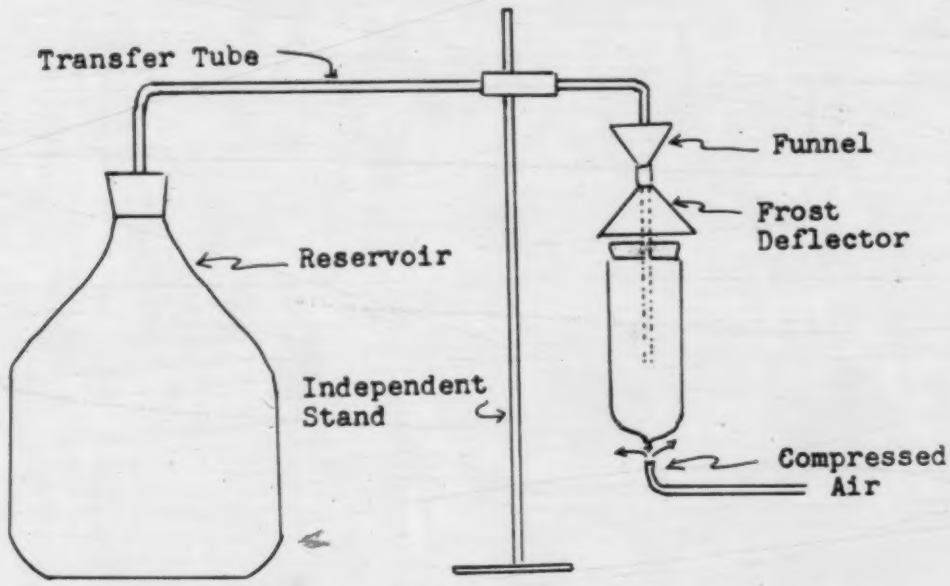


Figure 2-46 Nitrogen Transfer System

The actual transfer rate is somewhat slower as time is required for the dewar to pressurize, and for the transfer lines to cool. Further there will always be losses in transit through uninsulated lines. As a result the transfer time is about 3 minutes, and about three quarters of a litre of liquid nitrogen are consumed.

Transfer may be quickly terminated by venting the pressurized dewar and cutting the power to the resistor.

With regard to the details of the cooling system, a few extra measures were found to be necessary in practice. The contraction of the Tygon transfer line in cooling to liquid nitrogen temperatures is of the order of a few centimeters. As a result the line cannot be directly connected to the cryostat. Instead one end is left free, and the intervening span is supported independently of the cryostat. Liquid nitrogen falls from the free end, is collected by a funnel, and flows into the hollow copper chamber.

With the transfer line and funnel both uninsulated, there is a great deal of condensation and frost build up on both of these parts. To prevent particles of frost or droplets of water from contacting the optical surfaces, a simple frost deflector is mounted between the exposed cold components above the cryostat and the optical surfaces of the dewar below.

Finally, a gentle air flow is directed against the external optical surfaces of the dewar to avoid any possible condensation.

The sample temperature was monitored by a copper-constantan thermocouple which has a usable response extending from slightly below 77 K to well over 650 K. Since the operating temperature range of the cryostat is from 77 K to about 350 K, this is more than adequate. The measuring junction was mounted at the upper edge of the copper sample support pad, within a centimeter of the sample. Under semi-equilibrium conditions this proximity should guarantee that the junction temperature is within a few degrees of the sample temperature. To insure reasonably accurate readings, the second junction was immersed near the surface of a water-ice mixture. The thermal e.m.f. was amplified by 100 with a chopper-stabilized amplifier, and the amplifier output fed into the A/D convertor of the data acquisition system. A digital voltmeter, which served as a visual monitor of the temperature, was also connected to this amplifier output.

Within the data processing system, the e.m.f. to temperature function was approximated for computational ease by:

$$T(\varepsilon) = 273.16 + 26.1167\varepsilon - 0.799167\varepsilon^2 - 0.0316667\varepsilon^3 - 0.0358333\varepsilon^4$$

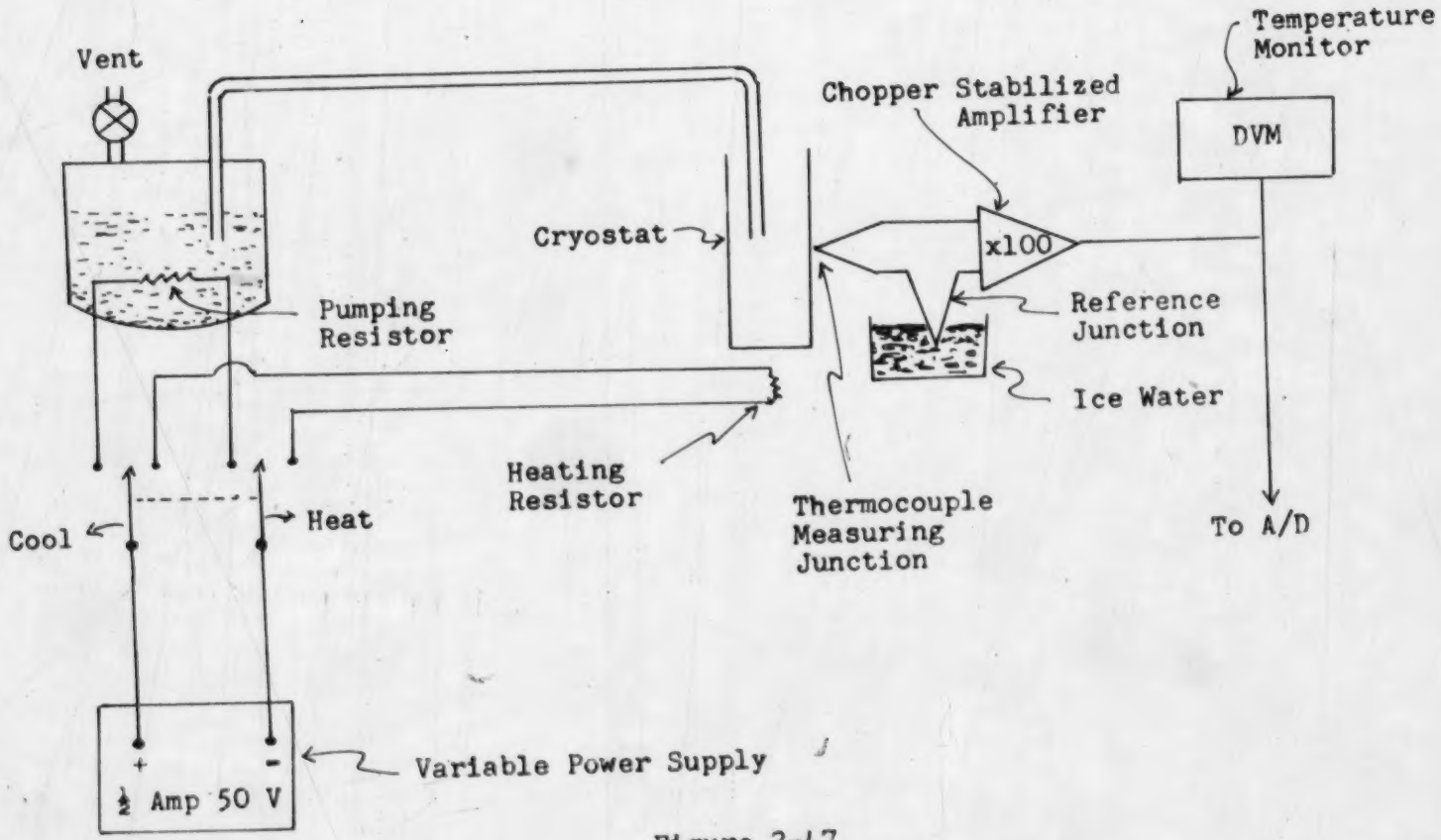


Figure 2-47
Temperature Control and Monitoring Circuit

where T is the temperature in K, and $\varepsilon$ is the e.m.f. in millivolts. This formula is accurate to better than 2 K over the temperature range 77 K - 100 K, with greatest error near the low temperature end; and to better than 0.5 K from 100 K to 340 K.

## 2.4 The Data Acquisition and Processing System

There remain basically two topics: the conditioning and acquisition of the luminescence signal; and the acquisition and processing of the rest of the information from the experiment.

Since the greatest experimental difficulty is the fluctuation of the laser power level, a significant part of the experimental system has already been discussed in the section describing the power monitor. The original design, as shown in figure 2-30, called for a high speed coincidence gate, and a fast rise time amplifier driving a coaxial delay cable, so that the fast luminescence peak could be captured in real time by a sample-and-hold. However, due to the incomplete state of these high speed components, a lower speed compromise version of the system was used to take the data reported here.

To allow for the 1 μsec decision-making time of the coincidence gate, the photomultiplier signal is integrated with a 30 μsec time constant before being fed

into the sample-and-hold amplifier. This integration is achieved simply with a 100 KΩ termination of the photomultiplier, in parallel with stray and cabling capacitance of about 300 pf. An active integrator-preamp, the Canberra 805 scintillation preamp, was tried, but found to be very sensitive to the large amount of electrical impulse noise present. A better signal to noise ratio was achieved with the simple RC circuit.

Integration itself however reduces the signal to noise ratio, as a brief analysis will show. The noise from the photomultiplier is almost entirely due to thermionic electron emission from the S-1 photocathode (unfortunately, the S-1 is the noisiest photocathode in commercial use). This thermionic noise can be mathematically approximated quite well by shot noise.

In the simplest shot noise approximation the following assumptions are made:

1. that the photomultiplier is a current source;

2. that although amplified, the anode current is directly proportional to the current from the photocathode;

3. that the photocathode noise is the direct sum of random single electron emissions;

4. that the probability of an electron emission from the photocathode is constant at all times, and is independent of previous emissions.

A mathematically rigorous analysis of the last two assumptions leads to a Poisson distribution for electron emission at the photocathode, and in simple approximation at "low frequencies" the Schottky formula:

$$\frac{dI^2(f)}{df} = \bar{n}e^2$$

where I(f) is the noise current as a function of bandwidth, $\bar{n}$ is average number of emitted electrons per unit time, and e is the electron charge. Since $i_{dark} = \bar{n}e$, it is easy to show that the rms noise current over a bandwidth $\Delta f$, $i_{noise}(\Delta f)$, is given by:

$$i_{noise} \approx \sqrt{i_{dark} e \Delta f} \quad .$$

A simple derivation can also be performed by merely considering the relationship between standard deviation and sample size. Given that the standard deviation of a sample is inversely proportional to the square root of the number of events in the sample, it follows that for a period $\tau$ the deviation from $\bar{n}\tau$ will be proportional to $1/\sqrt{\bar{n}\tau}$, but $\bar{n} = i_{dark}/e$, and $\tau = 1/\Delta f$, therefore:

$$i_n \propto \sqrt{e\Delta f/i_d}$$

i.e. $$i_n = A\sqrt{e\Delta f/i_d}$$

where A is a constant of proportionality. However,

letting $\tau_o = 1/\bar{n}$, and considering samples taken over a time of $\tau_o/2$, $(\Delta f = 2\bar{n})$, we have that the peak to peak noise current will be:

$$i_n \approx \frac{e}{(\tau_o/2)} = 2i_d$$

so that $$A = \sqrt{2}\, i_d$$

and we have in general that:

$$i_n = \sqrt{2 i_d e \Delta f} \quad .$$

We have, of course, so far only considered the current at the photocathode. If the gain of the multiplier stages is g, then:

$$i_N = g i_n \qquad i_D = g i_d$$

and $$i_N = \sqrt{2 g i_D e \Delta f} \quad .$$

If the tube is now terminated by a resistance R, the output voltage will be:

$$V_N = R\sqrt{2 g i_D e \Delta f} \quad .$$

Finally considering a parallel resistor and capacitor in a simple approximation as having an impedance of R for frequencies lower than $f = 1/2\pi RC$, and an impedance of zero for frequencies above this corner, we have for the RC terminated PM that:

$$V_N = \sqrt{\frac{Rgi_D e}{\pi C}} \quad .$$

From the RCA specifications for the 7102 we have that:

$$i_D = 1900 \text{ nA}$$

$$g = 0.23 \times 10^6$$

so that $V_N$ = 2.7 mV which closely agrees with the observed peak to peak noise voltage.

If for simplicity's sake we consider our signal to be a rectangular current pulse of amplitude $i_S$ lasting about 100 ns, then the integrated signal voltage will have a peak magnitude of:

$$V_o = \frac{Q}{C} = \frac{i_S \times 10^{-7}}{C}$$

however if the delay to signal acquisition is $t_D$, then the signal voltage will be:

$$V_S = \frac{i_S \times 10^{-7}}{C} \; e^{-\frac{t_D}{RC}} \quad .$$

Thus, with the integration circuitry, the signal to noise ratio will be given by:

$$\left(\frac{V_S}{V_N}\right)_{int} = \frac{i_S \times 10^{-7}}{\sqrt{RCgi_D e/\pi}} \; e^{-\frac{t_D}{RC}}$$

so that with $t_D \simeq 1$ μsec, we have:

$$e^{-\frac{t_D}{RC}} = 0.97$$

and

$$\left(\frac{V_S}{V_N}\right)_{int} = 1.19 \times 10^5 \frac{i_S}{amp} \quad .$$

Now if we consider instead a 50 Ω 10 MHz system capable of directly resolving the amplitude of the 100 ns pulse we have:

$$V_N = R\sqrt{2gi_D e\Delta f} = 5.9 \times 10^{-5} \text{ volts}$$

and

$$V_S = i_S R \quad .$$

Thus, for a $\Delta f$ bandwidth system of sufficient bandwidth to directly resolve the signal we have a signal to noise ratio of:

$$\left(\frac{V_S}{V_N}\right)_{\Delta f} = \frac{i_S}{\sqrt{2gi_D e\Delta f}} \quad .$$

We can now compare these signal to noise ratios. Define r as:

$$r = \frac{(V_S/V_N)_{\Delta f}}{(V_S/V_N)_{int}} \quad .$$

We then have:

$$r = \sqrt{\frac{RC}{2\pi\Delta f}}\ e^{\frac{t_D}{RC}} \times 10^7$$

so that with RC = 30 μsec, we have for bandwidths of 10 MHz and 100 MHz:

$$r_{10} = 7.1$$

$$r_{100} = 2.3 \quad .$$

Although RC = 30 μsec was chosen for technical reasons, it is mathematically possible to minimize r for fixed $\Delta f$ and $t_D$ by setting $RC = 2t_D$. We then have:

$$r_{10} = 2.9$$

$$r_{100} = 0.9 \quad .$$

From these calculations we may conclude that a fast system not only gives exact amplitude resolution of fast pulses, but also gives a better signal to noise ratio than integrating systems.

Cooling the 7102 photomultiplier to 77 K will reduce the thermal noise by 6 orders of magnitude; however, another limiting factor must be considered. To be usable a low level signal must be amplified. The fast amplifier immediately available, the Optical Electronics model 9826 has a gain bandwidth product of 1 GHz, but input noise figures of 20 nV/$\sqrt{\text{Hz}}$ and 10 pA/$\sqrt{\text{Hz}}$. In a 50 Ω 10 MHz system this gives an input noise voltage of about $6.3 \times 10^{-5}$ volts, which is already slightly greater than the room temperature noise from the photomultiplier under the same conditions. The best available

amplifiers have a noise figure of about 1 nV/$\sqrt{Hz}$ and therefore offer only a factor of twenty improvement.

With our present configuration, the integrated signal from the photomultiplier is usually of the order of 10 mV with source noise of about 3 mV. Since the A/D converter is currently set for 11 bit conversion over an input range of -10 to +10 volts, the resolution is about 10 mV per bit; therefore, for efficient and accurate acquisition the signal should be amplified to about 1 volt. Toward this end a suitable amplifier-sample-and-hold was designed and constructed. The immediate availability of an Analog Devices SHA-2a sample-and-hold amplifier greatly simplified the design.

The basic design requirements were for a pre-amplifier with a high input impedance, a 1 MHz bandwidth, less than 5 mV of input noise, gain of 100 (40 dB), and sufficient slew rate to settle in 1 μsec (about 10 V/μsec); and for a unity gain low output impedance post-amplifier to buffer the S/H module. (The high speed requirements in the preamp are necessary to allow for acquisition 1 μsec after excitation.) These needs are approximately met by the temporary design produced with available commercial integrated circuits. The active element used in this design is a Fairchild μA 749 integrated circuit, which is an uncompensated operational amplifier

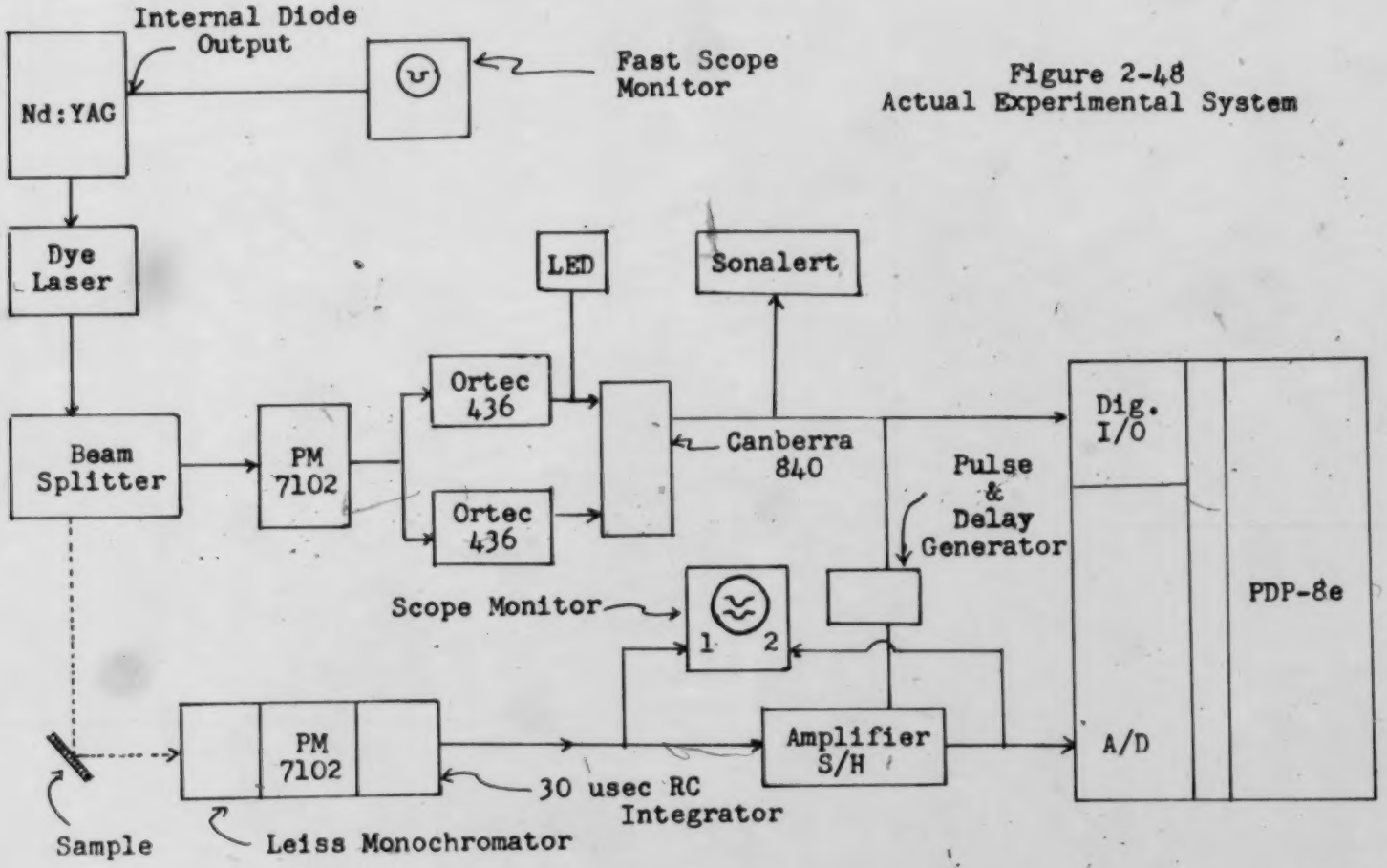


Figure 2-48
Actual Experimental System

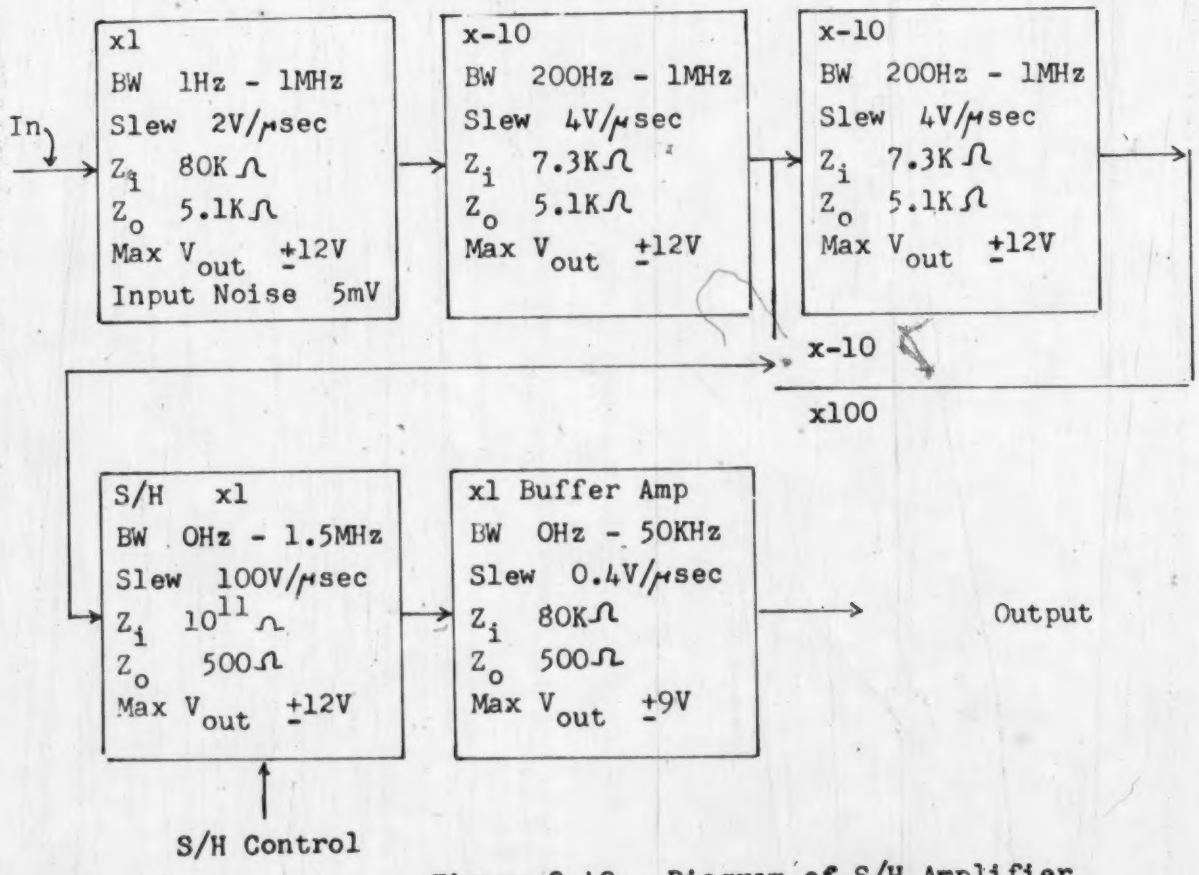


Figure 2-49 Diagram of S/H Amplifier

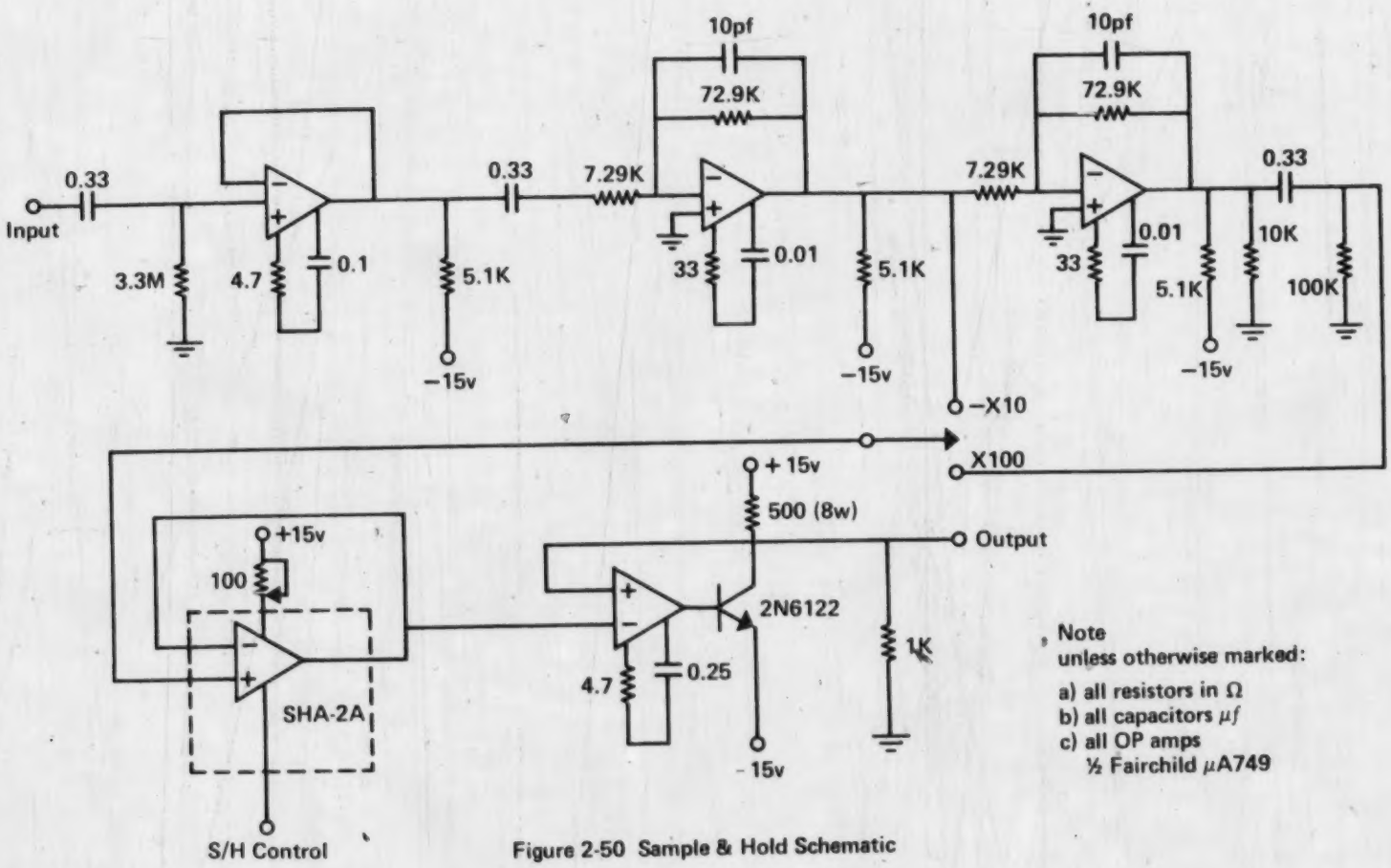


Note
unless otherwise marked:

a) all resistors in Ω
b) all capacitors μf
c) all OP amps
½ Fairchild μA749

Figure 2-50 Sample & Hold Schematic

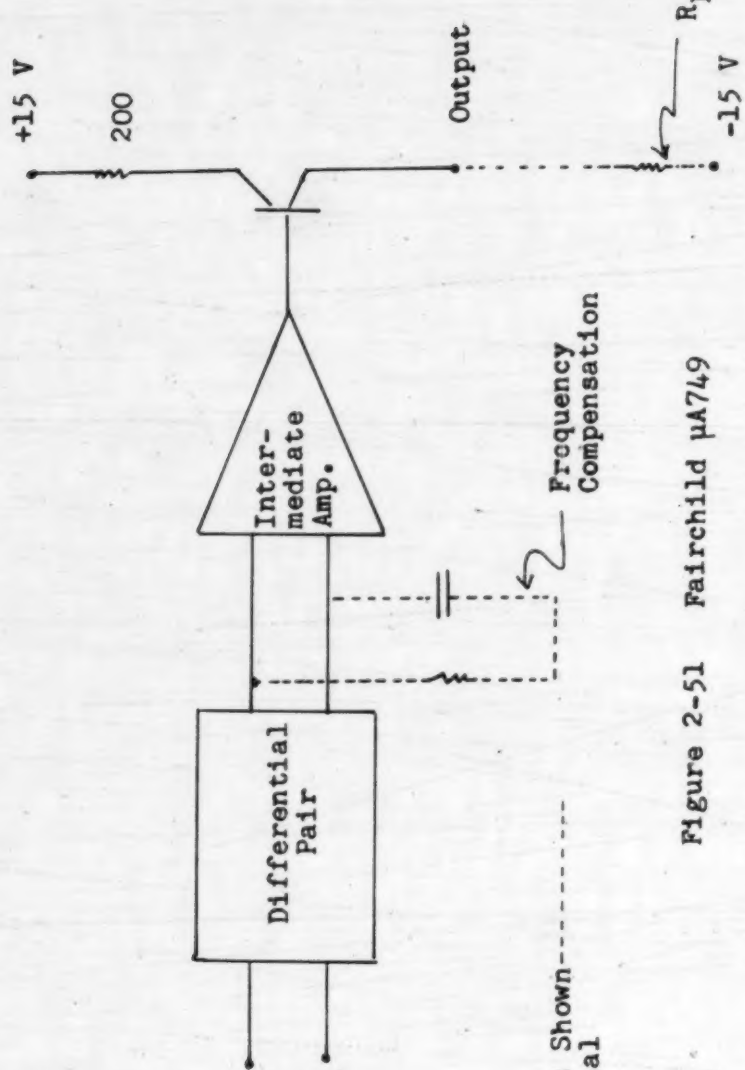


Figure 2-51 Fairchild μA749

which has a pnp transistor with an uncommitted collector for its output stage.

The sample/hold control of the SHA-2a is triggered by a pulse/delay generator which is itself triggered by the output of the coincidence date. The pulse/delay generator is present for two reasons:

1. To allow adjustment of the holding time.

2. To allow adjustment of the delay time between the experiment trigger pulse and the onset of the hold pulse. This second feature is especially important for measurement of the 0.83 μ luminescence which seems to reach a maximum nearly 110 μsec after excitation.

In our implementation the pulse-delay generator was constructed from two pulse generators: a General Radio 1340 pulse generator, and an Advance PG52 pulse generator, linked together and appropriately triggered. The Advance provides the hold pulse, and the pulse width on this generator determines the holding time. The GR-1340 is only inserted to add trigger delay for measurements of 0.83 μ luminescence; otherwise the Advance generator is triggered directly from the experiment trigger pulse.

For stable operation the holding time must be between 200 μsec and 12 ms. This insures unambiguous acquisition of the laser pulses which are separated by at least 13.3 ms, allows adequate settling time (20 μsec) for the buffer amplifier, and gives the computer adequate

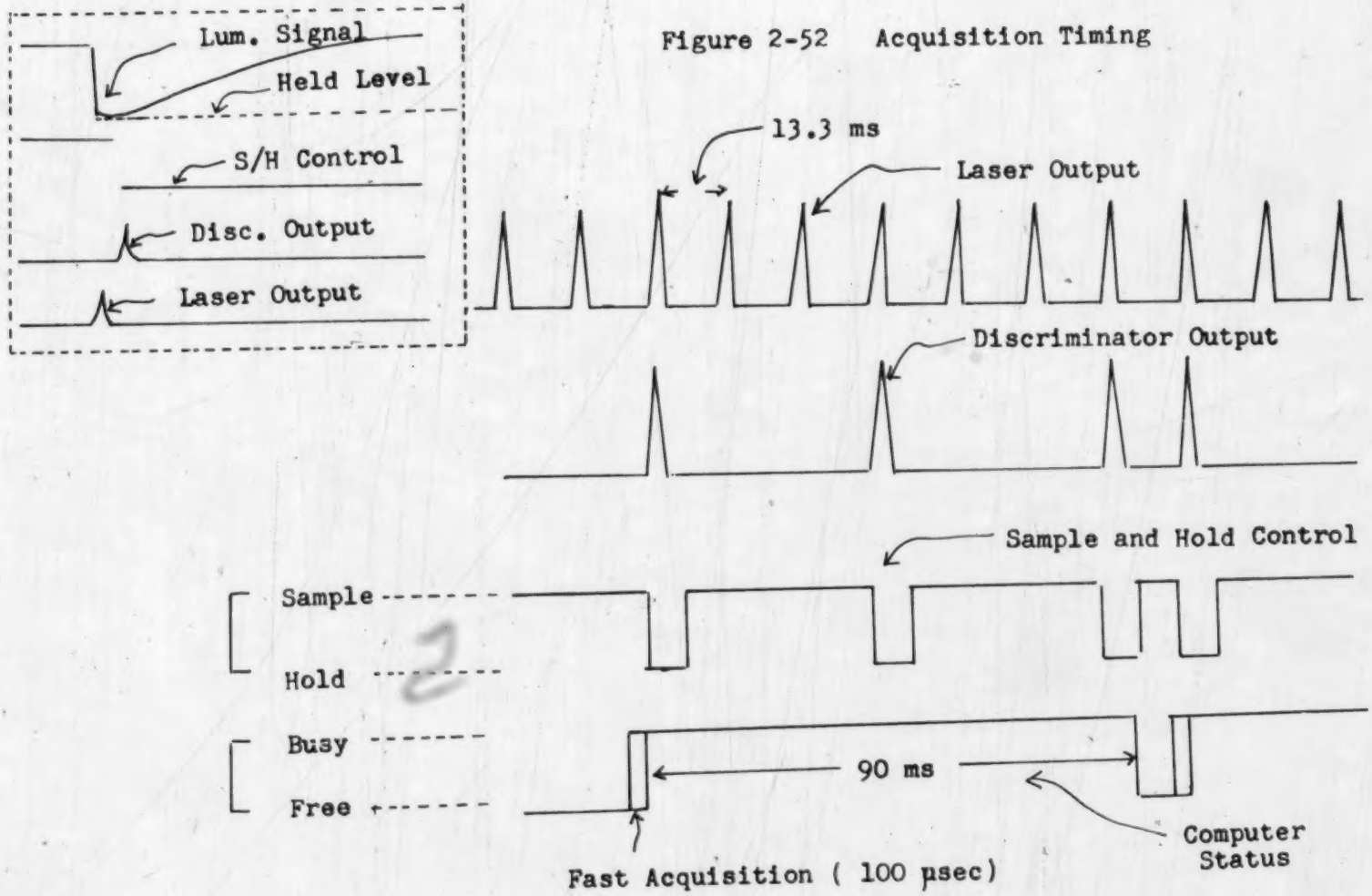


Figure 2-52 Acquisition Timing

time (100 μsec) to measure and store the signal level.

A holding time of about 10 ms is usually selected to facilitate observation of the sample-hold acquisition on the monitoring oscilloscope. Measurement by the computer will only take place if a trigger pulse arrives while the computer is not busy.

Signal averaging and further measures to reduce noise content take place in the computer. The computer used is a DEC PDP-8e with 8K words of storage. The PDP-8e operates with a 12 bit word, with two's component single precision integer arithmetic, and a memory cycle time of 1.2 μsec.

The PDP-8e is currently interfaced to two devices: an ASR-33 teletype/paper-tape-reader-and-punch; and an Analogic AN5800 A/D converter. Extensions have been made to the A/D interface to allow the implementation of two extra features:

1. 3 bits of buffered digital output capable of data transmission at rates of up to 250 KHz per bit;

2. An externally triggerable flag.

The Analogic AN5800 A/D conversion system is currently operating with a 4 channel multiplexer, an internal sample-and-hold to insure stable conversion, -10 to +10 volt range, and a 13 bit two's complement A/D converter. The 11 most significant of these 13 bits are transmitted to the computer. The multiplexer inputs are

single ended, and the multiplexer is operated in a random address mode. It has a full power bandwidth of about 200 KHz, and a settling time after channel switching of about 5 μsec. Because the sample-and-hold amplifier also requires about 5 μsec to settle (to 0.01% accuracy), it remains in sample mode for approximately 7 μsec after the convert command is issued before returning to the hold mode with the newly acquired data. (Jitter in the sample-and-hold triggering is of the order of 10 ns and not significant.) Conversion begins 0.2 μsec after the sample-and-hold acquisition, (thus allowing time for the switching transients to decay) and proceeds at the rate of about 6 μsec/bit. The total conversion time from the issuance of the convert command to the end of conversion is therefore about 86 μsec, so that the maximum throughput rate is about 11.6 KHz. With an acquisition time of about 7 μsec the A/D conversion system is capable of sampling signals up to a frequency limit of about 140 KHz. The converter suffers from slight scale, offset, and drift inaccuracies, and is accurate to only about 0.05%.

The computer system, with its limited I/O, is operated under the DECUS interpretive language FOCL/F. FOCL/F is a derivative and extension of the DEC interpretive language FOCAL. FOCL/F is a high level single user language specifically designed to be plastic and

flexible. It is capable of self-modification and allows definition in machine language of new commands and functions. It requires no supervisor since it has storage, editorial, and executive modes, and keyboard interrupt, to allow for easy development, modification, and execution of programs. By defining functions (in machine language) to handle the detailed I/O subroutines for the A/D converter and the experiment system, it is possible to retain great flexibility in the architecture of the software controlling the experiment system. Finally, FOCL/F operates with double precision (6.9 digit accuracy) floating point arithmetic, and contains the necessary supporting software for this.

The price of this flexibility and convenience is the loss of execution speed common to interpretive languages. With our current operating program about one tenth of a second is required to process each event acquired. This slightly slows data acquisition but is not a major problem.

In the specific configuration of this experiment the computer monitors four inputs from the experiment, and outputs data to the teletype and paper tape punch. When a laser pulse of suitable amplitude is produced the output of the coincidence gate sets the externally triggerable flag, and the computer measures and stores the signal level captured by the luminescence channel sample

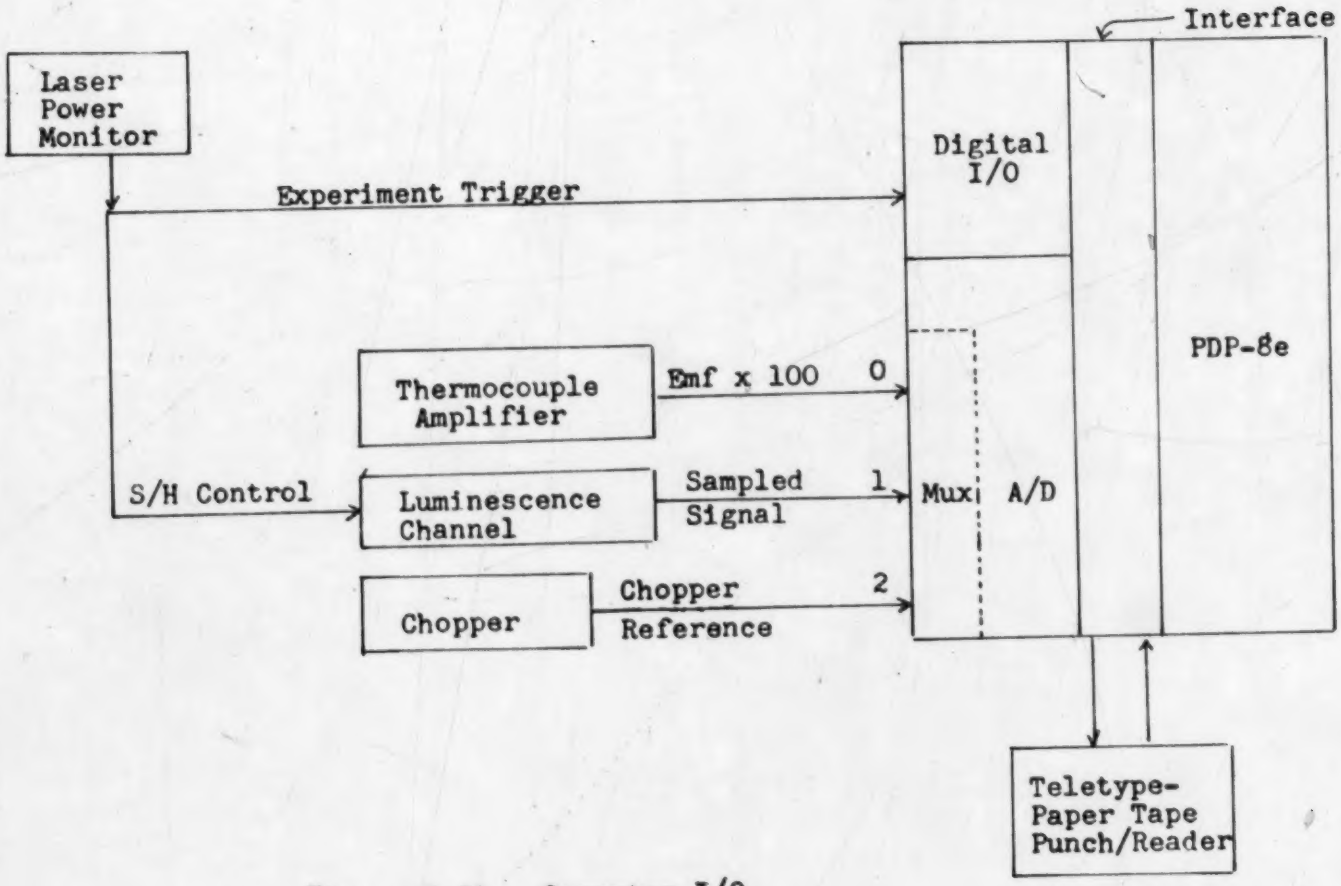


Figure 2-53 Computer I/O

Figure 2-54 Program Groupings

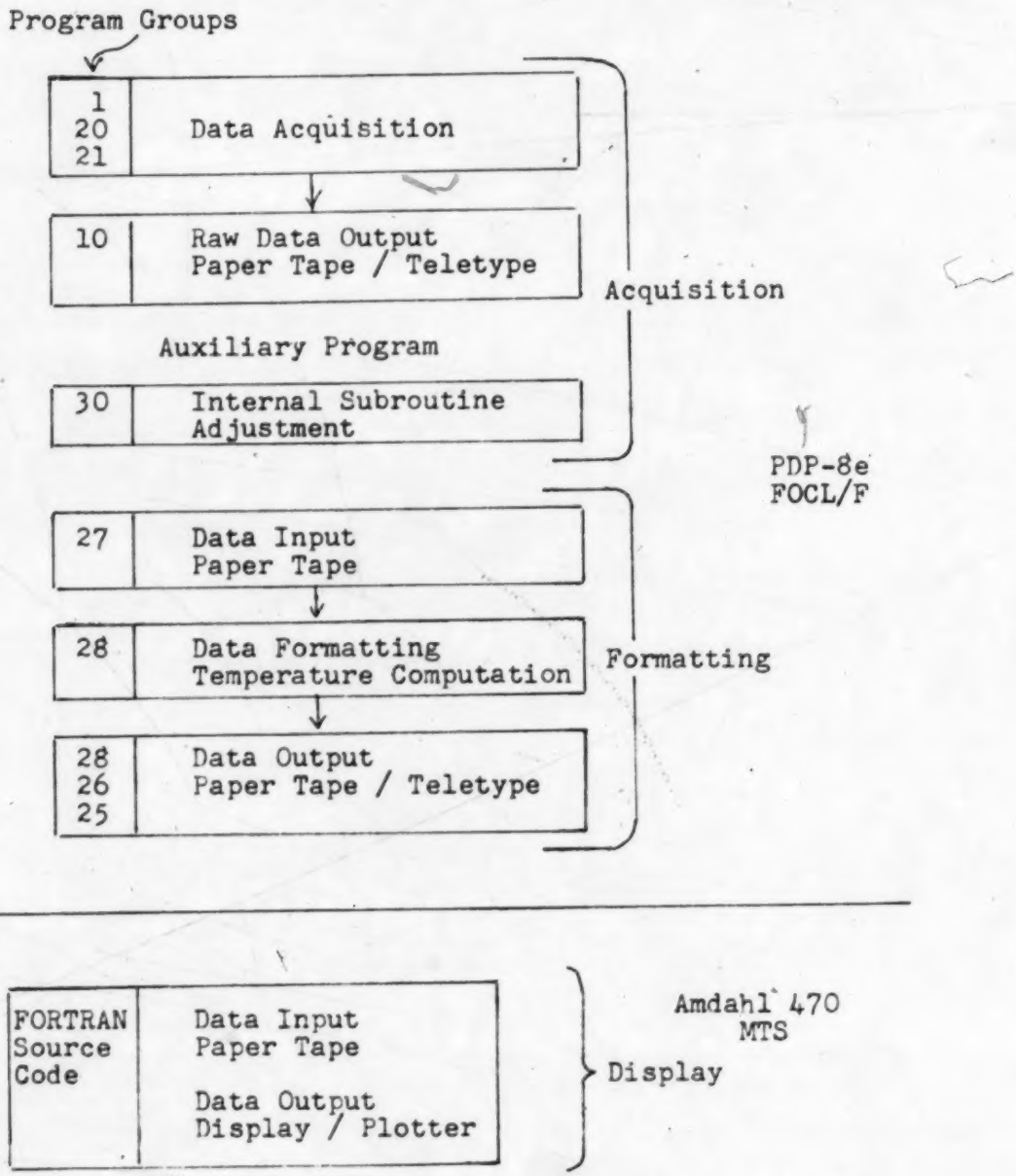

and hold the computer, then measures and stores the signal from the chopper reference output, and finally measures and stores the amplified output from the thermocouple. Thus, the luminescence signal, the state of the chopper, and the sample temperature are stored every time the computer is triggered. The data after processing is outputed to the teletype and punched out on paper tape. Since about 90 ms are required to process each event, and data events may occur as closely together as 13.3 ms, some data events are lost simply because the computer is busy and not receptive (see figure 2-52).

Because of this speed problem, the data processing done in real time, during acquisition, is minimized. As a result the data processing and formatting programs are separate from the acquisition program. To utilize the available Calcomp plotter and Tektronix CRT displays for data presentation, auxiliary programs were written for the MTS system. Data is transferred from program to program and machine to machine by means of punched paper tape. The organization and grouping of these programs and program segments is shown in figure 2-54. The actual source listing of all programs used are in Appendix I.

The acquisition program (FOCL/F groups 1, 20, and 21) acquires and organizes the data, producing a sequence of paired averages. Each pair consists of an averaged thermocouple e.m.f., and the averaged luminescence signal

level, so that the computer monitors L(T) at the externally specified $\lambda_i$, $I_i$, and $\lambda_o$. These pairs of averages are printed on the teletype in real time as they are acquired and computed. When sufficient data has been acquired, the operator stops the active acquisition with a keyboard interrupt, and initiates the output segment of the program (group 10) which produces a punched paper tape containing all the acquired data.

The data on this tape may then be re-entered into the computer. In the computer, the data is edited and the thermocouple e.m.f.'s converted to absolute temperatures. A labeled formatted tape with the sequence of temperature-luminescence pairs is then punched. This is achieved with the program material in FOCL/F groups 25, 26, 27 and 28.

The labeled formatted data may then be displayed graphically or plotted by means of programs written (in FORTRAN source code) for the Amdahl 470 MTS system.

Of greatest interest are the details of the data acquisition program. This program is a very straightforward averaging and noise subtraction routine. Because of the presence of the mechanical chopper in the path of the optical excitation, it is possible to maintain two separate averages: an average of luminescent response to excitation, and an average of electrical noise present under identical conditions with no

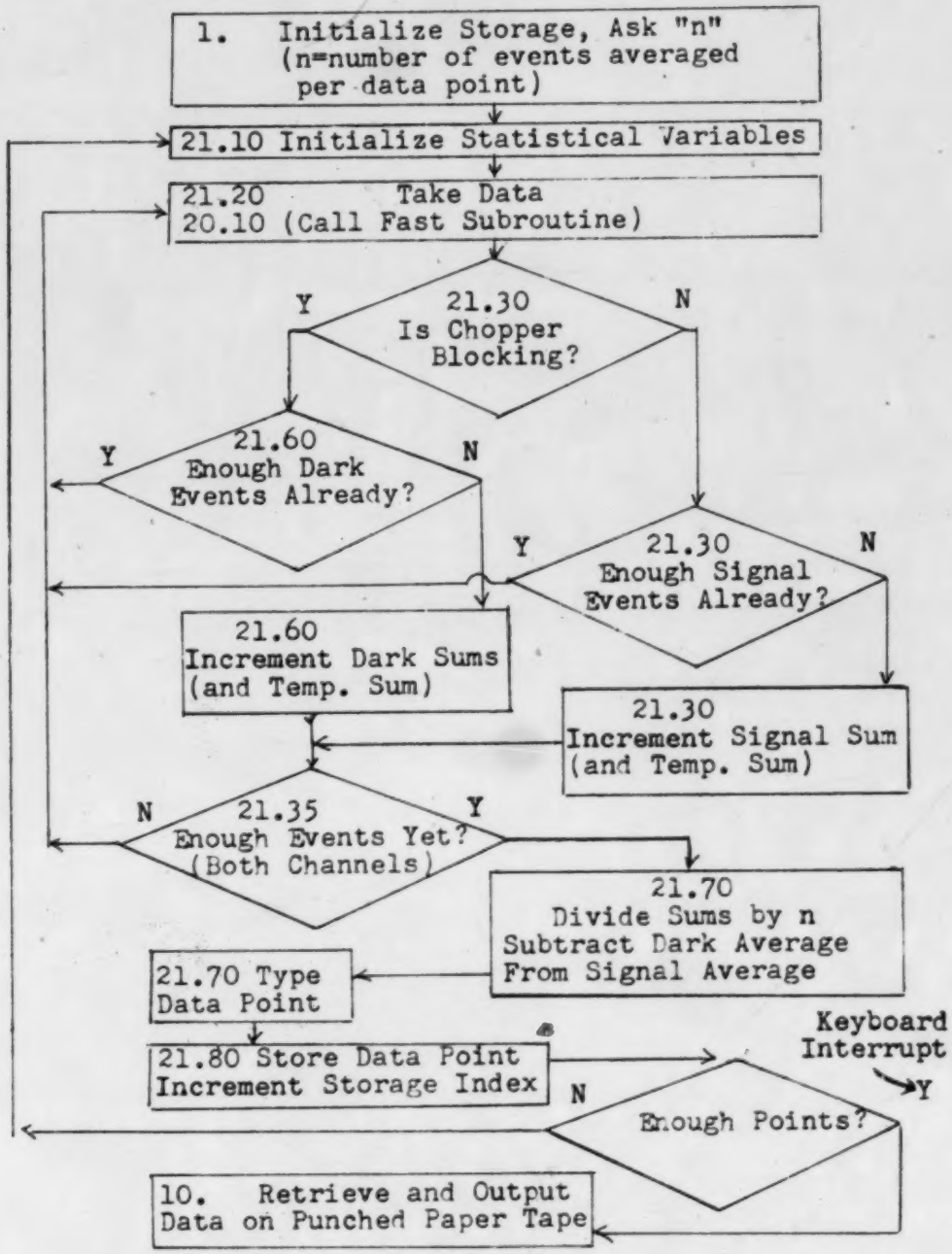


Figure 2-55 Acquisition Program

excitation. By subtracting the second from the first (dark from excited), it is possible to eliminate the effects of any offsets in the system (dark current, D.C. amplifier offsets, etc.) as well as the effects of any background pulse noise that might occur synchronously with the luminescence.

The number of events to be counted in each average, n, is specified by the operator at the program's initialitation (n is usually 50). The data acquisition program then begins by setting three sums equal to zero: a "temperature" (thermocouple e.m.f.) sum, a "dark" sum (luminescence channel, chopper blocking), and a "signal" sum (luminescence channel, chopper transmitting). Acquisition is initiated by calling the specially defined subroutine FNEW. When a suitable laser pulse occurs this subroutine will return three values: the luminescence signal, the chopper reference signal, and the amplified thermocouple e.m.f. The program will then decide according to the chopper state which sum should be incremented (if the chopper state is ambiguous, i.e. if the reference level is halfway between the light and dark values, the event is rejected, and the program returns to wait for a new event.) Before incrementing either the "dark" or "signal" sums the program checks whether a sufficient number of events have already been acquired in the selected channel. If the selected channel has sufficient

events (i.e. if the newly acquired event was a "dark" event, and n dark events have already been acquired) the newly acquired event will be rejected, and the program will return to await new events. If not, the selected sum will be incremented.

When either of the two luminescence channels is incremented, the thermocouple e.m.f. will then also be added to the "temperature" sum. The program now checks whether a sufficient number of events have yet occurred in both channels. If not the program returns to FNEW to wait for another event.

If n events have been reported in both luminescence channels (i.e. n events in the "dark" channel and n events in the "signal" channel) the program then divides the "signal" and "dark" sums by n and the "temperature" sum by 2n. The "dark" average is then subtracted from the "signal" average to produce a true average of the luminescence signal.

The program then turns the teletype on and types the acquired data point. The pair of averages will also be stored in a pair of long vectors and the storage index incremented.

When a sufficient number of data points (averaged pairs) have been acquired the operator may stop acquisition with a keyboard interrupt and direct the program to sequentially retrieve the data points and punch them

out on a paper tape.

Averaging the signal over n events reduces random fluctuations by a factor of $\sqrt{n}$ so that typically with 50 events to each average this reduction factor is about 7. The two most significant sources of error affected are: the random noise from the photomultiplier and amplifiers which will be reduced (in the mean) to about 0.7 mV (of effective input noise); and the fluctuations in signal due to the finite width of the discriminator aperture, thus a typical 7% fluctuation in signal (allowed by the discriminator) is reduced to a 1% fluctuation in the mean.

An earlier generation of this program also stored (during acquisition) the sums of the squares of the individual events thus allowing immediate specification of the standard deviation. This feature was eliminated for two reasons:

1. It required a considerable amount of extra computing time, and thus increased the system "dead time".

2. The consistency and reproducibility can be directly (and more authentically) measured by taking repeated readings under constant conditions.

The detailed structure of the fast machine language subroutine FNEW is very simple and shown in figure 2-56. The subroutine is called with the command format "Set Y= FNEW(X)". The quantity specified by the value

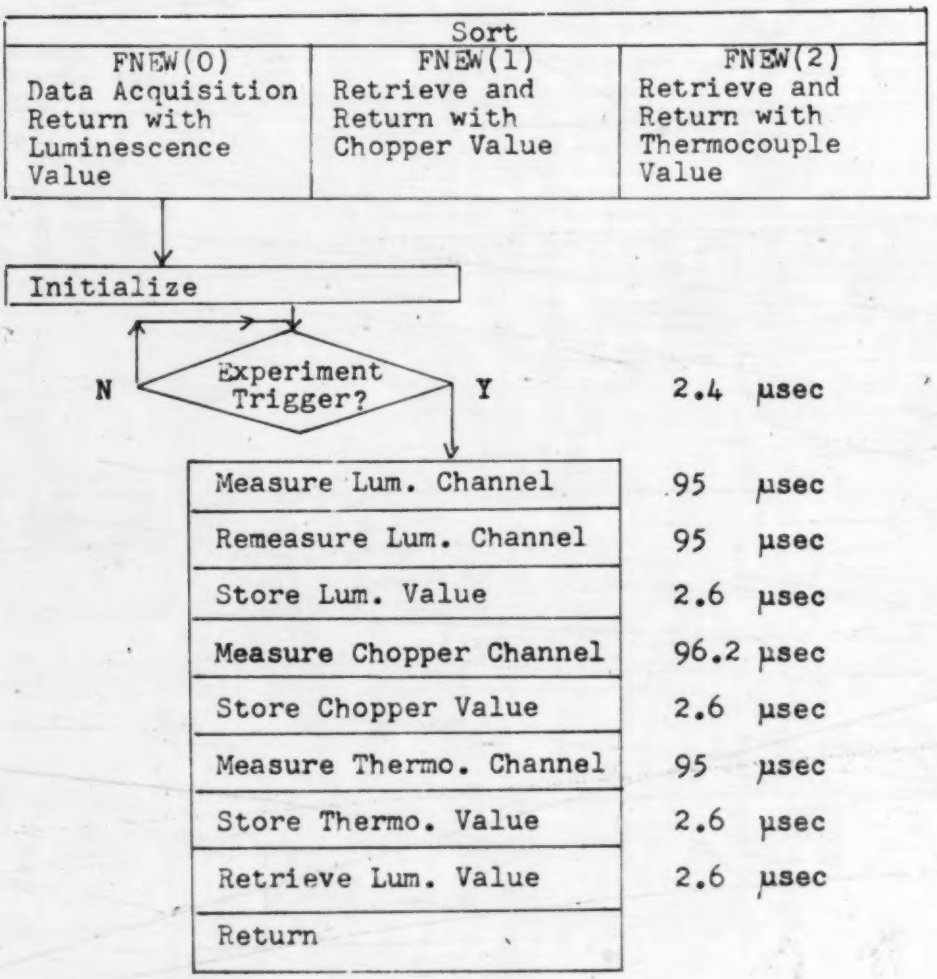


Figure 2-56 Fast Acquisition Subroutine

of the function is controlled by the value of its argument: FNEW(0) returns with the luminescence value, FNEW(1) returns with the chopper value, and FNEW(2) returns with the thermocouple value. This triple return is necessitated by the fact that function returns must be scalar in FOCL/F. As a result the first part of the FNEW subroutine simply sorts to select which of the three routines to execute. FNEW(0) however is special: it is also the call for the fast data acquisition routine.

The fast data acquisition routine begins in wait loop with a 2.4 μsec cycle time. Escape occurs only when the externally triggerable flag is set. Triggered, the routine calls an A/D subroutine which measures the signal level at multiplexer input 1 (the luminescence signal). This measurement then is repeated. Only the second value is stored. The purpose of the first measurement is simply to clear the circuit, and to allow the sampled luminescence signal to settle accurately in the electronics preceding the A/D converter module. Each of these measurements takes about 100 μsec, so that approximately 200 μsec after the experiment trigger, the chopper reference on multiplexer input 2 is measured and stored. (It is retrieved with FNEW(1).) The amplified thermocouple e.m.f. (on multiplexer input 0) is then measured and stored (to be retrieved with FNEW(2)).

Finally, the measured luminescence value is retrieved, and the subroutine returns to the main program.

The delays to the luminescence and chopper measurements (of 100 μsec and 200 μsec respectively) are responsible for slight errors. The SHA-2a sample-and-hold has a maximum droop rate of 100 μV/μsec, so that the 100 μsec delay could produce a droop in the held level of as much as 10 mV. The sample-and-hold is however at the output of the ×100 amplifier, so that this 10 mV corresponds to a loss of only 0.1 mV of signal at the input.

Considering the chopper error, the 200 μsec measurement delay is very short relative to the chopper rate of 13 Hz (aperture time 38 msec). As a consequence the simple probability of error in measuring the chopper state is about 0.005. This figure will however be further reduced with the rejection by the main program of transitional chopper states.

On an ordinary sample of 50 "signal" events and 50 "dark" events each error in evaluation of the chopper state would create a 2% decrease in the value of the difference "signal" minus "dark". Since the total sample size is 100, and the probability of this binomially distributed error is at worst 0.005, the expected number of chopper errors per sample is $100 \times 0.005 = 0.5$, so that the expected percentage error is at worst 1%.

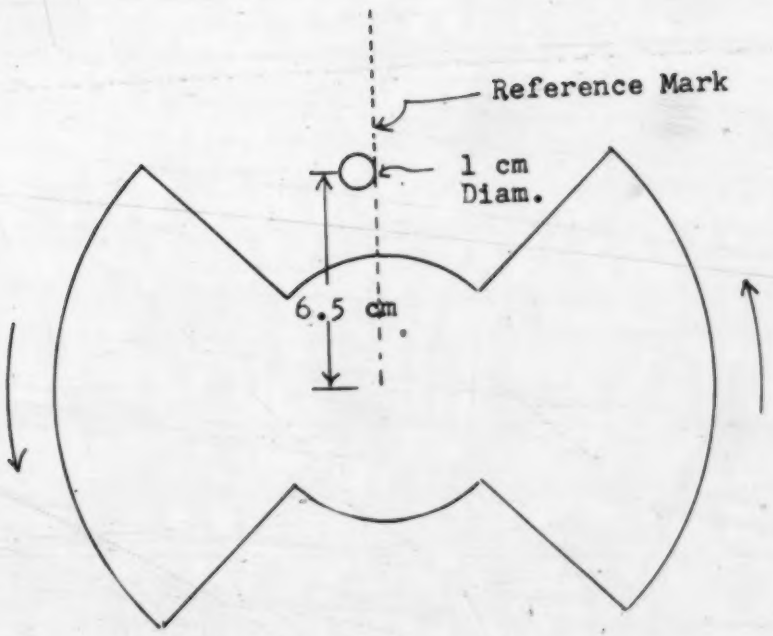


Figure 2-57 Chopper Geometry

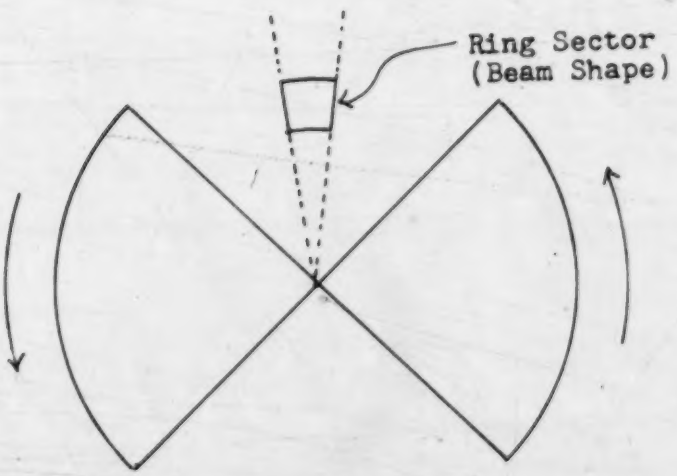


Figure 2-58 Ring Sector Approximation

To allow adjustments in FNEW a special auxiliary subroutine is present in FOCL/F group 30. The subroutine is principally used to make the alterations necessary for measurement of the 0.83 μ luminescence. Because of the slow rise time of this luminescence acquisition by the external sample-and-hold is delayed by about 110 μsec so that a similar delay must be inserted between the escape from the loop and the first acquisition. The subroutine in group 30 is also used to remove this delay before returning to normal operation.

One last topic remains, this is a discussion of some specific errors generated through the use of the chopper. The chopper aperture spans approximately 10 cm at the radius where the 1 cm diameter dye laser beam passes through. As a result for about 10% of the transmission time only a part of the laser beam is transmitted (as the chopper blade partially blocks the beam), and for about 10% of the dark time a part of the laser beam leaks through.

To simplify the mathematics let us assume that the beam shape is that of a sector of a ring, and that the aperture spans a sector angle v times that of the ring sector. Considering the transmission as a function of time, we then have for the open (transmitting) cycle:

$$T_o(t) = vt/\tau \qquad \text{for} \quad 0 \leq t < \tau/v$$

$$T_o(t) = 1 \qquad \text{for} \quad \tau/v \leq t \leq \tau$$

where $\tau$ is the aperture time; and we have for the dark cycle:

$$T_d(t) = (1 - vt/\tau) \quad \text{for} \quad 0 \leq t < \tau/v$$

$$T_d(t) = 0 \quad \text{for} \quad \tau/v \leq t \leq \tau \ .$$

The expected values of transmission therefore are:

$$E(T_o) = 1/\tau \int_0^\tau T_o(t)\ dt = 1 - (1/2v)$$

$$E(T_d) = 1/\tau \int_0^\tau T_d(t)\ dt = 1/2v \ .$$

Further,

$$E(T_o^2) = 1/\tau \int_0^\tau T_o^2(t)\ dt = 1 - (2/3v)$$

$$E(T_d^2) = 1/\tau \int_0^\tau T_d^2(t)\ dt = 1/3v$$

so that

$$\sigma_o^2 = \sigma_d^2 = \frac{4v - 3}{12v^2} \ .$$

For the difference $T = T_o - T_d$ we therefore have:

$$\mu_T = 1 - (1/v)$$

$$\sigma_T = \sqrt{\frac{4v - 3}{6v^2}} \ .$$

For a sample size of n we therefore have:

$$\sigma_{T_n} = \sqrt{\frac{4v - 3}{6nv^2}}$$

so that p the percentage of random error in the acquired data is:

$$p = 100 \times \sigma/\mu = \frac{100\sqrt{\frac{4v - 3}{6n}}}{v - 1} \quad .$$

For our particular case the sample size is 50, and the 1 cm laser beam interrupts the chopper blade about 6.5 cm from the center of the chopper so that:

$$v = \frac{6.5\pi}{2} = 10.2$$

$$\mu = 0.902$$

$$p = 3.86 \quad .$$

Thus this transmission timing error attenuates the measured signal by about 10% and contributes a random error of about 4% to the measured averages. Since the attenuation is a constant systematic error, and we are not making absolute measurements, it is of little significance. Unfortunately however the 4% random error is one of the most significant in the entire experimental system. It can easily be eliminated (for future data acquisition) by simple RC filtering of the chopper reference signal. This will prolong the "indeterminate"

states so that the partial transmissions and leakage will be rejected as data.

## 2.5 Summary

In brief, considering the experimental system as a whole, we are able to measure the near IR photoluminescent response to pulsed visible excitation. The system is currently set to measure the luminescence as a function of temperature at specified excitation wavelength, excitation intensity, and output wavelength (wavelength of measurement). Further the excitation wavelength, excitation intensity, and wavelength of measurement are all variable.

Specifically, the sample temperature can be controlled and measured to an accuracy of better than 3 K over the range 77 K to 340 K. The excitation wavelength is variable over the range 0.5700 μ to 0.6350 μ with a spectral purity of 0.0025 μ. The excitation is in the form of 150 ns pulses whose power level is directly variable between 1 and 100 watts.

The detection system is capable of monitoring luminescent emission from 0.6 μ to 1.0 μ with a spectral resolution of better than 0.033 μ. The system is further capable of detecting emissions of the order of $10^{-3}$ watts (at the sample surface), and of measuring emissions

of $10^{-2}$ watts or greater with an accuracy of better than 5%. Finally the system is reasonably quick, convenient, and efficient in operation.

# CHAPTER 3

# RESULTS

## 3.0 Results

The ultimate goal of the specific program of research established here was to measure the luminescence as a function of excitation wavelength, excitation intensity, and sample temperature for a number of carefully prepared samples. The development by other workers in our research group of improved annealing techniques promised to make available samples with reproducible characteristics. Unfortunately due to time limitations and equipment breakdowns only the most preliminary results have so far been obtained.

The measurements reported here are all on the luminescence of one specific single crystal sample prepared by Duvvury and designated SC-11. It was prepared by slow oxidation of a 0.5 mm thick strip of copper about 10 cm by 2.5 cm. The oxidation was done at 1000 C in a nitrogen atmosphere with slow oxygen feed. Oxidation took about 4 days. The completely oxidized sample was then annealed in a 5% oxygen 95% nitrogen atmosphere for about 20 hours. It was cooled in high vacuum (approximately $10^{-4}$ torr) at an approximately uniform rate of 150 C/hour. This produced a

sample which by its behavior would seem to be slightly copper enriched.

Although many specific choices are possible in the variation of the other experimental parameters $(\lambda_i, I_i, T, \lambda_o)$ the data were taken by varying T at fixed $\lambda_i, I_i$, and $\lambda_o$. The luminescence was measured in triplet data sets, one temperature variation being made for measurement at each of the three output peaks (0.72 μ - Leiss setting 918, 0.83 μ - Leiss 931, 0.93 μ - Leiss 938) so that we have at each excitation wavelength $L_{0.72}(T)$, $L_{0.83}(T)$, and $L_{0.93}(T)$. The excitation wavelength was altered by steps of about 120 Å so that we have triplet data sets at each of 5960 Å, 6080 Å, 6200 Å, and 6320 Å. (Additional data sets were taken for the 0.93 μ luminescence at an excitation wavelength of 5905 Å.) The incident intensity was held constant. $I_i$ was chosen to be a moderate level (about 30 watts) to allow for easy operation and stable variation of wavelength.

Although it might seem of more interest to measure $L_{\lambda_o}(\lambda_i)$ at specified T, this is technically difficult with our dye laser. The beam shift caused by the chromatic dispersion makes it very difficult to continuously sweep excitation wavelength and maintain well focused optics. It is easily possible however to measure $L_{\lambda_i,T}(\lambda_o)$ as was done in our preliminary paper[68].

The positions of the output peaks seem to be moderately stable so that measurements at the peaks yield fairly good data.

Certain systematic errors not discussed in Chapter 2 complicate comprehensive measurements. They are:

1. Misalignment of the collimator
2. Misalignment of the Leiss optics (equivalent to shifts in sample position)
3. Frost, vapor, or condensation in the optical path.

Within a given data set (set of points taken over varying temperatures at specified $\lambda_i, \lambda_o$) errors 1 and 2 do not seriously affect the quality of the results. Although they may decrease the absolute signal level the relative temperature function will remain approximately the same. It is unfortunate however that all three of these phenomena decrease the absolute signal level. As a result comparisons of output intensity at different wavelengths of excitation are slightly tenuous. The best that can be said is that of multiple data sets which have been taken under "identical" conditions, the one which shows the consistently largest values is most likely to be the truest data. For this reason it is a preferred procedure to take more than one data set for

each set of excitation conditions to allow for direct comparison and verification.

The results are shown in figures 3-1 to 3-24. These fitures are grouped according to output wavelength and appear in order of increasing wavelength. Within each group the results appear in order of increasing excitation wavelength. Where more than one data set has been taken at the same wavelength of measurement and excitation wavelength, the data is merged if very consistent. If there is significant variation in data each temperature set is first displayed separately, and then the merged data.

The excitation wavelength, wavelength of measurement (Leiss setting), and numerical label of the displayed data are shown on each figure. The data shown in figures 3-1 to 3-24 are all normalized so that the maximum value occurring in each temperature set appears as 10. A detailed list of the acquired data can be found in Appendix II.

Examining the figures a number of things are obvious:

1. The shape of the 0.72 μ luminescence temperature function seems to vary little with respect to wavelength of excitation. This is especially clear upon examining figure 3-25 which shows the 0.72 μ output curves overlaid for the various wavelengths of excitation. The

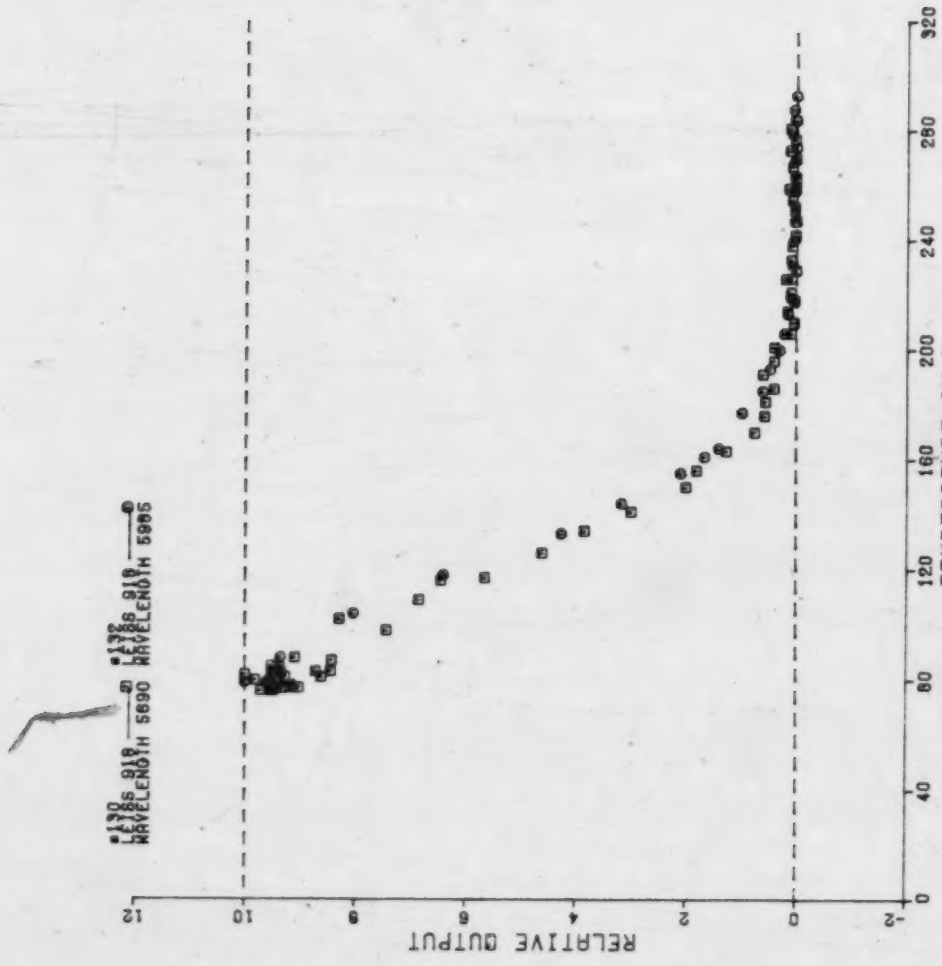


FIGURE 3-1 0.72 μ LUMINESCENCE EXCITED BY 5960 Å

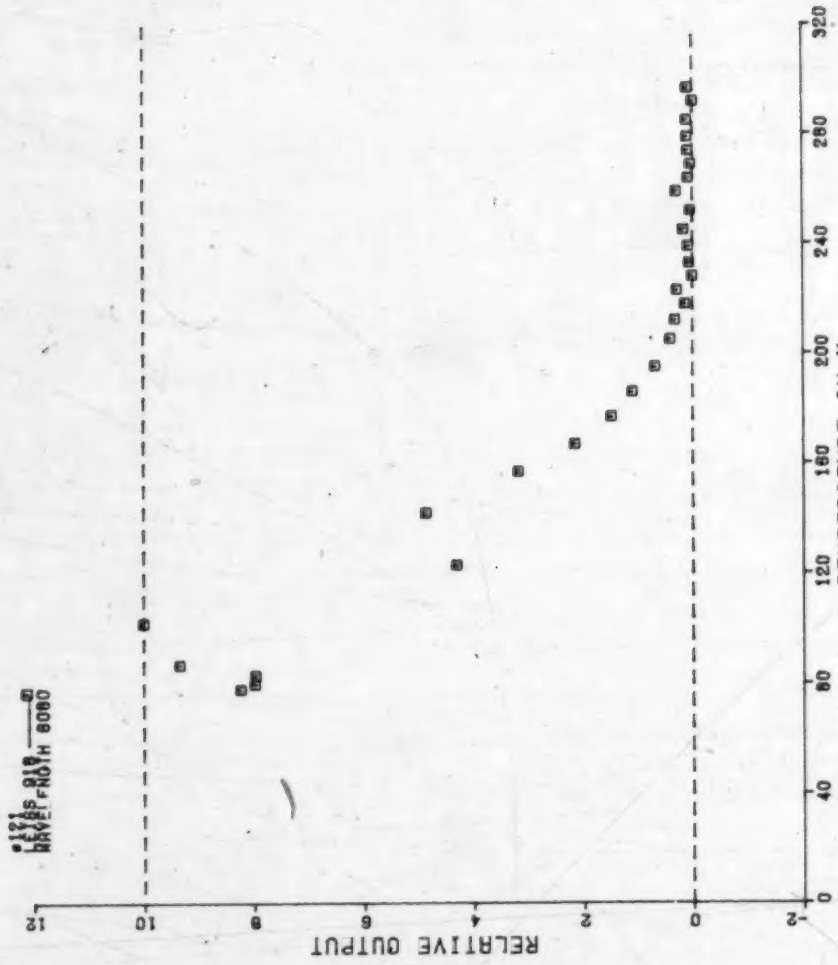


FIGURE 3-2 0.72 μ LUMINESCENCE EXCITED BY 6080 Å

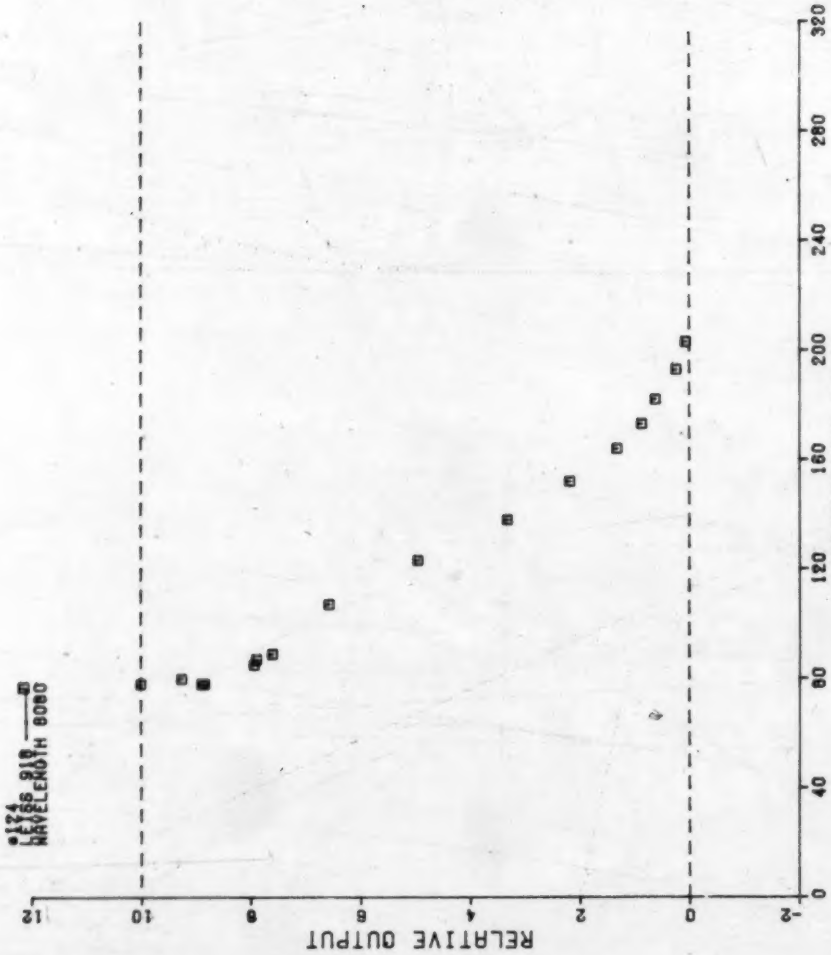


FIGURE 3-3 0.72 μ LUMINESCENCE EXCITED BY 6080 A

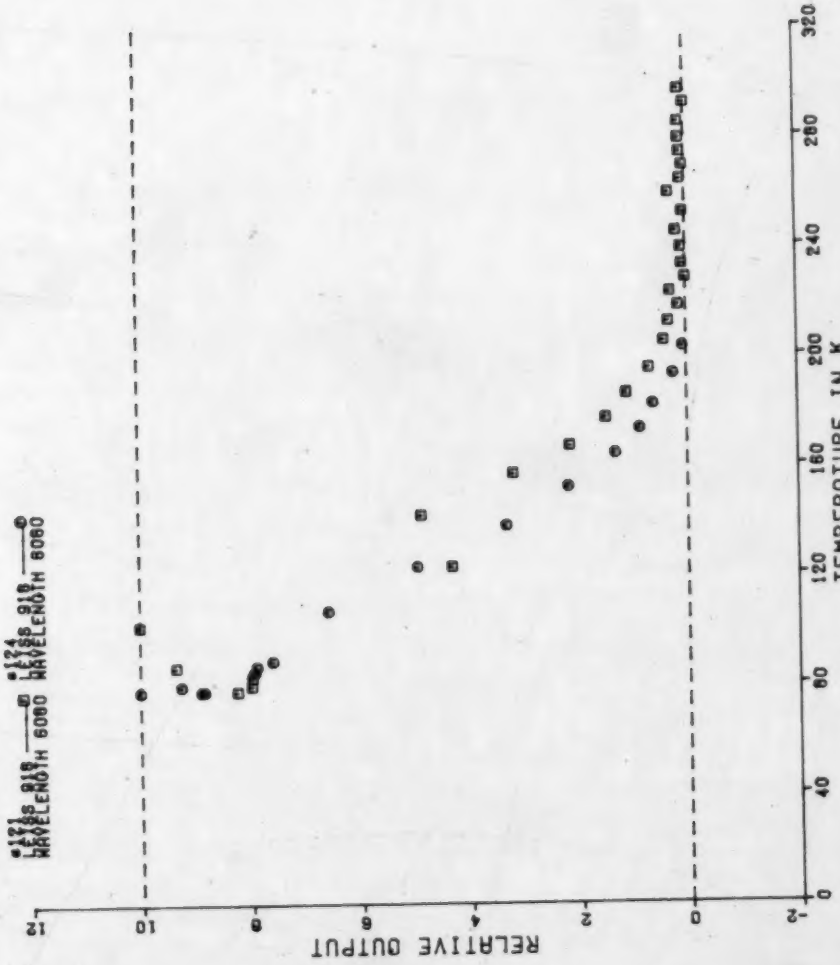


FIGURE 3-4 0.72 μ LUMINESCENCE EXCITED BY 6080 A

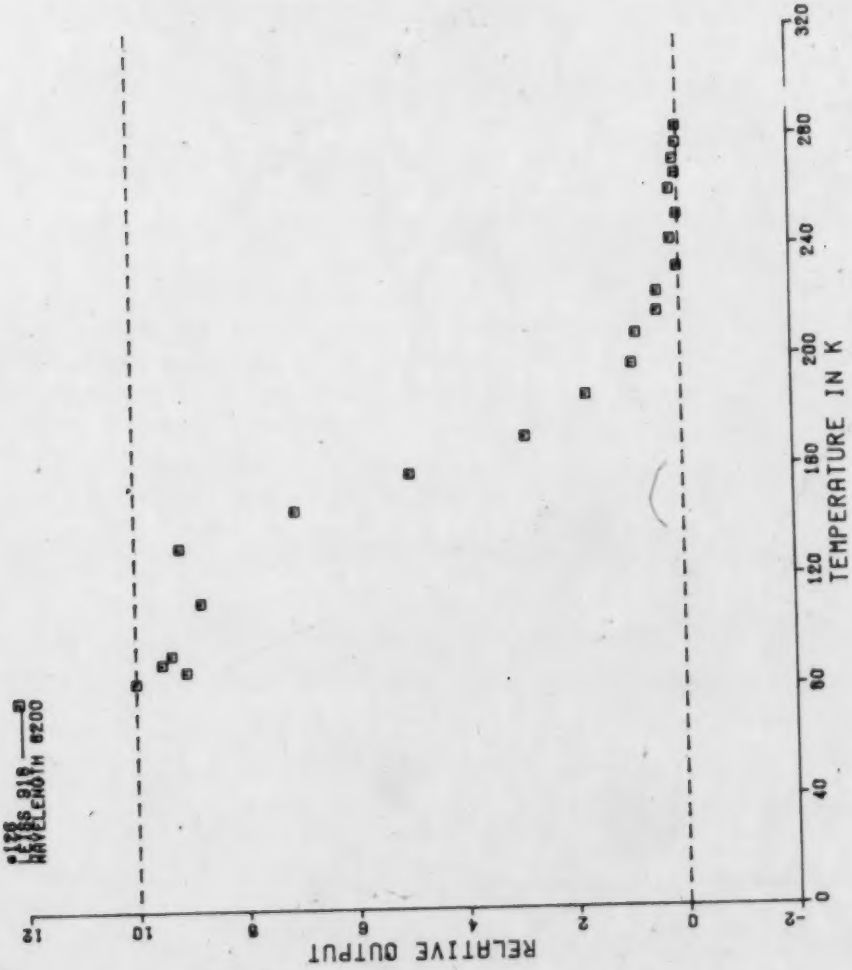


FIGURE 3-5 0.72 μ LUMINESCENCE EXCITED BY 6200 A

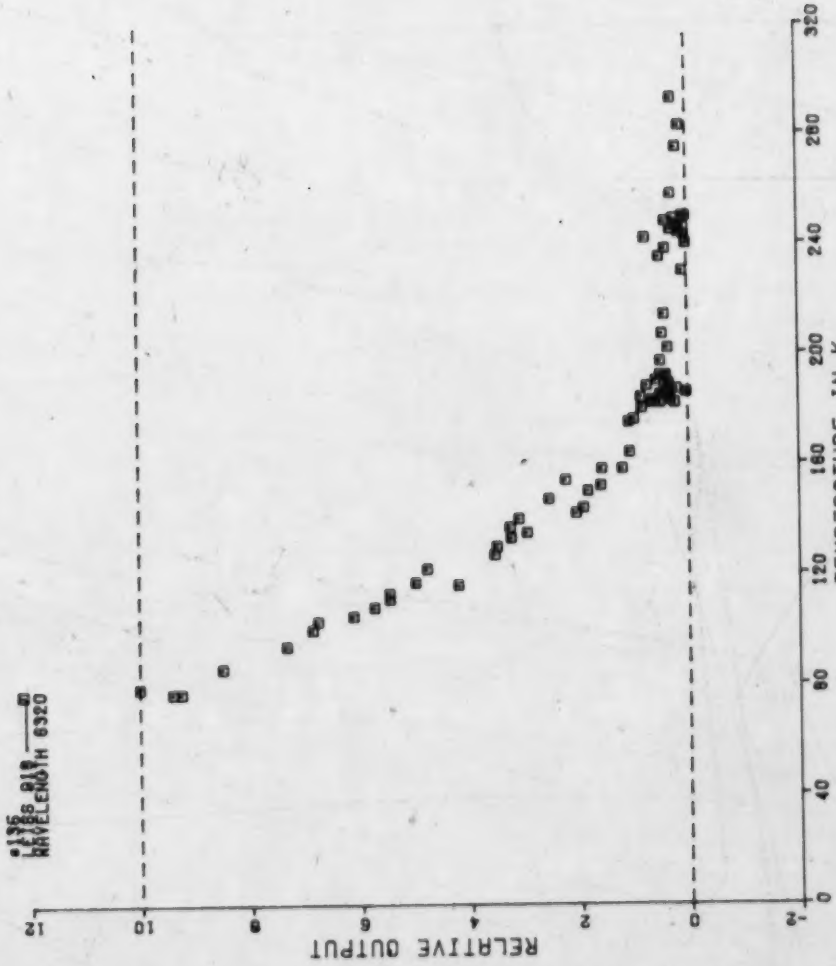


FIGURE 3-6 0.72 μ LUMINESCENCE EXCITED BY 6320 A

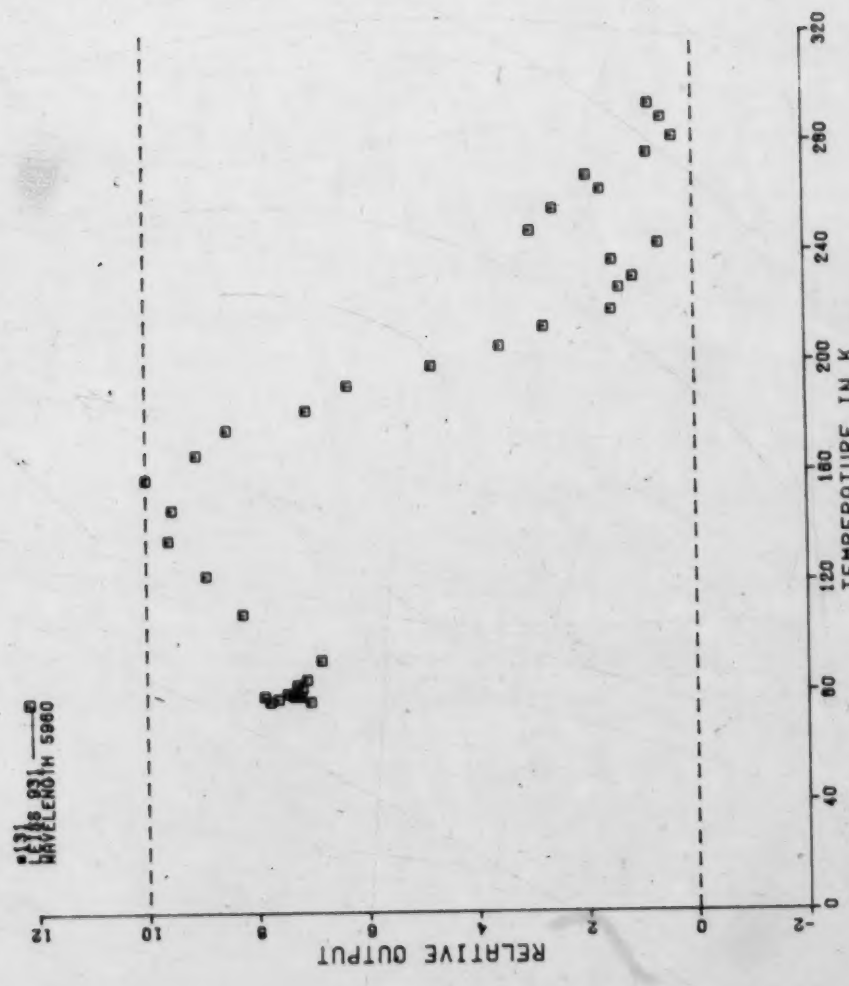


FIGURE 3-7 0.83 μ LUMINESCENCE EXCITED BY 5960 A

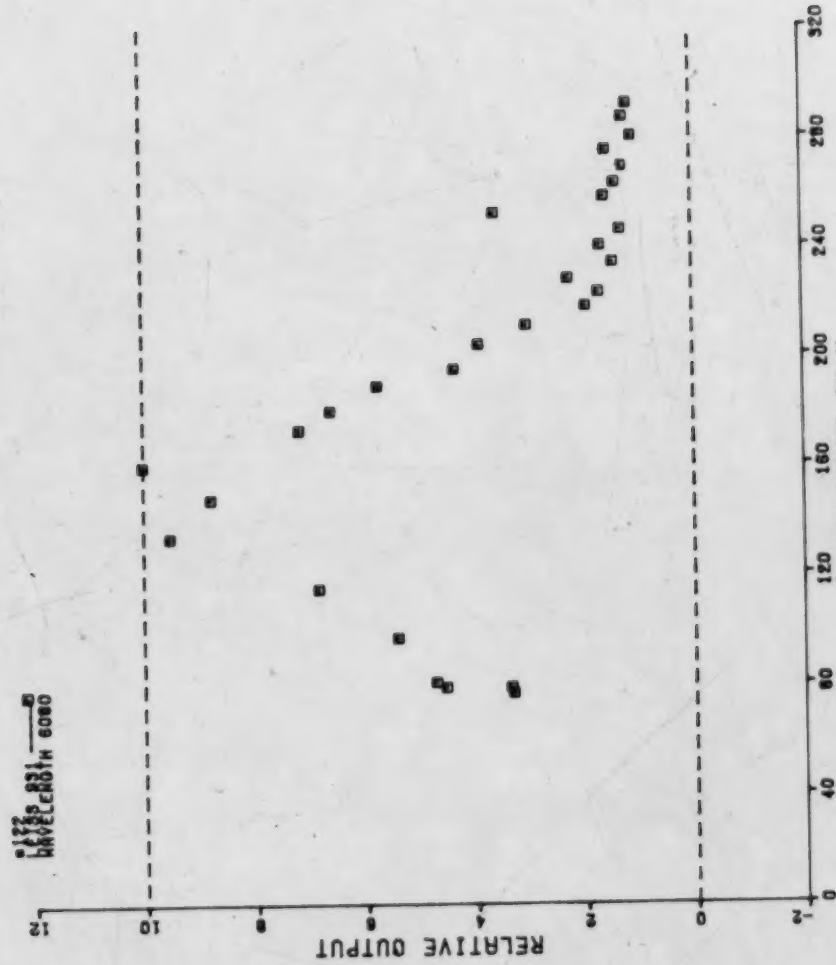


FIGURE 3-8 0.83 μ LUMINESCENCE EXCITED BY 6080 A

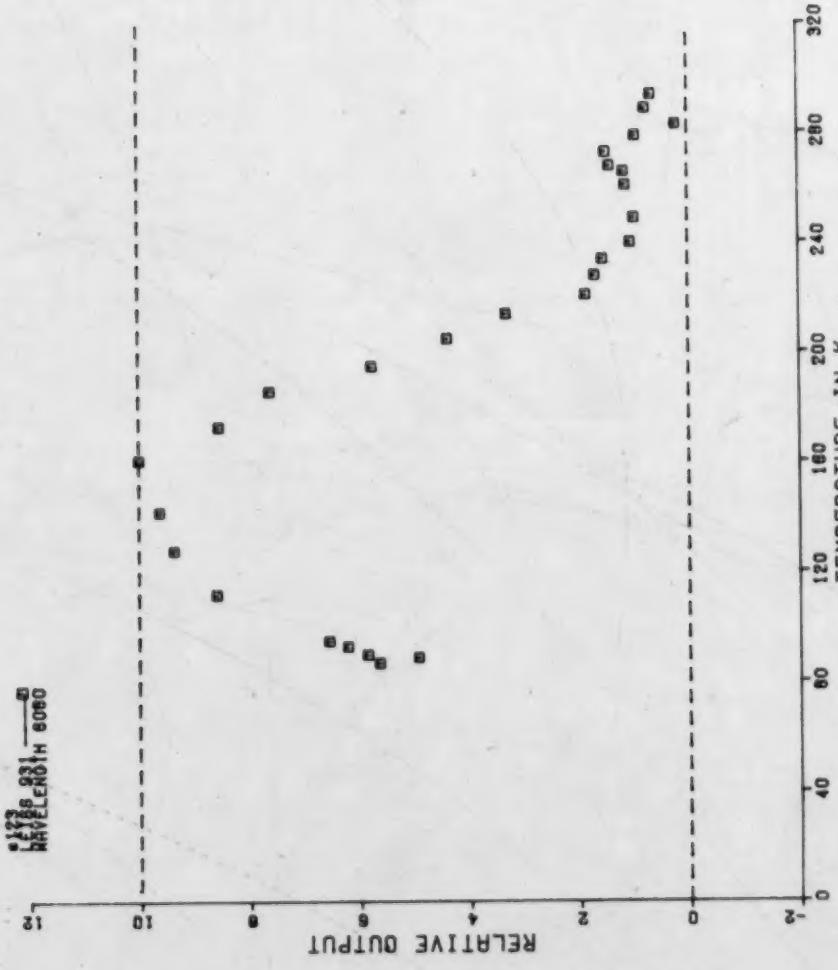


FIGURE 3-9 0.83 μ LUMINESCENCE EXCITED BY 6080 A

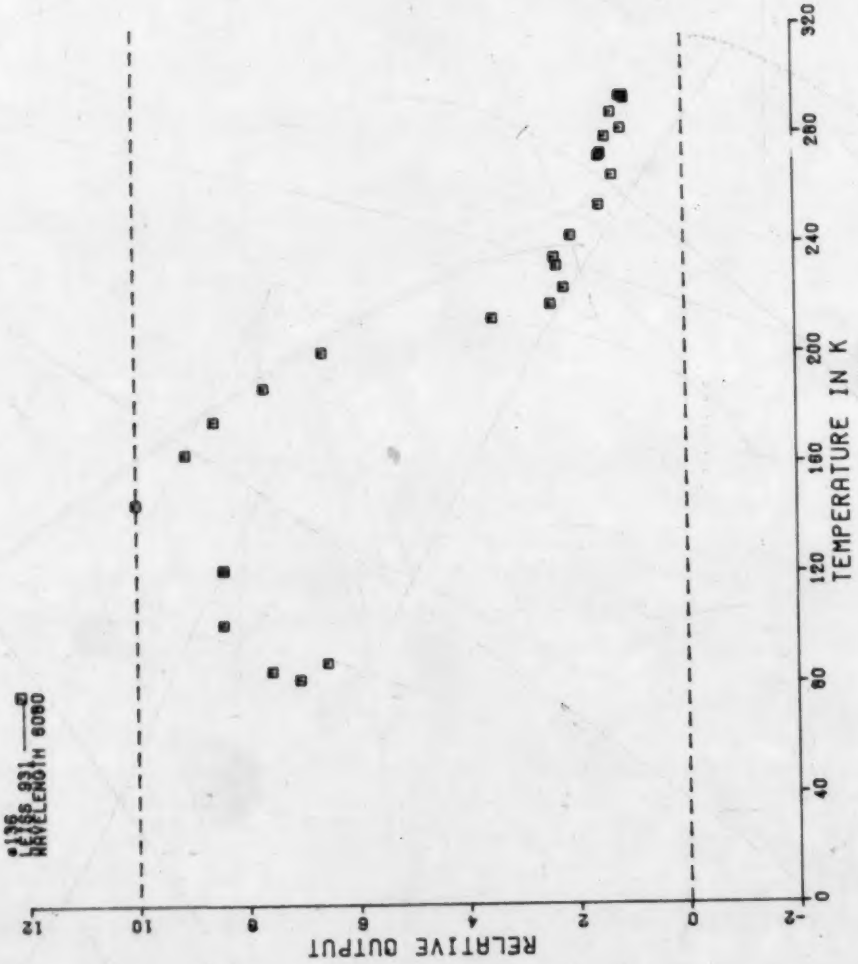


FIGURE 3-10 0.83 μ LUMINESCENCE EXCITED BY 6080 Å

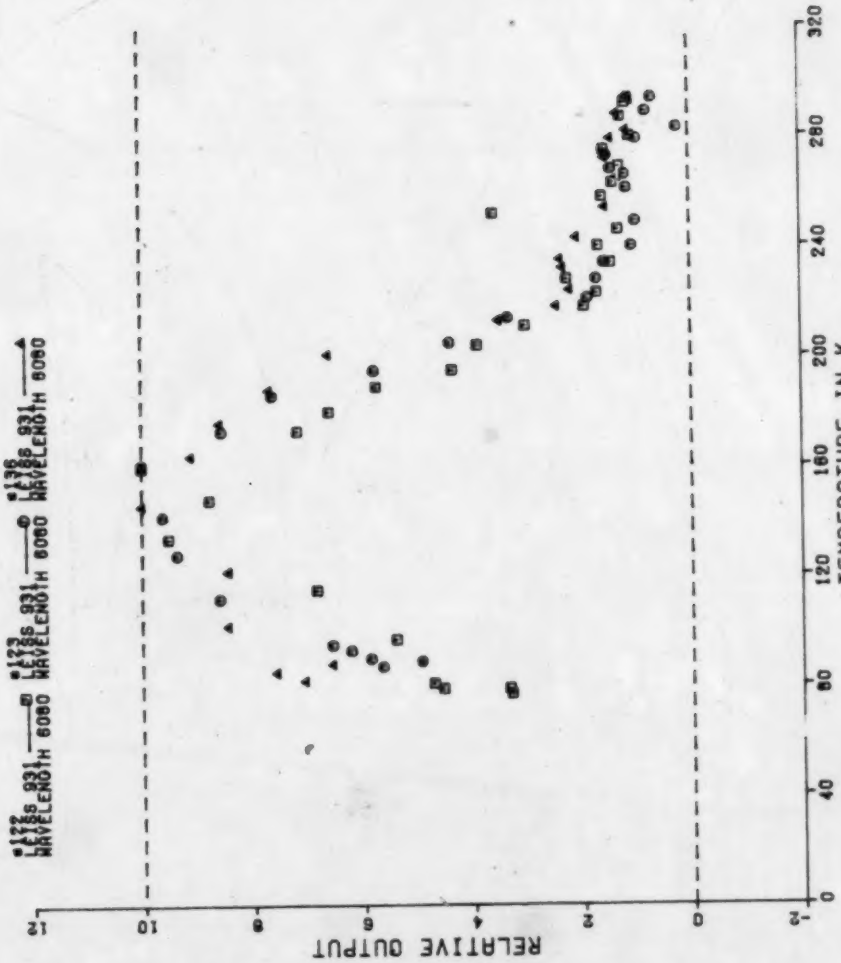


FIGURE 3-11 0.83 μ LUMINESCENCE EXCITED BY 6080 A

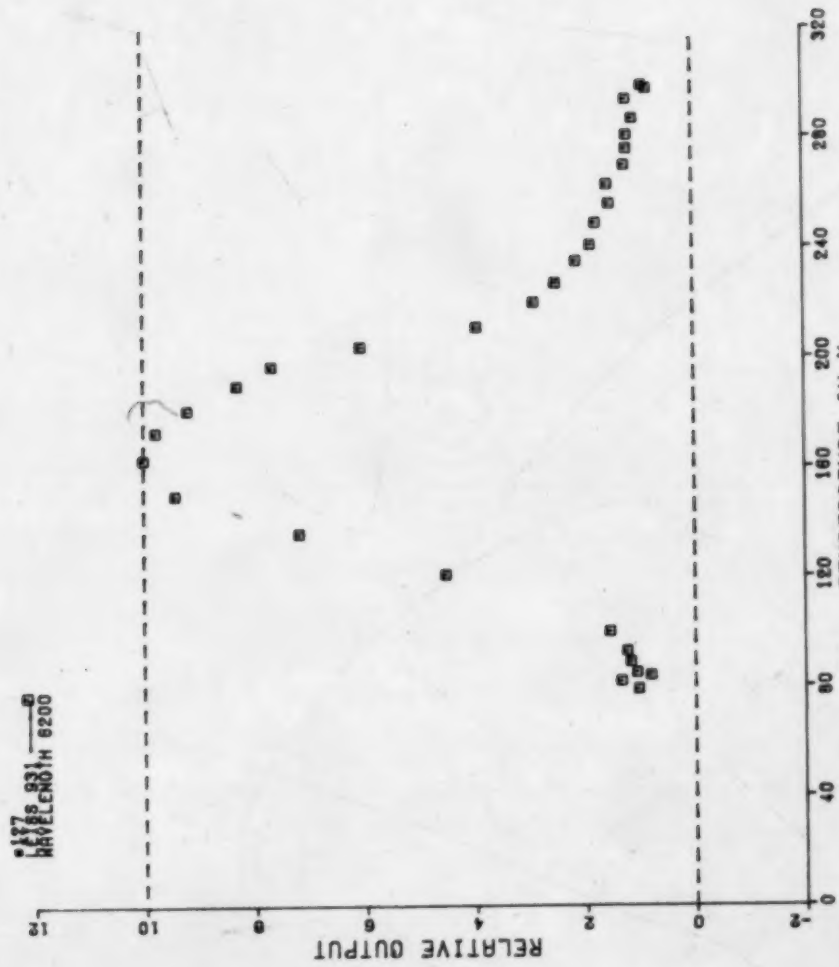


FIGURE 3-12 0.83 μ LUMINESCENCE EXCITED BY 6200 A

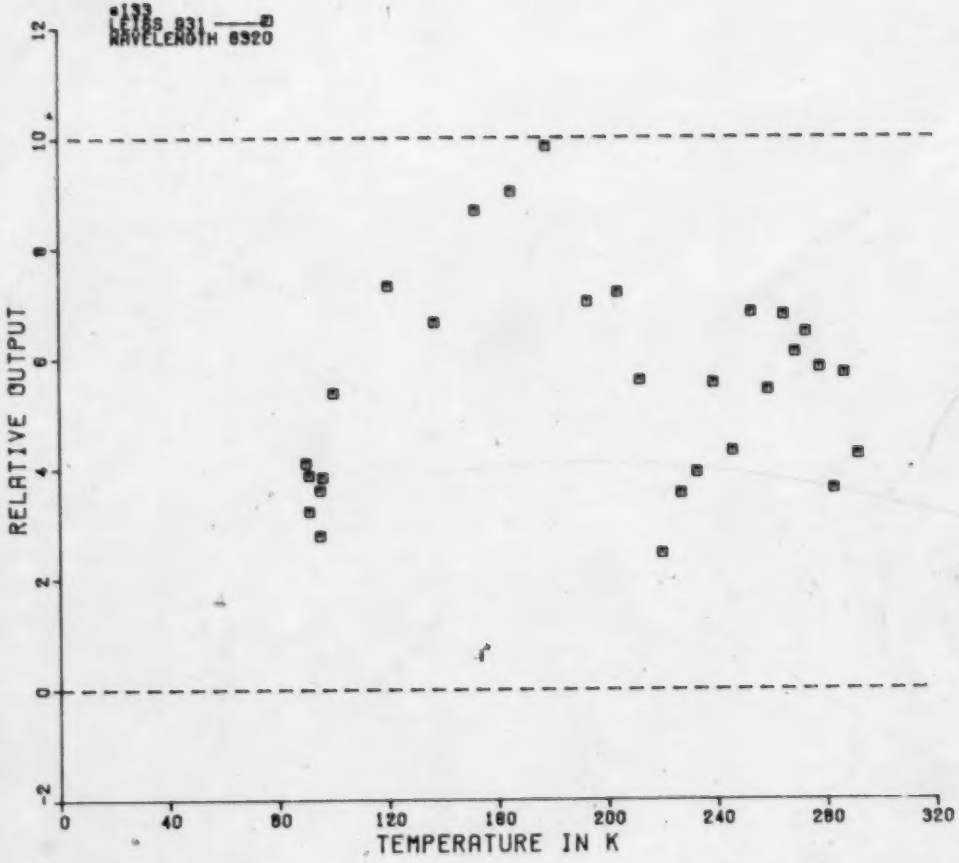


FIGURE 3-13 0.83 μ LUMINESCENCE EXCITED BY 6320 A

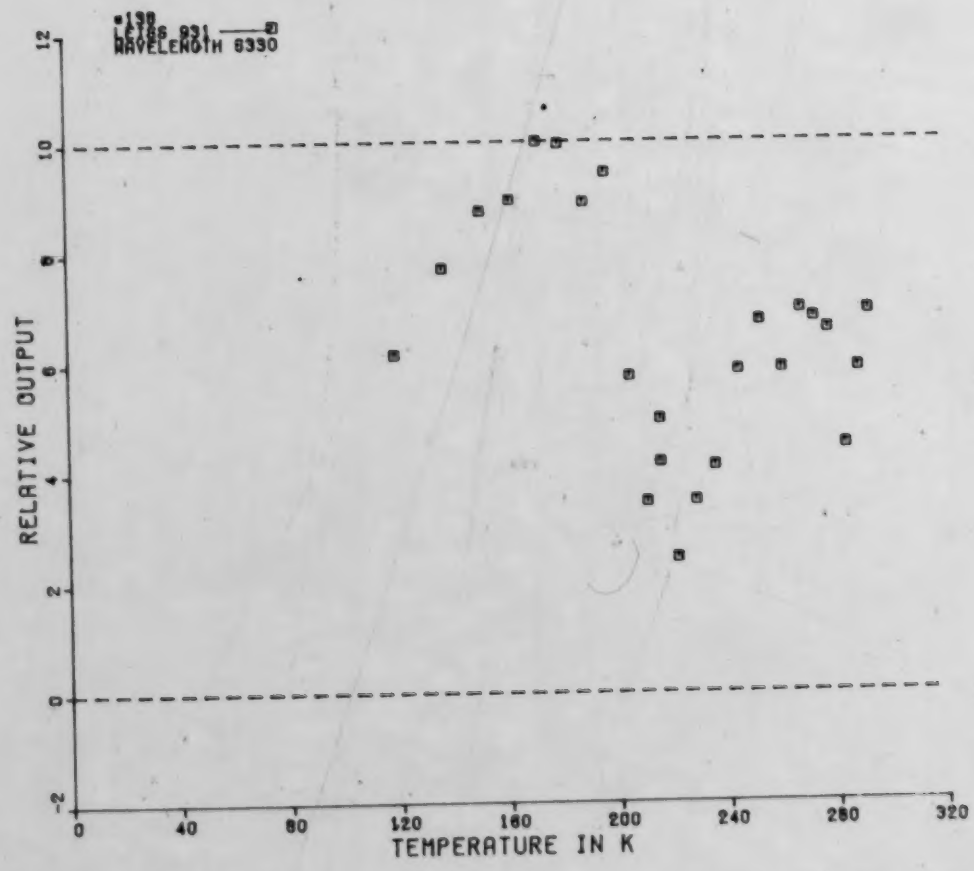


FIGURE 3-14 0.83 μ LUMINESCENCE EXCITED BY 6330 A

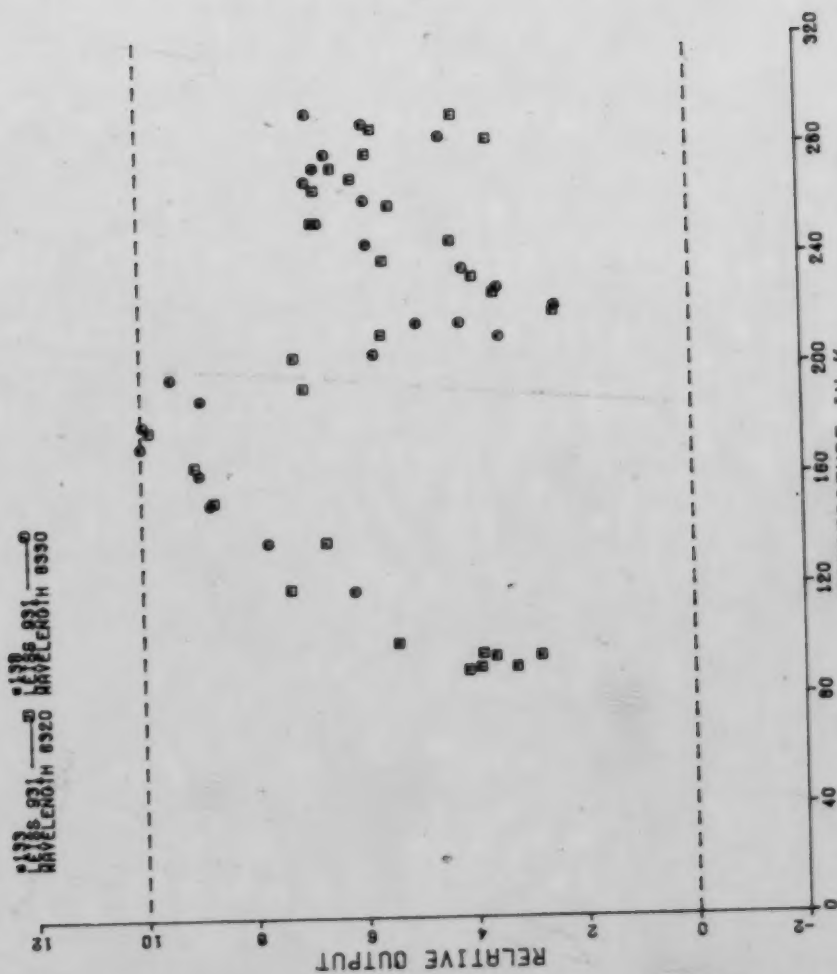


FIGURE 3-15 0.83 μ LUMINESCENCE EXCITED BY 6320 A

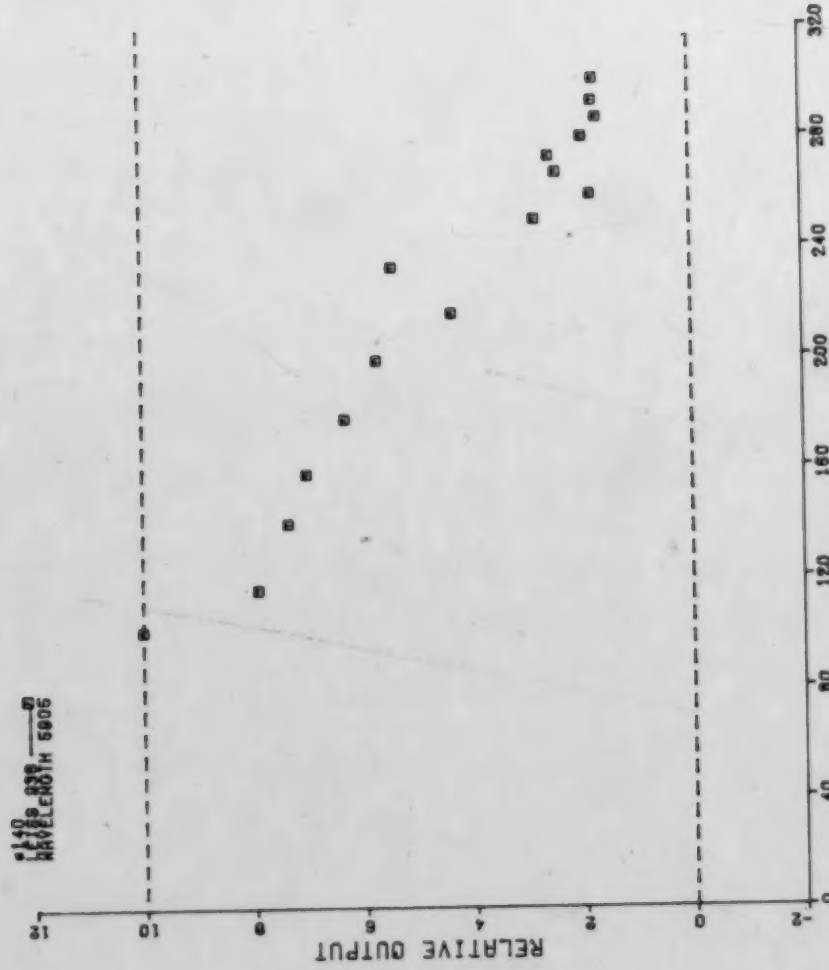


FIGURE 3-16 0.93 μ LUMINESCENCE EXCITED BY 5905 Å

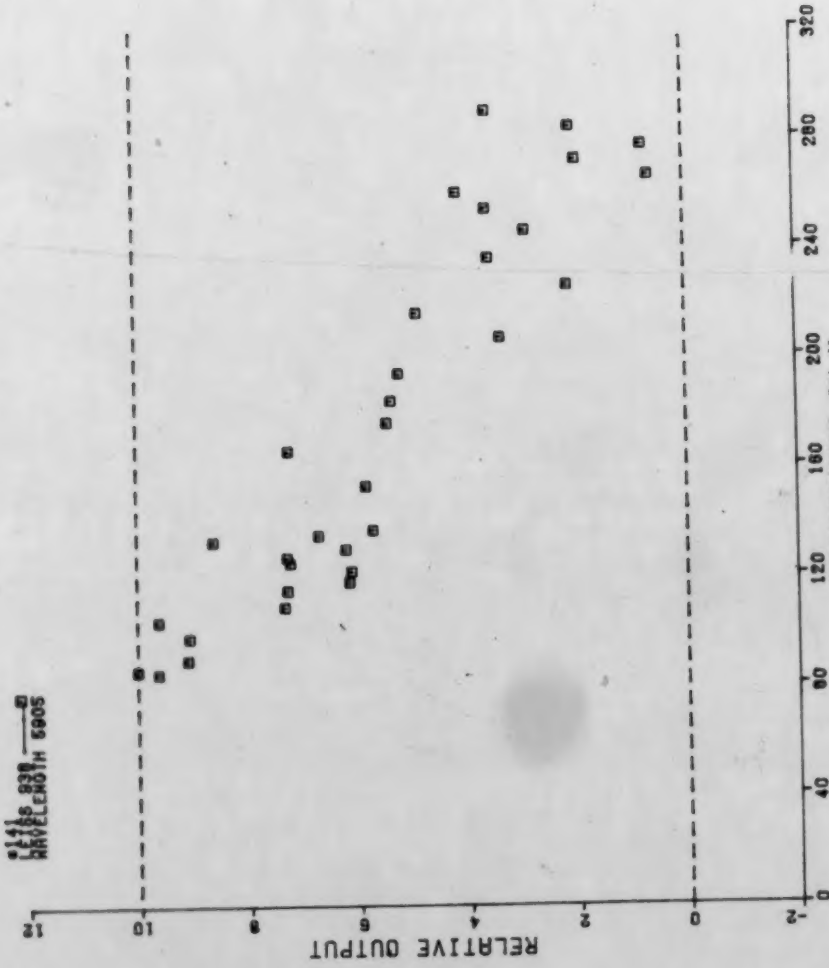


FIGURE 3-17 0.93 μ LUMINESCENCE EXCITED BY 5905 A

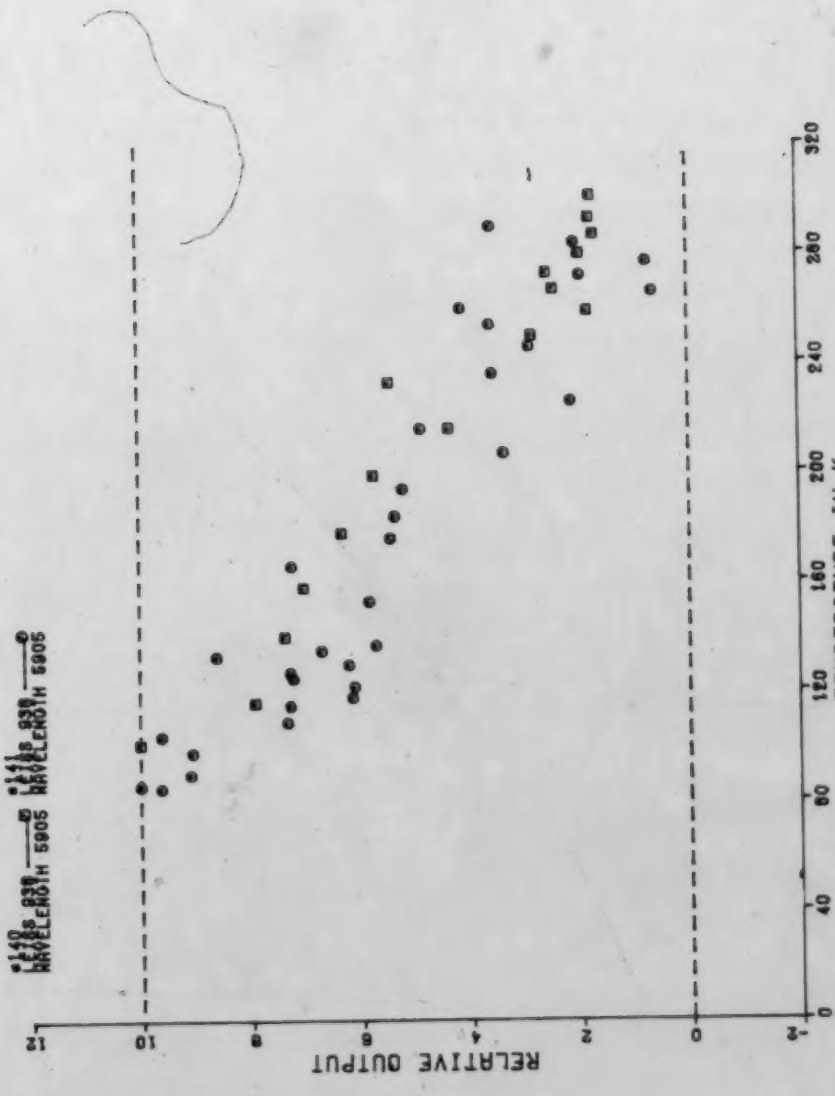


FIGURE 3-18 0.93 μ LUMINESCENCE EXCITED BY 5905 A

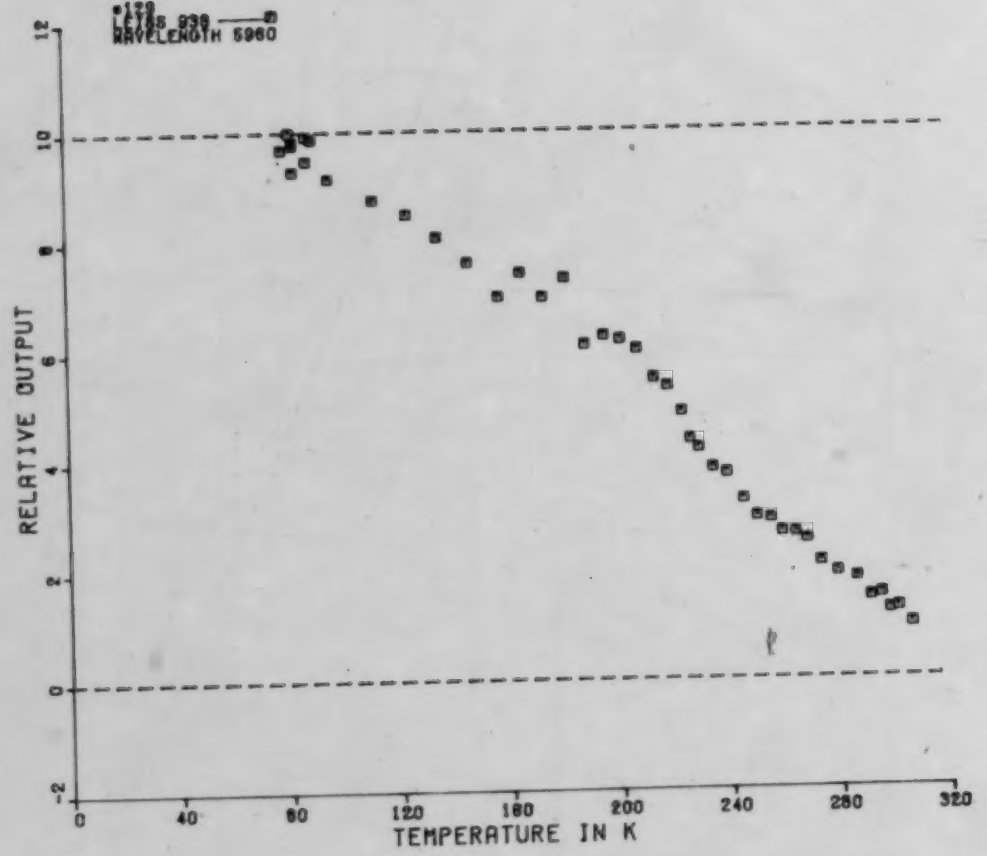


FIGURE 3-19 0.93 μ LUMINESCENCE EXCITED BY 5960 A

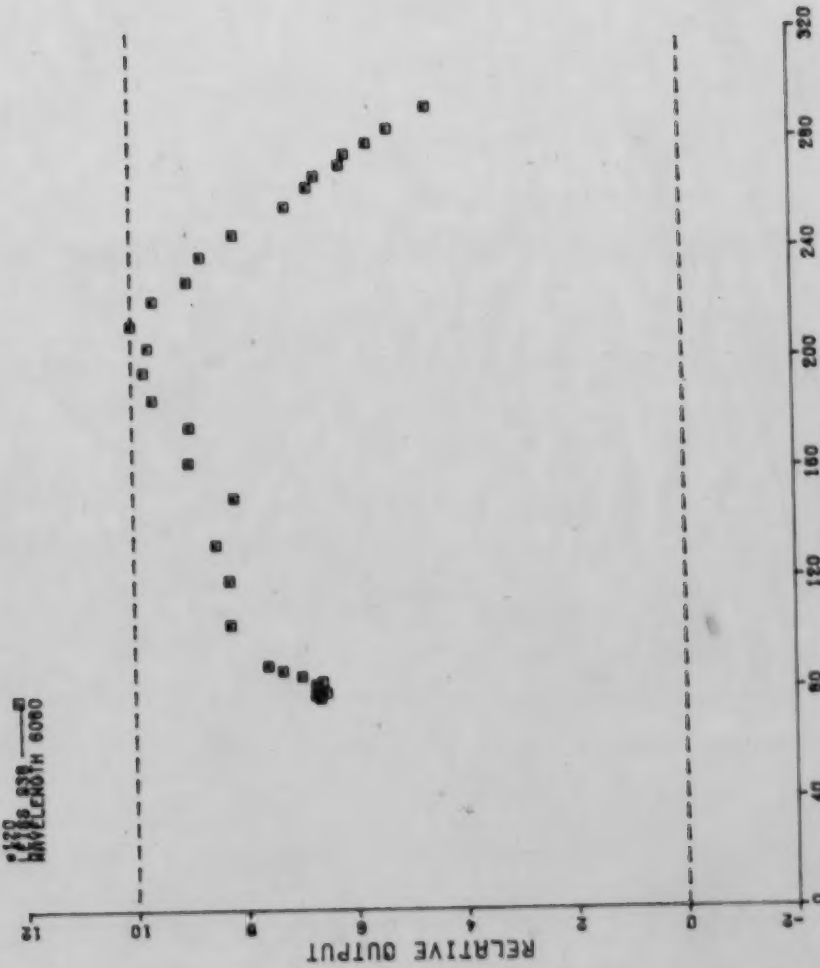


FIGURE 3-20 0.93 μ LUMINESCENCE EXCITED BY 6080 A

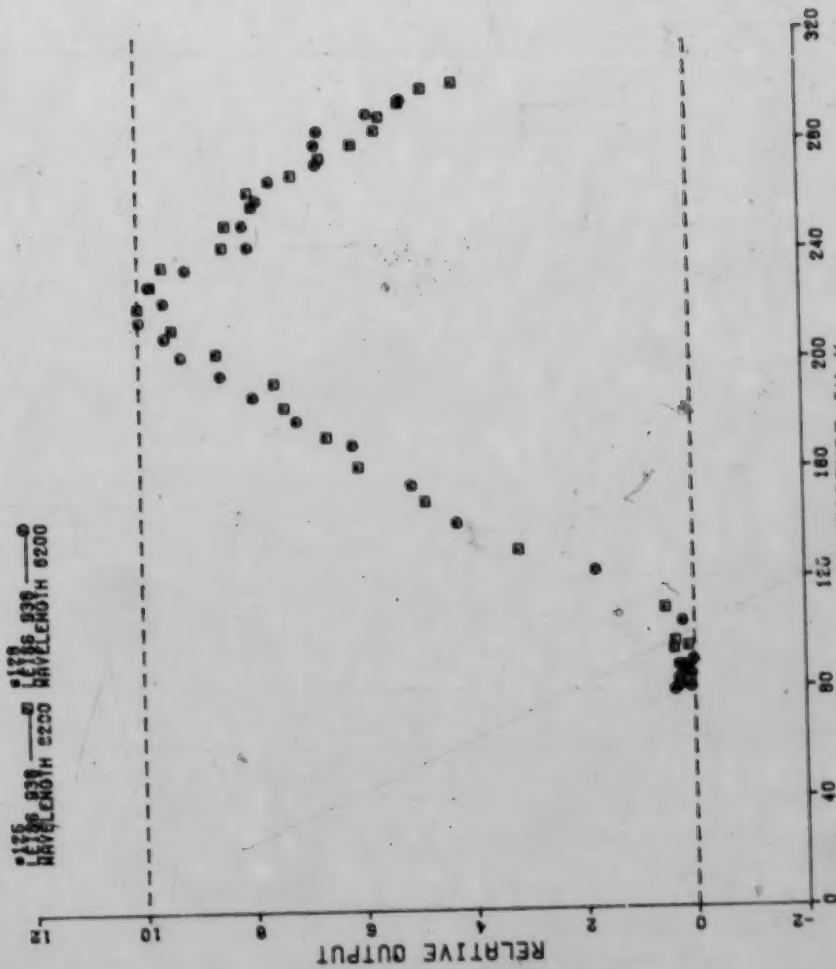


FIGURE 3-21 0.93 μ LUMINESCENCE EXCITED BY 6200 A

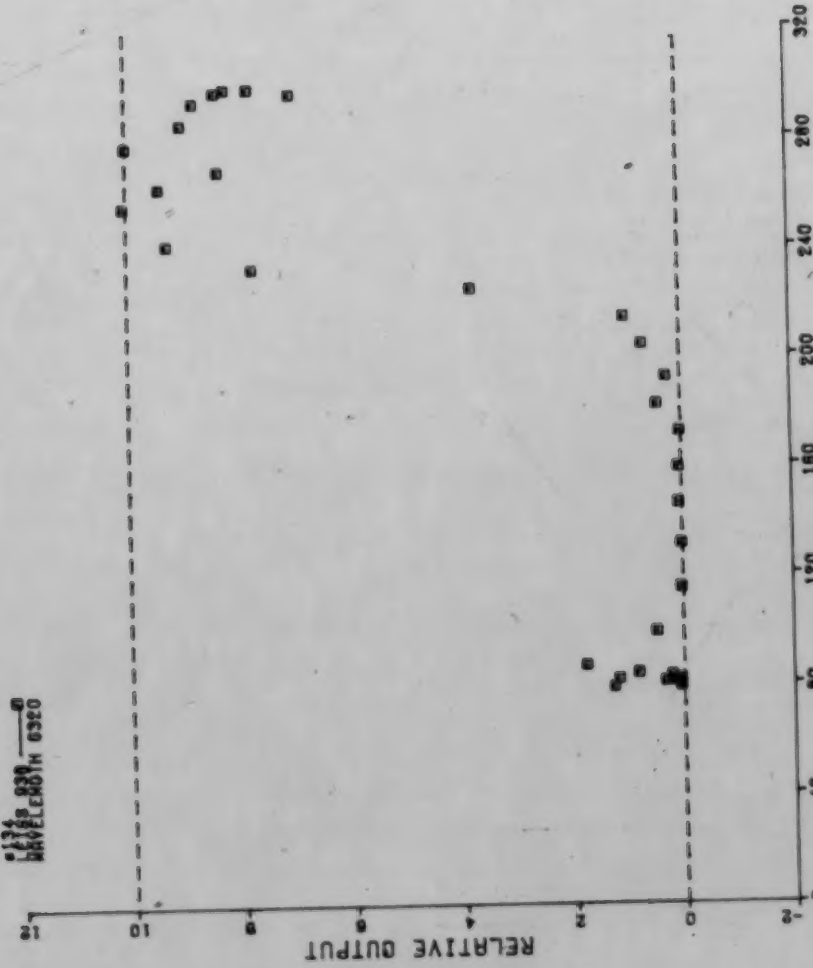


FIGURE 3-22 0.93 μ LUMINESCENCE EXCITED BY 6320 A

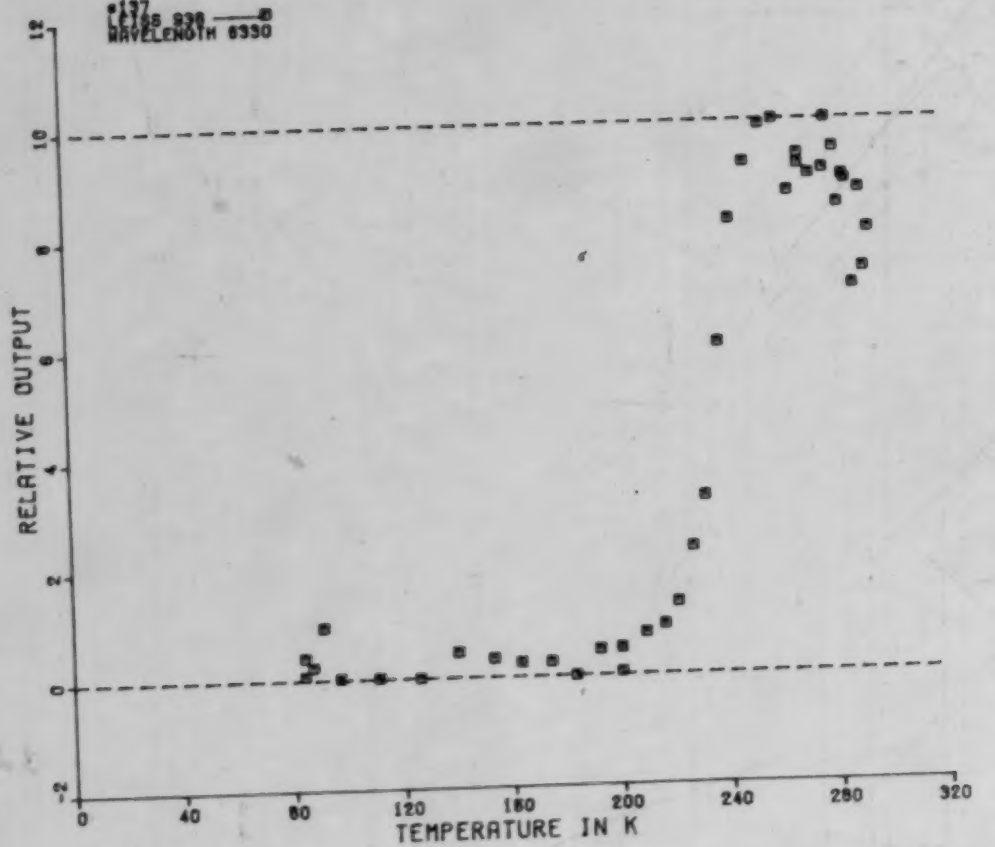


FIGURE 3-23 0.93 μ LUMINESCENCE EXCITED BY 6330 Å

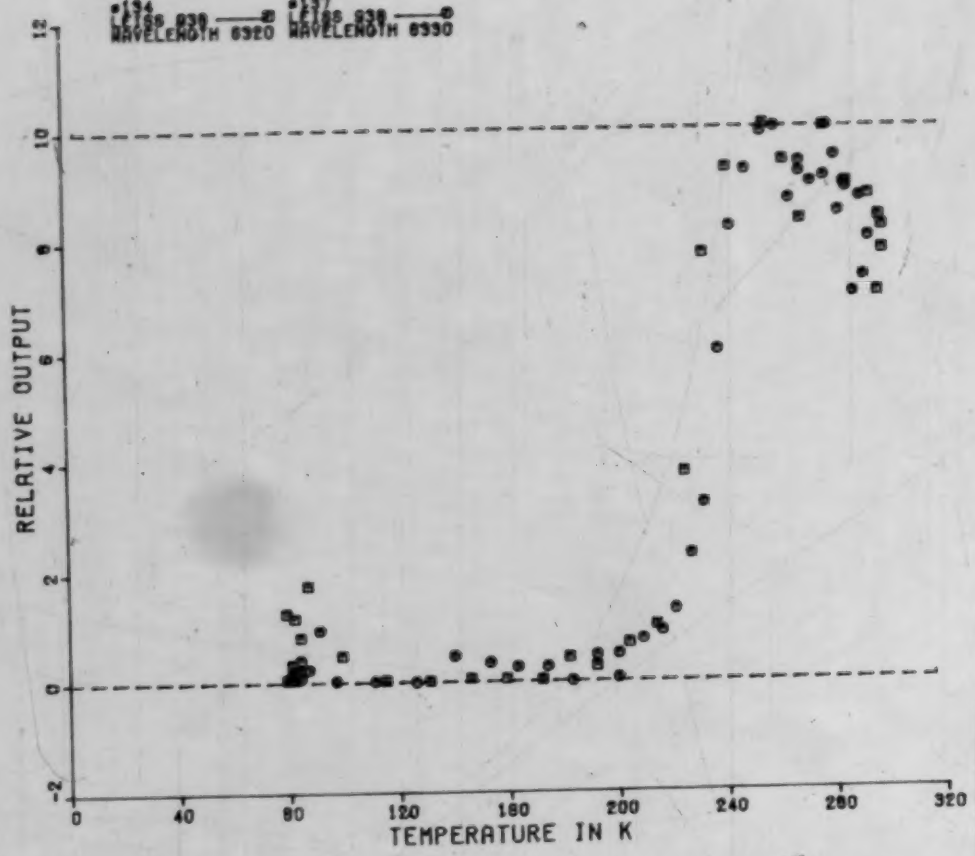


FIGURE 3-24 0.93 μ LUMINESCENCE EXCITED BY 6320 Å

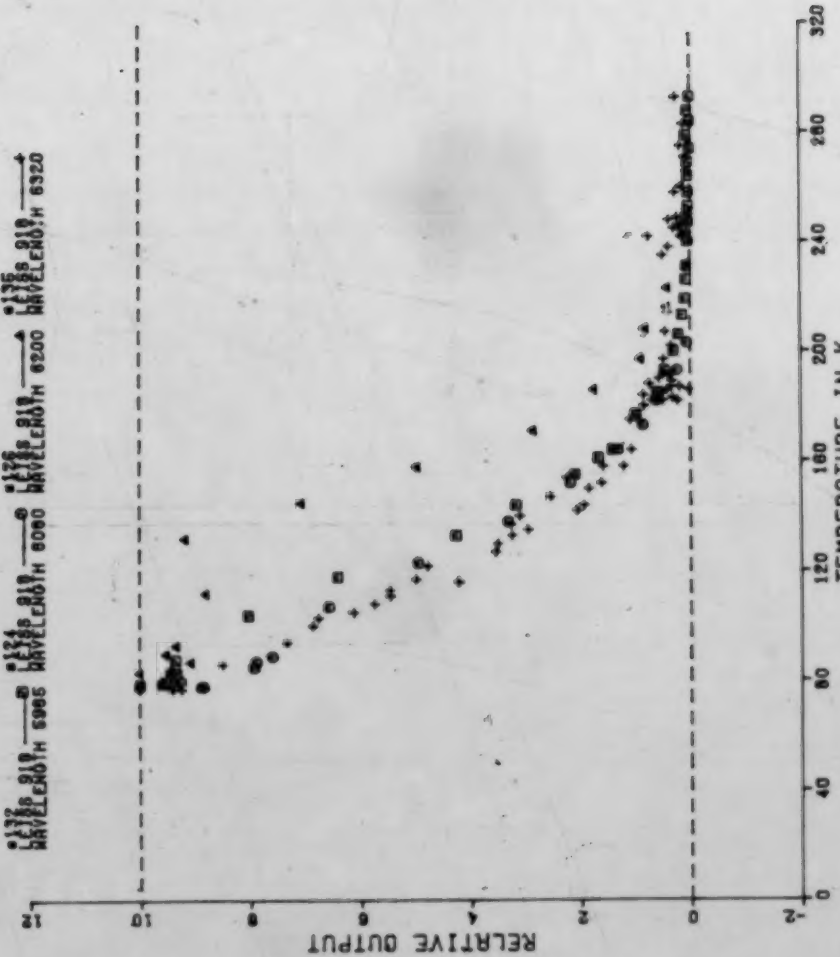


FIGURE 3-25 CUMULATIVE 0.72 μ DATA

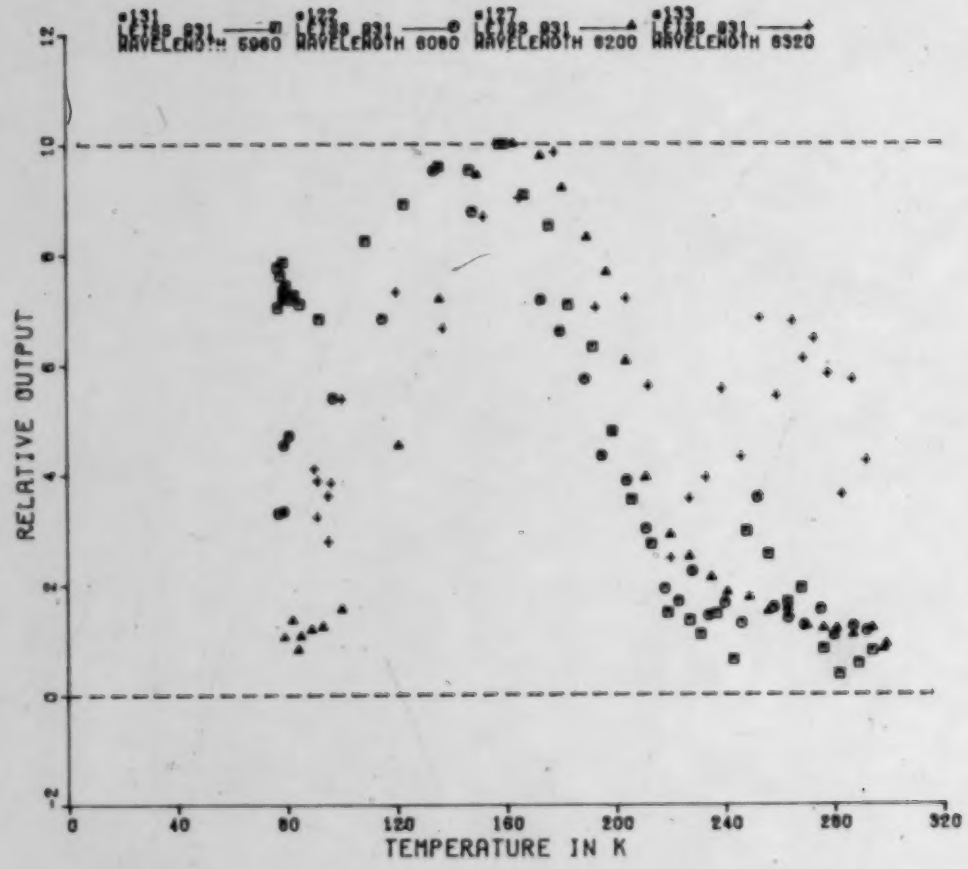


FIGURE 3-26 CUMULATIVE 0.83 μ DATA

shifted points from data set #126 are probably due to an erroneous low temperature point. The normalization then causes an apparent shift of the curve toward higher temperatures.

2. The 0.93 μ luminescence seems to show a preference for redder excitation at higher temperatures.

3. The 0.83 μ luminescence seems to display some similar sensitivity to the high temperature red excitation. Comparing figures 3-15 and 3-24 one finds the onset of the high temperature excitation at 6320 Å to occur at about the same temperature (220 K) in both cases.

4. Aside from this peculiarity the 0.83 μ temperature function appears to be fairly constant. Figure 3-26 displays the cumulative 0.83 μ data (over varying excitation wavelength) which appears to be stable, with the possible exception of a slight shift toward warmer temperatures with redder excitation.

As mentioned earlier set to set comparisons of absolute signal level are tenuous. The best data (i.e. the data with the largest values) has been selected for the non-normalized curves in figures 3-27, 3-28, and 3-29.

From figure 3-27 it is again apparent that the 0.72 μ luminescence is fairly regular in its temperature behavior showing a preference for yellow excitation but no basic structural change in the temperature function.

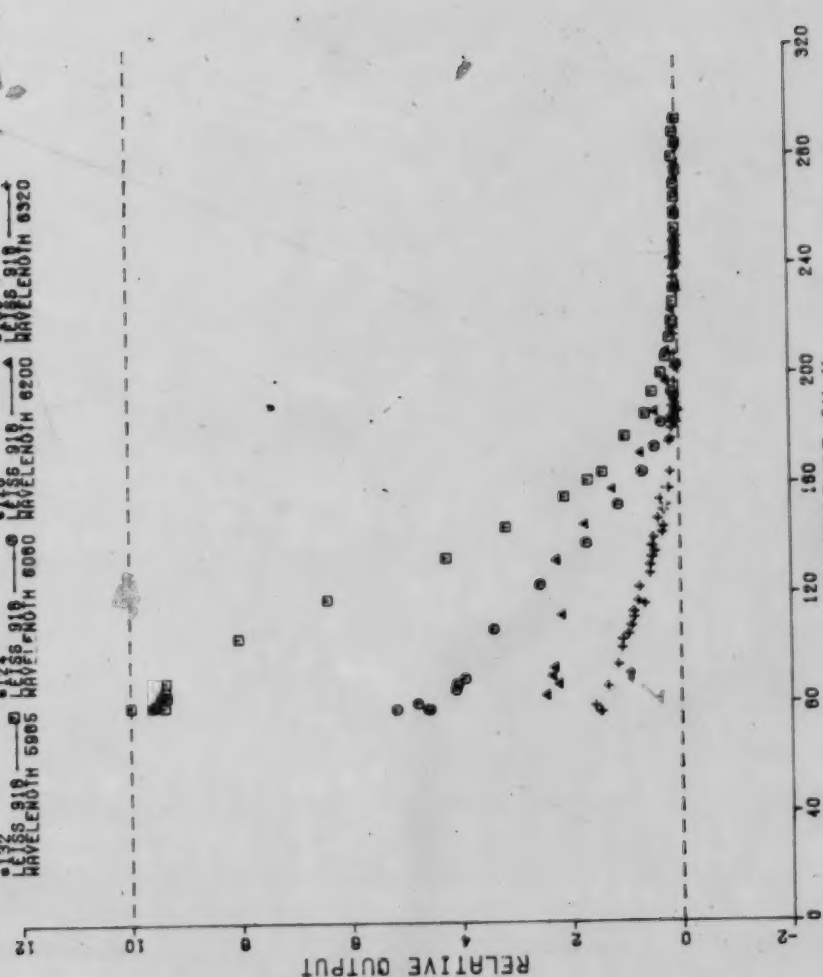


FIGURE 3-27 NON-NORMALIZED 0.72 μ DATA

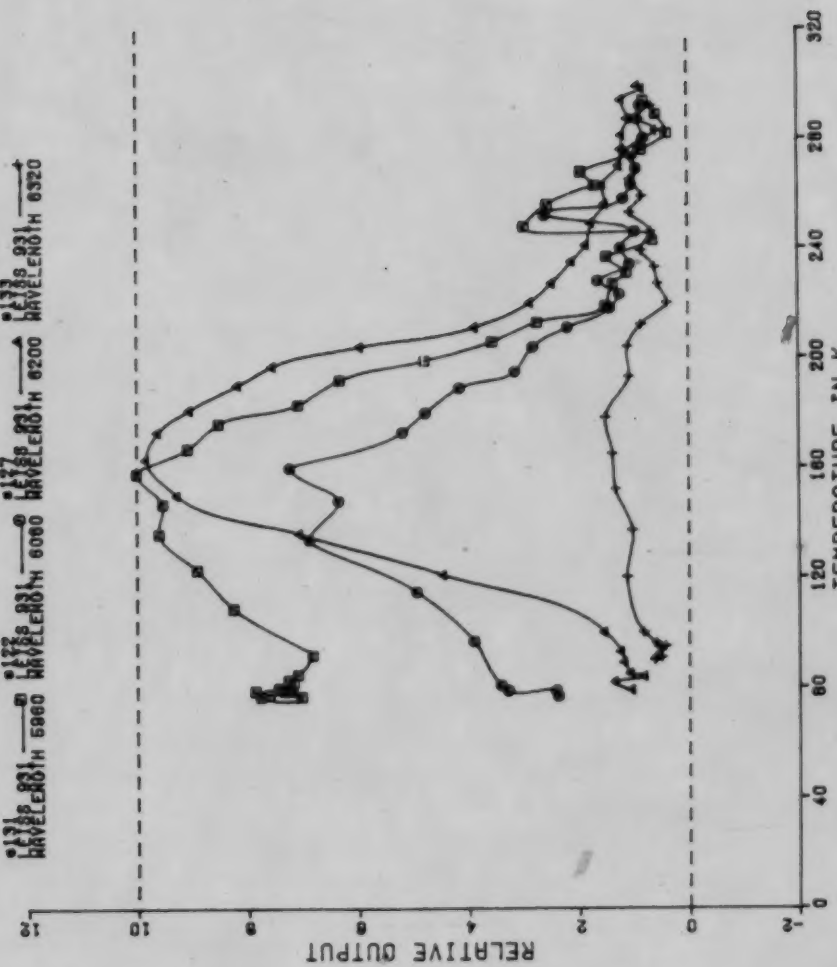


FIGURE 3-28 NON-NORMALIZED 0.83 μ DATA

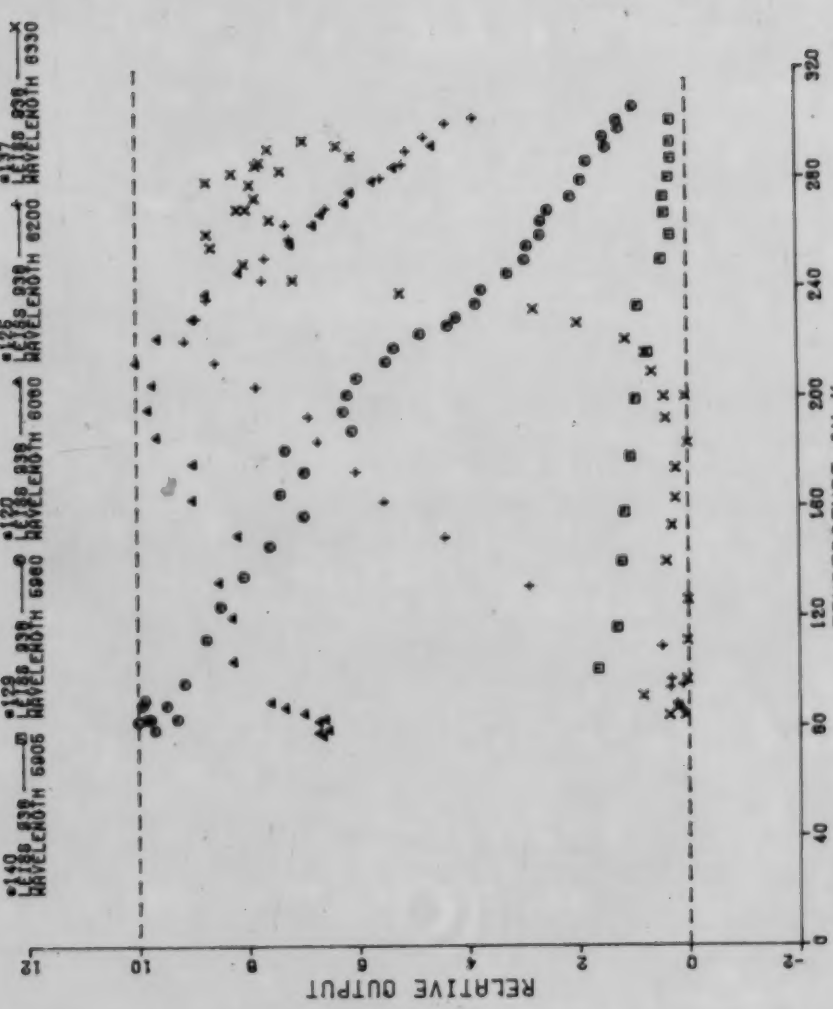


FIGURE 3-29 NON-NORMALIZED 0.93 μ DATA

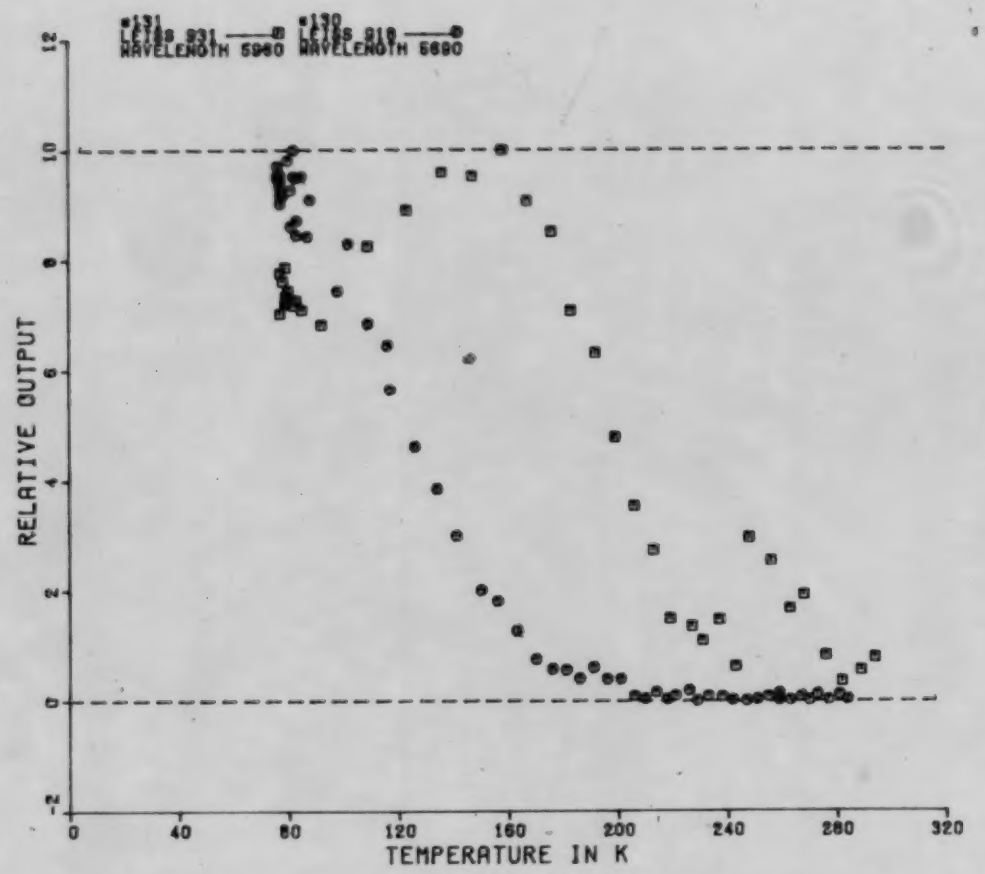


FIGURE 3-30 COMPARISON OF THE 0.72 μ AND 0.83 μ LUMINESCENCE TEMPERATURE FUNCTIONS

To simplify distinction of the separate data sets, the 0.83 μ output curves in figure 3-28 have been connected by lines. The regularity of the luminescence is approximate and not quite as evident with the quality of data presented here.

Finally the yield of 0.93 μ luminescence in figure 3-29 seems to show little absolute sensitivity to temperature, but a definite shift toward red excitation at warmer temperatures. The yield in the red may in fact be slightly larger than shown as the peak output wavelength shifts towards 0.96 μ at room temperature. The 5905 Å results seem to be anomalously low and this is probably an experimental error.

A few other observations can be made:

1. The amount of scatter and error in a given data set correspond approximately to the limits specified in Chapter 2. For example, examining the data in figure 3-18 the spread turns out to be approximately equivalent to 0.7 mV which is the specified PM-amplifier input noise.

2. As mentioned previously the temperature data curves are quite consistent within themselves even though the absolute value of the data varies from data set to data set. This is fairly evident in the data presented in figure 3-1. Here two separate data sets with absolute levels differing by more than a factor of two are merged

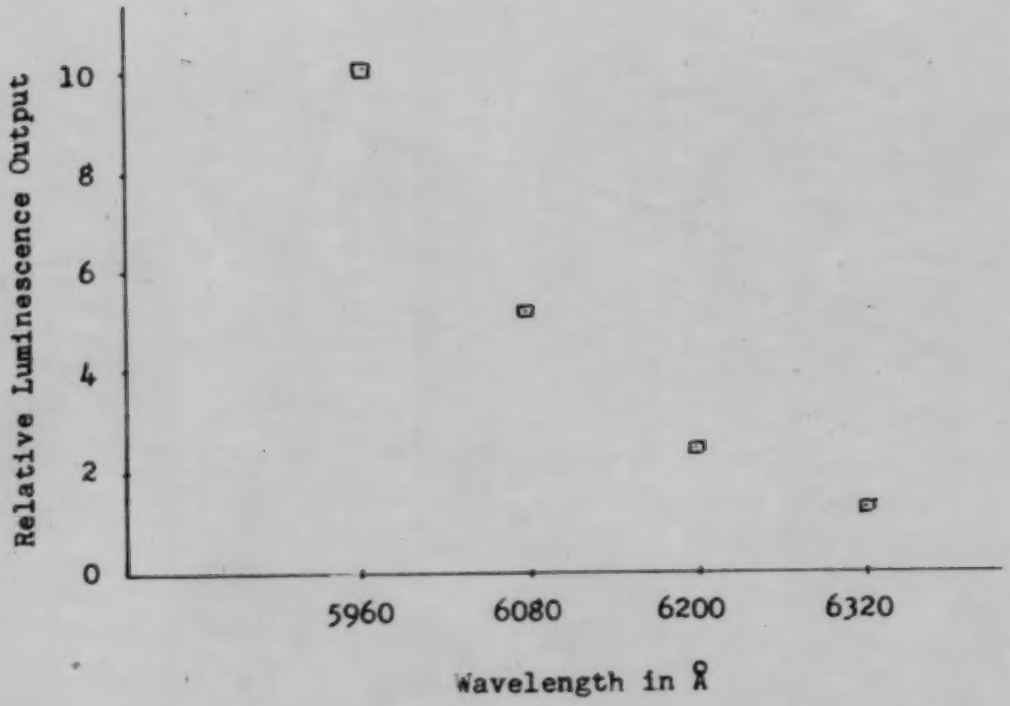


Figure 3-31 Excitation Spectrum of the 0.72 μ Luminescence at 77 K

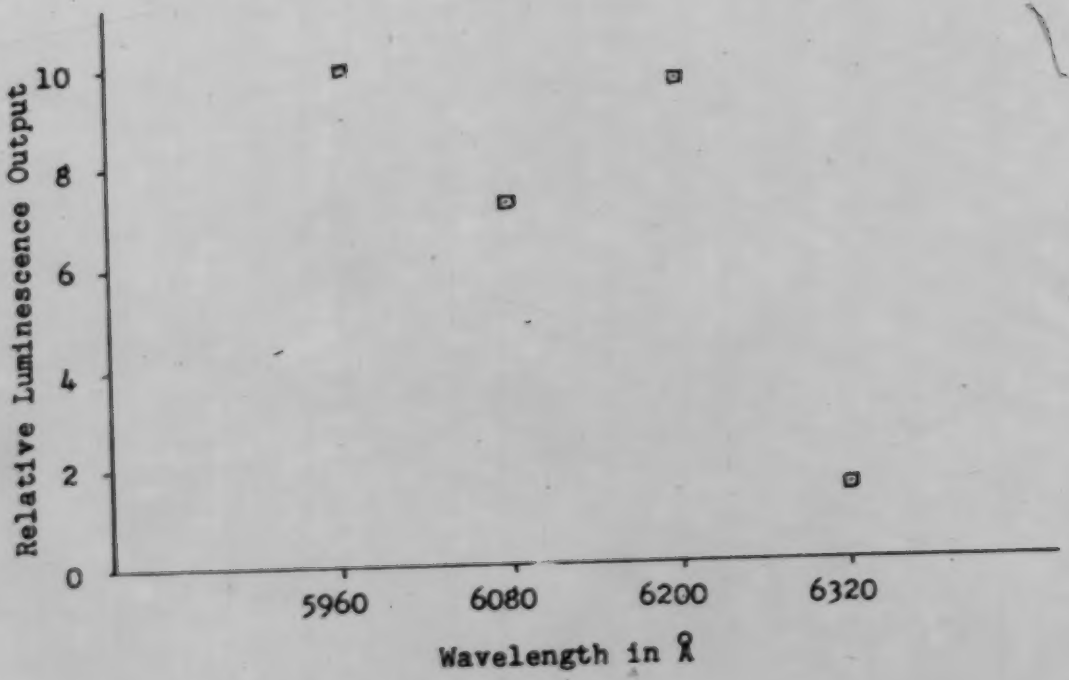


Figure 3-32 Excitation Spectrum of the 0.83 μ Luminescence at 160 K

almost indistinguishably.

3. The relationship with increasing temperature between the decline of the 0.72 μ luminescence and the increase in the 0.83 μ luminescence (see figure 3-30) is suggestive of competition or conversion of centres.

If our data set to data set comparisons may be believed then it also is apparent that the excitation functions of the 0.72 μ luminescence (figure 3-31) and of the 0.83 μ luminescence are quite different (figure 3-32). These excitation functions are reported for the temperature at which maximum output is observed, i.e. 77 K for the 0.72 μ luminescence and about 160 K for the 0.83 μ luminescence.

## 3.1 Summary and Conclusions

From our preliminary results we may tentatively conclude:

1. That the 0.72 μ and the 0.83 μ luminescence temperature characteristics show enough stability with respect to excitation to allow straightforward measurement (and possibly modelling) of the temperature function.

2. That the 0.72 μ and the 0.83 μ luminescences appear to have different excitation mechanisms. This is evident from the differences in their excitation

curves and time characteristics and is a point which has been very little discussed in the literature.

3. There is evidence of a possible link between the 0.83 μ and 0.93 μ luminescences in the high temperature red excitation. If this is the case it may indicate that the 0.83 μ luminescence may be specifically identified with the complex $V_{Cu}^{+}V_{0}^{-}$ as suggested by Bloem[18].

4. There is strong evidence that the excitation of the 0.93 μ luminescence is connected with the position of the optical absorption edge. According to the formula of Nikitine et.al.[69] the wave number of the absorption edge in $cm^{-1}$ is given by:

$$\gamma_{\infty} = 16510\ (1 - 2.695 \times 10^{-5} T - 3.689 \times 10^{-7} T^{2}) .$$

At 77 K this positions the absorption edge at about 6080 Å, and at 300 K at about 6320 Å giving a shift of about 240 Å over the 223 K temperature change. Examining the data we find a shift of about 330 Å over this temperature change. To clarify this point (i.e. whether the red shifting of excitation at high temperatures is related to the band shift) detailed studies on the same sample making specific comparisons of the shift in excitation versus the shift in absorption edge must be made. If this hypothesis is true it tends to indicate a strong excitonic mechanism in the visible. One thing is certainly true, any investigation of the

thermodynamics of the 0.93 μ luminescence must carefully take the excitation wavelength into account.

These results in themselves are very incomplete. More detailed work must be done on a large number of samples. However, an apparatus enabling better measurements has been developed and it is hoped that with the continuation of this research on the extrinsic luminescence of cuprous oxide a more concrete understanding of its mechanisms may be reached.

REFERENCES


1. Mott, N.F., On the absorption of light by crystals. Proc. Roy. Soc. A, 167: 384-391 (1938).
2. Gurney, R.W., and Mott, N.F., Luminescence in Solids. Trans. Faraday Soc., 35: 69-73, 1939.
3. Seibt, M., Verh. Deutsch. Phys. Ges., 20 (No.3): 99, 1939.
4. Lashkarev, V.E., and Kossonogova, K.M., IR luminescence of $Cu_2O$. C.R. Akad. Nauk (DAN.) S.S.S.R., 54 (No. 2): 125-6, 1946.
5. Karkhanin, Yu. I., Luminescence spectrum of $Cu_2O$. Izv. AN. (S.S.S.R., Ser-Fiz.), 16: 108-9, 1952.
6. Garlick, G.F.J., and Dumbleton, M.J., Phosphors emitting IR radiation. Proc. Phys. Soc. B, 67: 442-3, 1954.
7. Karkhanin, Yu. I., and Lashkarev, V.E., The nature of luminescence of $Cu_2O$. DAN. S.S.S.R., 97 (No.6): 1007-1010, 1954.
8. Tolstoi, N.A.,and Tkachuk, N.N., Temperature dependence of the relaxation time of $Cu_2O$. DAN. S.S.S.R., 95 (No. 1): 65-68, 1954.
9. Tolstoi, N.A., Tkachuk, N.N., and Preobrazhensky, R.K., Kinetics of the IR emission of $Cu_2O$ .I. Experimental part, Opt. Spektrosk., 2 (No.1): 116-126, 1957.
10. Garlick, G.F.J., Photoconductivity of $Cu_2O$. Encyc. of Phys., 19 (Sec.46): 377-380, 1956.

11. Gross, E.F., and Karriev, N.A., Absorption of light, visible and IR, in crystalline $Cu_2O$. DAN. S.S.S.R., 84 (No.2): 261-264, 1952.

12. Zhuze, V.P., and Ryvkin, S.M., The excitonic character of absorption of light and impurity photo conduction. DAN. S.S.S.R., 77: 241-244, 1951.

13. Grillot, M.E., IR emissions of crystalline minerals. Acta.Phys. Hung., 5: 445-461, 1955.

14. Tolstoi, N.A., Kinetics of the IR emission of $Cu_2O$. II. Theoetical Interpretations. Opt. Spektrosk., 2 (No.2): 210-219, 1957.

15. Khas, Z., Absorption and emission of light by bound exciton complexes. Czech. J. Phys. B, 15: 346-358, 1965.

16. Zhuze, V.P., and Ryvkin, S.M., On the mechanism of photoconductivity in $Cu_2O$. DAN. S.S.S.R., 68 (No.4): 673-676, 1949.

17. Bloem, J., Van der Houven van Oordt, A.J., and Kröger, F.A., A new luminescence emission in $Cu_2O$. Physica 22: 1254-1256, 1956.

18. Bloem, J., Discussion of some optical and electrical properties of $Cu_2O$. Philips Res. Repts. 13: 167-193, 1958.

19. Frerichs, Rudolph, and Weichman, Frank, Excitation of short infrared pulses with high repetition rate by electron bombardment of cuprous oxide. J. Appl. Phys. 29 (No.4): 710-713, 1958.

20. Frerichs, R., and Handy, R., Electroluminescence in cuprous oxide. Phys. Rev. 113 (No.5): 1191-1198, 1959.

21. Frerichs, R., and Liberman, I., Electroluminescence at point contacts in cuprous oxide and the mobility of $Cu^+$ ions at room temperature. Phys. Rev. Lett. 3 (No.5): 214-215, 1959.

22. Vorob'ev, Yu. V., and Karkhanin, Yu. I., Infrared luminescence of the surface layer of copper oxide. Fiz. Tverd. Tela.3 (No.1): 206-211, 1961. [Sov. Phys. Solid State 3 (No.1): 150-153, 1961.]

23. Peka, G.P., Karkhanin, Yu. I., Effect of an external electric field on luminescence of cuprous oxide. DAN. S.S.S.R. 141 (No.1): 63-65, 1961. [Sov. Phys. Doklady 6 (No.11): 983-984, 1962.]

24. Peka, G.P., Investigation of the effect of an electric field, applied at the surface, on the luminescence and electrical conductivity of cuprous oxide. Fiz. Tverd. Tela. 4 (No.5): 1118-1123, 1962. [Sov. Phys. Solid State 4 (No.5): 822-826, 1962.]

25. Karkhanin, Yu. I., Peka, G.P., and Yarmola, T.M., Quenching of infrared luminescence of cuprous oxide by hydrogen ions. Fiz. Tverd. Tela. 4 (No.9): 2306-2311, 1962. [Sov. Phys. Solid State 4 (No.9): 1689-1692, 1963.]

26. Peka, G.P., and Karkhanin, Yu. I., Effect on luminescence and electrical conductivity of cuprous oxide of an electric field applied to the surface. Fiz. Tverd. Tela. 4 (No.12): 3618-3625, 1962. [Sov. Phys. Solid State 4 (No.12): 2646-2651, 1963.]

27. Zinets, O.S., Peka, G.P., and Karkhanin, Yu. I., Certain problems of the theory of the luminescence field effect. Fiz. Tverd. Tela. 6 (No.12): 3515-3523, 1964. [Sov. Phys. Solid State 6 (No.12): 2817-2822, 1965.]

28. Peka, G.P., and Guzii, A.S., Investigation of surface levels in cuprous oxide by the field-effect method and by means of the luminescence field-effect. Fiz. Tverd. Tela. 8: 2293-2299, 1966. [Sov. Phys. Solid State, 8 (No.8): 1830-1835, 1967.]

29. Peka, G.P., and Zhdanov, G.P., Effect of surface band bending on luminescence kinetics in copper oxide. Fiz. Tverd. Tela. 11 (No.6): 1732-1735, 1969. [Sov. Phys. Solid State 11 (No.6): 1405-1407, 1969.]

30. Peka, G.P., Effect of adsorption of molecules on the luminescence, electrical conductivity and the luminescent field effect of $Cu_2O$. Fiz. Tverd. Tela. 5 (No. 7): 2017-2019, 1963. [Sov. Phys. Solid State 5: 1473-1475, 1964.]

31. Vol'Kenshtein, F.F., Peka, G,P., and Malakhov, V.V., Effect of adsorption on the luminescence of semiconductors. II. Exciton luminescence. Kinet. Katal.

14 (No.5): 1269-1273, 1973. [Kinet. and Catal. 14: 1114-1118, 1973.]

32. Wolkenstein, Th., Peka, G.P., and Malakhov, V.V., The influence of adsorption on the luminescence of semiconductors. Part II. Exciton luminescence. J. Lum. 5: 261-268, 1972.

33. Gross, E.F., and Kreingol'd, F.I., Exciton luminescence in $Cu_2O$ crystals. ZhETF Pis'ma 7 (No.8): 281-283, 1968. [JETP Lett. 7: 218-220, 1968.]

34. Gross, E.F., and Kreingol'd, F.I., Lifetimes of free and bound excitons in $Cu_2O$ crystals. ZhETF. Pis. Red. 10 (No.5): 219-223, 1969. [JETP Lett. 10: 139-142, 1969.]

35. Kreingol'd, F.I., and Fokin, V.M., Exciton electroluminescence in $Cu_2O$ crystals. Fiz. Tekh. Poluprov. 4 (No.11): 2198-2199, 1970.- [Sov. Phys. Semicon. 4 (No.11): 1888-1889, 1971.]

36. Gross, E.F., and Kreingol'd, F.I., Biexiton in $Cu_2O$ crystal. ZhETF Pis. Red. 12 (No.2): 98-100, 1970. [JETP Lett. 12: 68-70, 1970.]

37. Kreingol'd, F.I., Luminescence of $Cu_2O$-Cd crystals at 4 - 15 K. Opt. Spektrosk. 30 (No. 2): 286-290, 1971. [Opt. Spec. 30: 153-155, 1971.]

38. L'vov, O.I., and Pavinskii, P.P., Biexciton in $Cu_2O$ crystal. ZhETF Pis. Red. 14 (No.2): 253-256, 1971. [JETP Lett. 14: 167-169, 1971.]

39. Gadomskii, O.N., and Samartsev, V.V., Exciton induction and echo. Fiz. Tverd. Tela. 13 (No.9): 2806-2808, 1971. [Sov. Phys. Solid State 13 (No.9): 2354-2355, 1972.]

40. Kreingol'd, F.I., and Kulinkin, B.S., Temperature dependence of the exciton luminescence and photon spectra of $Cu_2O$ and $Ag_2O$ crystals. Opt. Spektrosk. 33: 706-711, 1972. [Opt. Spec. 33: 390-393, 1972.]

41. Gross, E.F., Kreingol'd, F.I., and Makarov, V.L., Resonant interaction between ortho- and para-excitons with participation of phonons in a $Cu_2O$ crystal. ZhETF Pis. Red. 15 (No.7): 383-387, 1972. [JETP Lett. 15: 269-271, 1972.]

42. Compaan, A., and Cummins, H.Z., Raman scattering, luminescence, and exciton-photon coupling in $Cu_2O$. Phys. Rev. B 6 (No. 12 : 4753-4757, 1972.

43. Petroff, Y., Yu, P.Y., and Shen, Y.R., Luminescence of $Cu_2O$-excitonic molecules,or not? Phys. Rev. Lett. 29 (No.23): 1558-1562, 1972.

44. Kreingol'd , F.I., and Makarov, V.L., Effect of a paraexciton level on the temperature dependence of exciton luminescence in a cuprous oxide crystal. Fiz. Tverd. Tela. 15: 1307-1309, 1973. [Sov. Phys. Solid State 15 (No.4): 890, 1973.]

45. Kreingol'd, F.I., and Makarov, V.L., Resonant interaction between ortho- and para-excitons involving phonons in a cuprous oxide crystal.

Izvest. A.N. (Ser.Fiz.) 37 (No.4): 714-717, 1973. [Bull. Acad. Sci. U.S.S.R.(Physical Series) 37: 22-25, 1973.]

46. Kreingol'd, F.I., and Makarov, V.L., Investigation of the mechanism of the deformation stimulation of a paraexciton level in the luminescence of cuprous oxide crystals. Fiz. Tekh. Poluprov. 8: 1475-1481, 1974. [Sov. Phys. Semicond. 8 (No.8): 962-965, 1975.]

47. Petroff, Y., Yu, P.Y., and Shen, Y.R., Study of photoluminescence in $Cu_2O$. Phys. Rev. B 12 (No. 6): 2488-2495, 1975.

48. Bairamov, B. Kh., and Khashkhozhev, Z.M., Luminescence of $Cu_2O$ crystals in the case of ultraviolet excitation. Fiz. Tverd. Tela. 17: 2497-2499, 1975. [Sov. Phys. Solid State 17 (No.8): 1666-1667, 1976.]

49. Kinoshita, Akira, and Nakano, Tomayasu, $Cu_2O$ crystal growth by hydrothermal technique. Jap. J. Appl. Phys. 6: 656-657, 1967.

50. Kuzmina, I.P., Lobachev, A.N., Predtechenskii, B.S., Starostina, L.S., Stopachinskii, V.B., and Khaidukov, N.M., Luminescence of cuprous oxide single crystals. Kristallografia 18: 635-637, 1973. [Sov. Phys. Crystallogr. 18 (No.3): 400-401, 1973.]

51. Agekyan, V.T., Lobachev, A.N., Starostina, L.S., Kuz'mina, I.P., Predtechenskii, B.S., and Khaidukov, N.M., Optical properties of cuprous oxide crystals grown by various methods. Zhur. Prikla. Spektrosk. 22 (No.4): 740-745, 1975. [J. Appl. Spect. 22: 562-566, 1975.]

52. Merle, J.C., and Robino, Mrs. M., On the luminescence of $Cu_2O$ in the vicinity of the n=1 line of the excitonic yellow series. Opt. Comm. 14 (No.2): 240-243, 1975.

53. Gorban, I.S., Rudko, S.N., and Shishlovskii, A.A., Luminescence of semiconductor crystals with excitation in the discrete structure region of the absorption spectrum. Izv. A.N. S.S.S.R.(Ser. Fiz.) 25: 6-12, 1961. [Bull. Acad. Sci. U.S.S.R. 25: 7-13, 1961.]

54. Gorban, I.S., Gritsenko, Yu.I., and Rudko, S.N., Photoluminescence and current carrier recombination in copper oxide crystals. Fiz. Tverd. Tela. 3 (No.7): 2147-2153, 1961. [Sov. Phys. Solid State 3 (No.7): 1559-1563, 1962.]

55. Gorban, I.S., and Rudko, S.N., Energy spectrum of defects in copper-oxide crystals. Zhur. Prikla. Spektrosk. 7 (No. 2): 249-254, 1967. [Jour. Appl. Spec. 7 (No.2): 178-181, 1967.]

56. Karkhanin, Yu. I., and Vorob'ev, Yu.V., On the relaxation time of the short wavelength luminescence bands of $Cu_2O$. Opt. Spektrosk. 13: 148, 1962. [Opt. Spect. 13: 82-83, 1962.]

57. Vorob'ev, Yu. V., and Karkhanin, Yu. I., Effect of oxygen vacancies on the luminescence and photoconductivity of cuprous oxide. Fiz. Tverd. Tela. 4 (No.11): 3336-3337, 1962. [Sov. Phys. Solid State 4: 2442-2443, 1963.]

58. Vorob'ev, Yu. V., and Karkhanin, Yu. I., Mechanism of luminescence excitation in cuprous oxide in the impurity absorption region. Opt. Spektrosk. 15 (No.3): 389-393, 1963. [Opt. Spec. 15: 207-210, 1963.]

59. Berkovskii, F.M., and Shreter, Yu. G., Radiative recombination in cuprous oxide at high excitation intensities. Fiz. Tekh. Poluprov. 2 (No.5): 757-759, 1968. [Sov. Phys. Semicon. 2 (No.5): 631-632, 1968.]

60. Tolstoi, N.A., and Abramov, A.P., Nonlinear dependence of the luminescence of cuprous oxide on the photoexcitation intensity. Fiz. Tverd. Tela. 9 (No. 11): 3340-3341, 1967. [Sov. Phys. Solid State 9 (No.11): 2630-2631, 1968.]

61. Tolstoi, N.A., Bonch-Bruevich, V.A., and Gerlovin, I. Ya., Long-wave luminescence of cuprous oxide over a large range of photoexcitation intensities.

Fiz. Tverd. Tela. 11 (No. 7): 2005-2007, 1969. [Sov. Phys. Solid State 11 (No. 7): 1617-1618, 1970.]

62. Tolstoi, N.A., and Bonch-Bruevich, V.A., Luminescence of oxygen vacancies in cuprous oxide. Fiz. Tverd. Tela. 13 (No. 5): 1357-1359, 1971. [Sov. Phys. Solid State 13 (No.5): 1135-1137, 1971.]

63. Bonch-Bruevich, V.A., and Tolstoi, N.A., New results on the luminescence of cuprous oxide. Izv. A.N. S.S.S.R. (Ser. Fiz.) 35: 1425-1429, 1971. [Bull. Acad. Sci. U.S.S.R. (Phys. Ser.) 35: 1302-1305,1971.]

64. Taylor, J.C.W., and Weichman, F.L., Role of excitons in the luminescence of cuprous oxide. Phys. Rev. 185 (No.3): 1214-1217, 1969.

65. Taylor, J.C.W., Lomnes, R.K., and Weichman, F.L., Exciton structure and exciton decay probabilities from luminescence in cuprous oxide. J. Lum. 3: 405-418, 1971.

66. Pastrnak, J., Spectral distribution of quantum yield of infrared luminescence of $Cu_2O$ at low temperatures. Czech. J. Phys. B 11: 452-453, 1961.

67. Taylor, J.C.W., Weichman, F.L., and McClung, R.E.D., Electron paramagnetic resonance in $Cu_2O$ compared with other semiconducting properties. Can. J. Phys. 49 (No. 10): 1275-1283, 1971.

68. Duvvury, C., Kenway, D.J., and Weichman, F.L., Excitation characteristics of the IR luminescence

in $Cu_2O$. J. Lum. 10: 415-418, 1975.

69. Nikitine, S., Sieskind, M., and Perny, G., The displacement of the absorption spectrum of cuprous oxide as a function of temperature. C.R. Acad. Sci. Paris 238: 1987-1989, 1954.

## ADDITIONAL BIBLIOGRAPHY


Bonch-Bruevich, A.M., Karazin, I.M., Molchanov, V.A., and Shirokov, V.I., An experimental model of a phase fluorometer. Prib. I. Tekh. Eksp. 2: 53-56, 1959. [Inst. & Exp. Tech. 2: 53-56, 1959.]

Dahl, J.P., and Switendick, A.C., Energy bands in cuprous oxide. J. Phys. Chem. Solids 27: 931-942, 1966.

Daveport, Jr., Wilbur, B., and Root, William L., "An Introduction to the Theory of Random Signals and Noise". McGraw-Hill Book Company, Inc., New York, 1958.

Karkhanin, Yu. I., and Vorob'ev, Yu. V., The mechanism and kinetics of the electroluminescence of cuprous oxide. DAN. S.S.S.R. 152 (No.4): 855-857, 1963. [Sov. Phys. Doklady 8 (No. 10): 975-977, 1964.]

Karkhanin, Yu. I., and Vorob'ev, Yu. V., Injection-chemical effect and electroluminescence of $Cu_2O$. Fiz. Tverd. Tela. 10 (No. 6): 1880-1882, 1968. [Sov. Phys. Solid State 10 (No. 6): 1479-1480, 1968.]

Mott, N.F., and Gurney, R.W., "Electronic Processes in Ionic Crystals". Oxford University Press, London, Second Edition, 1948.

Schäfer, F.P. (Editor), "Dye Lasers" (Volume 1), Springer-Verlag, New York, 1973.

Steele, Earl L., "Optical Lasers in Electronics". John Wiley and Sons Inc., New York, 1968.

Taylor, J.C.W., "Luminescence and Excitons in Cuprous Oxide". (Thesis), U. of Alberta, Edmonton, Alberta, 1971.

Vorob'ev, Yu. V., and Karkhanin, Yu. I., Expansion of temperature range of electroluminescence of $Cu_2O$ with the help of an MOS system. Surf. Sci. 13: 491-493, 1969.

Weichman, F.L., "The Electrical and Optical Properties of Cuprous Oxide". (Thesis), Northwestern University, Evanston, Illinois, 1959.

Zucker, Richard S., Growth of single crystal cuprous oxide from the melt and luminescence of cuprous oxide. J. Electrochem. Soc. 112 (No. 4): 417-420, 1965.

# APPENDIX I

## Computer Programs

# FOCL/F Acquisition Routine

```
C-FOCL/F        12/01/72

01.05 V K;E V;V L,200;V O,WW,1;V O,WT,101
01.10 A "NUMBER OF SAMPLES?",N,!!!;S L=0;G 21.1

10.05 F I=1,300;S X=FSIN(1)
10.10 T :25;F K=0,L-1;T %6.04,WW(K),WT(K),!
10.20 T :60;D 10.05;Q

20.10 S XX=FNEW(0);S DD=FNEW(1);S YY=FNEW(2)

21.10 S X=0;S D=0;S Y=0;S I=0.1;S J=0.1
21.20 D 20
21.30 I (DD-2) 21.6;I (DD-120) 21.2;I (N-I) 21.2;  $
      S I=I+1;S X=X+XX;S Y=Y+YY
21.35 I (I-N) 21.2;I (J-N) 21.2;G 21.7
21.60 I (N-J) 21.2;S J=J+1;S D=D+XX;S Y=Y+YY
21.63 G 21.35
21.70 S X=X/N;S D=D/N;S Y=Y/(2*N);  $
      L O,N;T %3,L+1,%6.04,9.9*(X-D)/1023,9.9*Y/1023,!;  $
      F K=1,20;S AQ=FSIN(K)
21.80 L O,T;S WW(L)=9.9*(X-D)/1023;S WT(L)=9.9*Y/1023;  $
      S L=L+1;G 21.1

25.10 S XX=FSIN(1)
25.20 S J=FOUT(J)

26.05 I (X) ,26.12,;I (FITR(X)-X) 26.1;S X=X+0.5
26.10 S X=X+0.00005;S Y=FLOG(X)/2.30259;S Y=FITR(Y);S X=X/(10↑Y)
26.11 I (Y) ,,26.2
26.12 S J=FITR(X);S X=10*(X-J);S J=176+J;D 25;S J=174;D 25
26.13 F I=1,4;;S J=FITR(X);S X=10*(X-J);S J=176+J;D 25;R
26.20 F I=1,Y+1;S J=FITR(X);S X=10*(X-J);S J=176+J;D 25

27.10 F L=0,100;A WW(L),WT(L),!

28.05 A "#",N,!,"LEISS",LE,!,"WAVE",WA,!,"MAX",M,!;D 10.05
28.06 F I=1,250;S J=0;S XX=FSIN(1);S XX=FSIN(1);D 25
28.07 T "#";S X=N;D 26;T !,"LEISS ";S X=LE;D 26
28.08 T "   ",!,"WAVELENGTH ";S X=WA;D 26;T "  ",!," ";S X=M
28.09 D 26;T " ";S X=I;D 26;T !
28.10 F I=0,L-1;S WT(I)=10.07*(WT(I)-0.0097)
28.20 F I=0,L-1;S WT(I)=273.16+(WT(I)*26.1167)+  $
      (-0.799167*WT(I)↑2)+(-0.0316667*WT(I)↑3)+  $
      (-0.0358333*WT(I)↑4)
28.40 F K=0,L-1;T %3,WT(K),%6.04,WW(K),!
28.50 D 28.06;D 10.05;Q

30.10 A X;T %5,FX(8,FX(1,FX(10,X)));A Y;S X=FX(1,  $
      FX(10,X),FX(10,Y));T !
```

| | |
|---|---|
| 15200 | 4453 |
| 15201 | 7450 |
| 15202 | 5210 |
| 15203 | 1207 |
| 15204 | 7450 |
| 15205 | 5237 |
| 15206 | 5243 |
| 15207 | 7777 |
| 15210 | 7300 |
| 15211 | 1277 |
| 15212 | 6534 |
| 15213 | 6531 |
| 15214 | 5213 |
| 15215 | 7301 |
| 15216 | 4260 |
| 15217 | 7301 |
| 15220 | 4260 |
| 15221 | 3276 |
| 15222 | 7301 |
| 15223 | 7001 |
| 15224 | 4260 |
| 15225 | 3275 |
| 15226 | 7300 |
| 15227 | 4260 |
| 15230 | 3274 |
| 15231 | 1276 |
| 15232 | 3045 |
| 15233 | 3046 |
| 15234 | 1273 |
| 15235 | 3044 |
| 15236 | 5527 |
| 15237 | 7300 |
| 15240 | 1275 |
| 15241 | 5232 |
| 15242 | 7300 |
| 15243 | 1274 |
| 15244 | 5232 |
| 15245 | 7300 |
| 15246 | 1257 |
| 15247 | 3256 |
| 15250 | 2256 |
| 15251 | 5250 |
| 15252 | 7301 |
| 15253 | 5216 |
| 15254 | 0000 |
| 15255 | 0000 |
| 15256 | 0000 |
| 15257 | 7745 |
| 15260 | 0000 |
| 15261 | 6534 |
| 15262 | 6536 |
| 15263 | 6532 |
| 15264 | 6531 |
| 15265 | 5264 |
| 15266 | 6536 |
| 15267 | 5660 |
| 15270 | 0000 |
| 15271 | 0000 |
| 15272 | 0000 |
| 15273 | 0013 |
| 15274 | 0000 |
| 15275 | 0000 |
| 15276 | 0000 |
| 15277 | 2001 |

Fast Machine Language

Subroutine

Absolute Address and

Contents shown in Octal

## Normalized Display Routine (FORTRAN)

```
1           REAL T(120),L(120)
2           INTEGER CHAR(14)/0,1,2,3,4,5,6,7,8,9,10,11,12,13/
3           DIMENSION T2(3),T3(4)
4         97 FORMAT(A4)
5         98 FORMAT(3A4)
6         99 FORMAT(4A4)
7        100 FORMAT(I2,F6.4)
8        101 FORMAT(F7.4,T8,I3)
9        102 FORMAT(T3,F3.0,T8,F7.4)
10       103 FORMAT(2I2)
11          READ(1,103)KK,KI
12          CALL PLOTS
13          CALL PLOT(2.0,-8.0,-3)
14          DO 250 JJ=1,KK
15          CALL PLOT(0.0,10.5,-3)
16          READ(1,100)K,FACT
17          CALL FACTOR(FACT)
18       105 CALL AXIS2(0.0,0.0,'TEMPERATURE IN K',-16,8.0,0.0,0.0,40.0,1.0)
19          CALL AXIS2(0.0,0.0,'RELATIVE OUTPUT',15,7.0,90.0,-2.0,2.0,1.0)
20          CALL PLOT(0.0,1.0,3)
21          CALL DASHPT(8.0,1.0,0.1)
22          CALL PLOT(8.0,6.0,3)
23          CALL DASHPT(0.0,6.0,0.1)
24          DO 200 J=1,K
25          READ(1,97)T1
26          READ(1,98)  (T2(I),I=1,3)
27          READ(1,99)  (T3(I),I=1,4)
28          XX=0.5+(2.5*(J-1))
29          CALL SYMBOL(XX,7.2,0.15,T1,0.0,4)
30          CALL SYMBOL(XX,7.0,0.15,T2,0.0,12)
31          CALL SYMBOL(XX,6.8,0.15,T3,0.0,16)
32          CALL SYMBOL(XX+1.5,7.07,0.15,J+4042321 91,0.0,4)
33          READ(1,101)S,N
34          N=-N
35          DO 110 I=1,N
36          READ(1,102)T(I),L(I)
37       110 L(I)=L(I)*10/S
38          T(N+1)=0
39          L(N+1)=-2.0
40          T(N+2)=40.0
41          L(N+2)=2.0
42       200 CALL FLINE(T,L,N,1,KI,J-1)
43       250 CONTINUE
44          CALL PLOT(2.0,2.0,999)
45          STOP
46          END
```

## Non-Normalized Display Routine (FORTRAN)

```
      REAL T(120),L(120)
      INTEGER CHAR(14)/0,1,2,3,4,5,6,7,8,9,10,11,12,13/
      DIMENSION T2(3),T3(4)
   97 FORMAT(A4)
   98 FORMAT(3A4)
   99 FORMAT(4A4)
  100 FORMAT(I2,2F6.4)
  101 FORMAT(F7.4,T8,I3)
  102 FORMAT(T3,F3.0,T8,F7.4)
  103 FORMAT(2I2)
      READ(1,103)KK,KI
      CALL PLOTS
      CALL PLOT(2.0,-8.0,-3)
      DO 250 JJ=1,KK
      CALL PLOT(0.0,10.5,-3)
      READ(1,100)K,FACT,R
      CALL FACTOR(FACT)
  105 CALL AXIS2(0.0,0.0,'TEMPERATURE IN K',-16,8.0,0.0,0.0,40.0,1.0)
      CALL AXIS2(0.0,0.0,'RELATIVE OUTPUT',15,7.0,90.0,-2.0,2.0,1.0)
      CALL PLOT(0.0,1.0,3)
      CALL DASHPT(8.0,1.0,0.1)
      CALL PLOT(8.0,6.0,3)
      CALL DASHPT(0.0,6.0,0.1)
      DO 200 J=1,K
      READ(1,97)T1
      READ(1,98)  (T2(I),I=1,3)
      READ(1,99)  (T3(I),I=1,4)
      XX=0.5+(2.5*(J-1))
      CALL SYMBOL(XX,7.2,0.15,T1,0.0,4)
      CALL SYMBOL(XX,7.0,0.15,T2,0.0,12)
      CALL SYMBOL(XX,6.8,0.15,T3,0.0,16)
      CALL SYMBOL(XX+1.5,7.07,0.15,J+404232191,0.0,4)
      READ(1,101)S,N
      M=-N
      DO 110 I=1,N
      READ(1,102)T(I),L(I)
  110 L(I)=L(I)*10/R
      T(N+1)=0
      L(N+1)=-2.0
      T(N+2)=40.0
      L(N+2)=2.0
  200 CALL PLINE(T,L,M,1,KI,J-1)
  250 CONTINUE
      CALL PLOT(2.0,2.0,999)
      STOP
      END
```

# APPENDIX II

## List of Data

## List of Data

| Label # | Wavelength of Measurement μ | Excitation Wavelength Å | Maximum Signal Level mV |
|---|---|---|---|
| 130 | 0.72 | 5960 | 32.3 |
| * 132 | 0.72 | 5985 | 70.9 |
| 121 | 0.72 | 6080 | 26.3 |
| * 124 | 0.72 | 6080 | 36.7 |
| * 126 | 0.72 | 6200 | 17.3 |
| * 135 | 0.72 | 6320 | 11.1 |
| * 131 | 0.83 | 5960 | 21.5 |
| * 122 | 0.83 | 6080 | 15.5 |
| 123 | 0.83 | 6080 | 11.2 |
| 136 | 0.83 | 6080 | 15.9 |
| * 127 | 0.83 | 6200 | 21.2 |
| * 133 | 0.83 | 6320 | 3.3 |
| 138 | 0.83 | 6330 | 3.2 |
| * 140 | 0.93 | 5905 | 3.3 |
| 141 | 0.93 | 5905 | 2.7 |
| * 129 | 0.93 | 5960 | 20.2 |
| * 120 | 0.93 | 6080 | 20.2 |
| * 125 | 0.93 | 6200 | 18.4 |
| 128 | 0.93 | 6200 | 16.8 |
| 134 | 0.93 | 6320 | 8.5 |
| * 137 | 0.93 | 6330 | 17.3 |

Sets indicated with an * were used in non-normalized data plots.